

F-theory and the LHC: Stau Search

Jonathan J. Heckman^{1*}, Jing Shao^{2†} and Cumrun Vafa^{3‡}

¹School of Natural Sciences, Institute for Advanced Study, Princeton, NJ 08540, USA

²Department of Physics, Syracuse University, Syracuse, NY 13244, USA

³Jefferson Physical Laboratory, Harvard University, Cambridge, MA 02138, USA

Abstract

F-theory GUT models favor a relatively narrow range of soft supersymmetry breaking parameters in the MSSM Lagrangian. This leads to the specific predictions that a 10 – 100 MeV mass gravitino is the LSP, and the NLSP is quasi-stable, with a lifetime between a second to an hour. In a wide range of parameter space, the NLSP turns out to be a stau, though a bino-like lightest neutralino is also possible. Focusing on F-theory GUTs with a stau NLSP, we study the discovery potential at the LHC for such scenarios. Models with a quasi-stable stau predict a striking signature of a heavy charged particle passing through the detector. As a function of the parameters of minimal F-theory GUTs, we study how many of such events to expect, and additional signatures correlated with the presence of quasi-stable staus. We also study the prospects for staus to become stopped in or near the detector, as well as potential ways to distinguish such models from minimal gauge mediation models with similar spectra.

January, 2010

*e-mail: jheckman@sns.ias.edu

†e-mail: jishao@syr.edu

‡e-mail: vafa@physics.harvard.edu

Contents

1	Introduction	2
2	Parameter Space of F-theory GUTs	5
3	The LSP, NLSP and NNLSP	9
3.1	Masses and the Messenger Scale	10
3.2	PQ Deformation of the Masses	12
3.3	Benchmark Models	13
3.4	PQ Deformation of the Branching Fractions	16
3.5	Right-Handed Sneutrino NLSP and Dirac Neutrinos	18
4	Event Generation of Long-Lived Staus	21
4.1	Production Cross Sections	22
4.2	Candidate Staus	25
5	Search Channels	27
5.1	Inclusive Stau Channels	28
5.1.1	β_{min} and Cross Sections	28
5.1.2	Λ and Δ_{PQ} Dependence	29
5.1.3	Discovering Staus	29
5.2	Exclusive Two Stau Channel	33
5.3	Two Stau Plus Lepton(s) Channels	36
5.4	Inclusive Lepton Signals	38
6	Stopped Staus	42
7	Mass Spectra and Distinguishing Look-Alikes	46
7.1	Mass Reconstruction with Staus	47
7.2	Comparison with Minimal Gauge Mediation	50
8	Conclusions	57

1 Introduction

A few decades of theoretical research has led to many novel ideas for what to expect at the TeV energy scale. Perhaps the most well motivated idea is that supersymmetry will soon be discovered. In addition to its aesthetic appeal, supersymmetry provides a relatively simple resolution of the hierarchy problem. There is also circumstantial evidence for supersymmetry both from the prescient prediction of a heavy top mass, and the remarkable unification of the gauge coupling constants in the MSSM, which does not work with only Standard Model degrees of freedom. Though the lack of detection necessarily constrains the available parameter space, leading to a mild degree of fine-tuning (the mini-hierarchy problem), supersymmetry remains among the most robust, and motivated options for beyond the Standard Model physics.

Another motivation for supersymmetry is that at high energies it is predicted by string theory. Given the existence of meta-stable vacua where supersymmetry is broken, this suggests the attractive possibility that at least for matter charged under the Standard Model gauge group, supersymmetry persists down to the TeV scale.

Even so, this by itself is not particularly predictive, because the details of supersymmetry breaking strongly affect the superpartner masses and interactions with the Standard Model. This in turn directly affects the expected collider signatures of a particular model.

In the past few years, F-theory based models have emerged as promising candidates for particle phenomenology [1–48]. In these models, the Standard Model gauge group and matter originate in a compact region of the six extra dimensions of string theory. Physically, this corresponds to a regime where particle physics can be treated in a limit decoupled from gravity. Gauge groups localize on four real-dimensional subspaces, chiral matter localizes on two real-dimensional Riemann surfaces, and cubic interaction terms between chiral matter localize at points of the geometry. Flavor physics in particular appears to play a key role in constraining candidate geometries [14, 24, 32], requiring a point of E_8 enhancement [32].

Combining this with the assumption that supersymmetry persists down to the TeV scale severely limits consistent scenarios. A deformation of minimal gauge mediated supersymmetry breaking seems to be the most natural option in F-theory GUTs [6, 8, 9], though other approaches are also possible.¹ Parameterizing the effects of supersymmetry breaking through the vev of a GUT singlet $\langle X \rangle = x + \theta^2 F$, in F-theory GUT deformations of minimal gauge mediation models, the μ -term is generated through the Giudice-Masiero type operator

$$\int d^4\theta \frac{X^\dagger H_u H_d}{\Lambda_{UV}}, \quad (1)$$

where Λ_{UV} is fixed by the internal scale of the geometry to be near the GUT scale. In

¹See for example [49–52] and in the context of moduli mediation [4, 53–57].

order to generate a weak scale value for μ , this requires a specific scale of supersymmetry breaking

$$F \sim M_{weak} M_{GUT} \sim 10^{17} \text{ GeV}^2.$$

This fixes a narrow range of values for $\sqrt{F} \sim 10^8 - 10^9 \text{ GeV}$, which implies that the gravitino is the lightest superpartner (LSP) of mass $10 - 100 \text{ MeV}$, and that the next lightest superpartner (NLSP) is quasi-stable on timescales probed by collider detectors, with a lifetime on the order of one second to an hour. The primary decay chains of all MSSM superpartners involve the NLSP, which strongly influences the experimental signatures of an F-theory GUT.

This begs the question: Which particle is the NLSP? In F-theory GUTs, constraints from other sectors of the model force the lightest stau $\tilde{\tau}_1$ to be the NLSP over much of parameter space. This is due to two effects: First, in minimal models with a point of E_8 unification, the messengers of the gauge mediation model tend to be in vector-like pairs transforming in the $10 \oplus \overline{10}$ of $SU(5)$. In comparison with messengers in the $5 \oplus \overline{5}$, the higher dimension of the 10 representation lowers the mass of the stau relative to the gauginos. Requiring that gravity can be decoupled requires an asymptotically free $SU(5)$ GUT group which constrains the number of vector-like pairs in the $10 \oplus \overline{10}$ to $N_{10} \leq 2$. Moreover, there is also a stringy ‘‘PQ deformation’’ of the spectrum due to heavy gauge boson exchange of an anomalous $U(1)_{PQ}$ [9]. This also has the effect of lowering the stau mass by an amount Δ_{PQ} which tends to be on the order of the weak scale. Even so, for a smaller range of parameter space a bino-like lightest neutralino $\tilde{\chi}_1^0$ may be the NLSP. In a very particular Dirac neutrino scenario the right-handed sneutrino can also be the NLSP, but in this case the next to next to lightest superpartner (NNLSP) is also quasi-stable, and is typically the stau.

If the NLSP is a stau, it will have dramatic consequences for the LHC. It is a heavy charged particle leaving the detector! Moreover, since R-parity is preserved, the number of such staus will always come in pairs. As a massive quasi-stable charged particle, the stau will initially register as a muon in the detector. The primary challenge is therefore to distinguish such ‘‘fake muons’’ from actual muons. Such stau events have extremely low Standard Model background, and can easily be isolated from actual muons through suitable selection cuts. Stau NLSP scenarios have been extensively studied in the literature [58–63]. One of the most attractive phenomenological features of such scenarios is that because it is relatively easy to detect, it is possible to extract its mass. Correlating this with the four-momenta of other final state products, this provides a means to proceed up a decay chain, extracting the masses of other superpartners [62].

In this paper we perform a parameter space scan over F-theory GUTs, showing that over a broad range of parameter space the stau is an NLSP. Next, we study the prospects for detecting signatures of stau NLSP F-theory GUT scenarios at the LHC. See [22] for a

study of related F-theory GUT scenarios with a bino NLSP. The expected signatures in stau NLSP scenarios greatly depend on both the center-of-mass energy and the integrated luminosity, and with increases in each, the prospects for detecting staus improve. We find that with energies which will soon be achieved at the LHC, such signatures will indeed be within reach!

Though the primary signature of stau NLSP scenarios is the presence of “fake muons”, the parameters of an F-theory GUT also strongly determine the additional signatures expected. We find that the number of leptons in the final state also depends on the number of messengers N_{10} , and the size of Δ_{PQ} . For a single $10 \oplus \overline{10}$ pair of messengers and moderate PQ deformation, many of the staus are unaccompanied by other final states. For larger values of the PQ deformation, and for more messengers, additional sleptons become lighter than gauginos, providing new decay channels. This tends to increase the number of leptons expected with a given stau signature.

We also study the prospects for generating staus which can become stuck in or near the detector and then decay at some later time. When these staus eventually decay to a gravitino and tau, observing such events would provide additional evidence for quasi-stable staus. Further, for staus stopped in the detector, correlating the presence of the tau produced from the decay of the stau with the initial collision event can in principle provide a means to measure the lifetime of the NLSP, and consequently the scale of supersymmetry breaking.

Another remarkable feature of such scenarios is that because a stau NLSP is detectable, it is possible to reconstruct with high precision the masses of sparticles which decay into a stau. We review the expected level of precision in such mass fits, and then explain how this level of accuracy provides a means to break degeneracies between F-theory GUTs and minimal gauge mediation models with a stau NLSP which might otherwise be present with cruder signatures.

The organization of the rest of this paper is as follows. In section 2 we review the salient features of F-theory GUTs. In section 3 we show that for a wide range of parameter space, the stau is the NLSP, while over a smaller range, the bino is the NLSP. We next move to collider signatures of F-theory GUTs with a quasi-stable stau NLSP. In section 4 we discuss details of the simulation performed and compute the production cross sections for supersymmetric events, and in section 5 we study search channels of potential interest. Section 6 discusses the prospects for observing stopped staus, and in section 7 we study whether mass reconstruction based on the stau NLSP can be used to distinguish F-theory GUTs from minimal gauge mediation models with similar spectra. Section 8 contains our conclusions. Appendix A contains additional details on the simulation, Appendix B contains some additional discussion on the selectron mass in F-theory GUTs and minimal gauge mediation, and Appendix C contains miscellaneous plots.

2 Parameter Space of F-theory GUTs

Our aim in this paper will be to study the phenomenological consequences of a particularly minimal class of F-theory GUT models based on a point of E_8 unification [32], and the corresponding supersymmetry breaking scenarios. See [4] for other supersymmetry breaking scenarios in F-theory GUTs, and their experimental signatures.

In an F-theory GUT, all of the particle content of the Standard Model localizes on a spacetime filling seven-brane which wraps a complex two-dimensional surface. The matter fields of the MSSM localize on complex one-dimensional curves formed by pairwise intersections of the GUT stack with other seven-branes, and the Yukawa couplings of the MSSM localize at points of the geometry formed by triple intersections of seven-branes. In this type of setup, achieving realistic flavor hierarchies requires that these Yukawa points be close together. In minimal setups, there is a single point where the geometry enhances up to a point of E_8 symmetry which is broken down to $SU(6)$ and $SO(10)$ along curves supporting respectively 5's and 10's of $SU(5)$, and is broken down to $SU(5)_{GUT}$ over the bulk of the seven-brane worldvolume. Minimal F-theory GUT models are especially predictive, and these are the scenarios we study in this paper.

The supersymmetry breaking sector localizes on another seven-brane, which supports an anomalous $U(1)_{PQ}$ gauge boson. This seven-brane intersects the GUT seven-brane, leading to the matter of the MSSM, all of which is charged under $U(1)_{PQ}$. Supersymmetry breaking is triggered by the vev of a GUT singlet X :

$$\langle X \rangle = x + \theta^2 F. \quad (2)$$

Supersymmetry breaking is communicated to the visible sector through gauge mediation [64–73] as well as through the exchange of a heavy anomalous $U(1)$ gauge boson. See [74] for a review of gauge mediation. In the deformation of minimal gauge mediation considered in [9] (see also [8]), the effects of supersymmetry breaking are transmitted to the messengers through the cubic interaction term:

$$\int d^2\theta XYY', \quad (3)$$

for messenger fields Y and Y' in vector-like pairs of complete $SU(5)$ GUT multiplets. Once X develops a supersymmetry breaking vev, loops with gauge fields will then communicate this to the visible sector. Assuming that the interaction XYY' also localizes at the same point of E_8 unification, it can be shown that in all but one Dirac neutrino scenario, the messenger fields are *forced* to transform in the $10 \oplus \overline{10}$ of $SU(5)_{GUT}$ [32]. We denote the number of such vector-like pairs by N_{10} . Heuristically, the requirement that we can decouple gravity from the gauge theory requires that $SU(5)_{GUT}$ is an asymptotically free

gauge theory, which implies $N_{10} = 1$ or 2 .

When the μ -term is generated through the higher-dimension operator of equation (1), the scale of supersymmetry breaking is fixed to be:

$$F \sim M_{weak} \cdot M_{GUT}. \quad (4)$$

Introducing the characteristic scale:

$$\Lambda \equiv \frac{F}{x} \quad (5)$$

of minimal gauge mediation, we can express the messenger scale M_{mess} in terms of x and the remaining parameters as:

$$x \equiv M_{mess} \sim \frac{M_{weak} \cdot M_{GUT}}{\Lambda}. \quad (6)$$

Phenomenologically, we require $\Lambda \sim 100$ TeV to achieve a realistic mass spectrum. Including all order one coefficients, we have [9]:

$$F \sim 10^{17} \text{ GeV}^2 \quad (7)$$

$$x \sim 10^{12} \text{ GeV}. \quad (8)$$

The specific range of supersymmetry breaking and messenger scales, as well as the constrained messenger content constitutes one important prediction of this class of models. The vev x also doubles as the effective axion decay constant, which is in accord with the present window of viable values.

At the messenger scale, localization on seven-branes allows an F-theory GUT to generate a weak scale value for the μ -parameter. Localization on seven-branes also implies that both $B\mu$ and the A-terms vanish at the messenger scale:

$$B\mu(M_{mess}) = 0 \quad (9)$$

$$A_{ijk}(M_{mess}) = 0. \quad (10)$$

At lower energy scales the parameter $B\mu$ is radiatively generated, and the ratio of the Higgs up and down vevs, $v_u/v_d \equiv \tan \beta \sim 20 - 30$ is large [75]. Another consequence of generating $B\mu$ in this way is that proper electro-weak symmetry breaking then requires $\mu M_{1/2} \tan \beta > 0$, where $M_{1/2}$ denotes the gaugino masses (see for example [75–77]). Our sign convention is the same as [78] where $M_{1/2}, \tan \beta > 0$, which in turn implies $\mu > 0$. To a large extent, the value of Λ determines the amount of fine-tuning in the Higgs sector. In particular, the current bound on the Higgs mass of ~ 114 GeV translates to a lower bound on Λ which we denote as Λ_{\min} . The value of Λ_{\min} also depends on the messenger content,

so that for $N_{10} = 1$ and 2, we have:

$$\Lambda_{\min}(N_{10} = 1) = 50 \text{ TeV} \quad (11)$$

$$\Lambda_{\min}(N_{10} = 2) = 28 \text{ TeV}. \quad (12)$$

To illustrate the broader features of this parameter space scan, we shall sometimes allow slightly lower values of Λ . The maximal value of Λ we consider is based on the requirement that we not overly fine-tune the Higgs sector, which to some extent is a matter of aesthetics. The upper bound on Λ we take is:

$$\Lambda_{\max}(N_{10} = 1) = 95 \text{ TeV} \quad (13)$$

$$\Lambda_{\max}(N_{10} = 2) = 53 \text{ TeV}. \quad (14)$$

Since the messenger scale also plays a role in setting the scale of the axion decay constant, we shall effectively treat M_{mess} as a fixed parameter. A change in Λ therefore corresponds to altering the scale of supersymmetry breaking.

The soft masses at the messenger scale receive additional corrections from integrating out the heavy PQ gauge boson:

$$L \supset -4\pi\alpha_{PQ}e_X e_\Psi \int d^4\theta \frac{X^\dagger X \Psi^\dagger \Psi}{M_{U(1)PQ}^2} \quad (15)$$

where e_X and e_Ψ respectively denote the PQ charges of X and the MSSM chiral superfield Ψ , and $M_{U(1)PQ}$ is the mass of the PQ gauge boson. Once X develops a supersymmetry breaking vev, this induces a shift in the soft masses at the messenger scale:

$$m_{soft}^2 = m_{mGMSB}^2 + q_\Psi \Delta_{PQ}^2. \quad (16)$$

Compatibility with minimal Majorana and Dirac neutrino scenarios [24] yields two different choices for the PQ charges. In a normalization where the operator

$$-4\pi\alpha_{PQ}e_X e_X \int d^4\theta \frac{X^\dagger X \Psi^\dagger \Psi}{M_{U(1)PQ}^2} \quad (17)$$

has the same coefficient in both Majorana and Dirac scenarios, the constant of proportionality q appearing in equation (16) is:

	10_M	$\bar{5}_M$	5_H	$\bar{5}_H$	
q_{Majorana}	$-4/5$	$-8/5$	$+8/5$	$+12/5$.
q_{Dirac}	-1	-1	$+2$	$+2$	

(18)

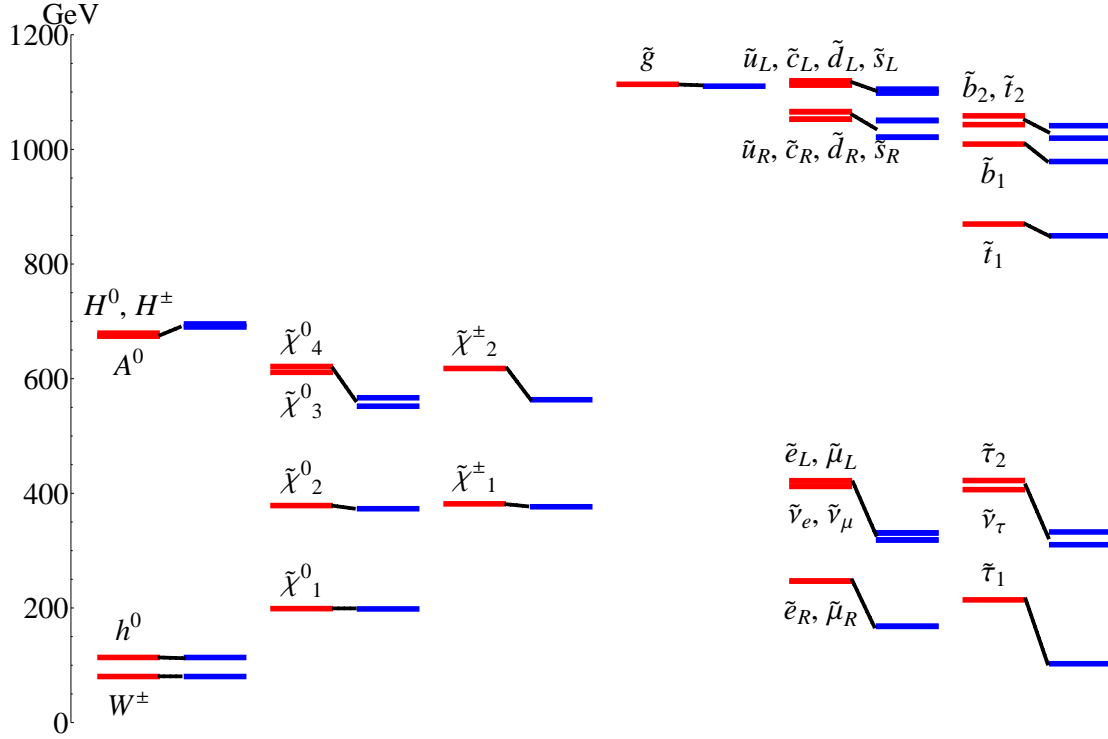


Figure 1: Spectrum of an F-theory GUT Majorana neutrino scenario with $N_{10} = 1$, $\Lambda = 50$ TeV for minimal (red left columns) and maximal (blue right columns) PQ deformation of order 200 GeV. At small values of the PQ deformation, the bino is the NLSP, whereas for larger values this transitions to the stau. Further note that at larger PQ deformation, the right-handed selectron and smuon are also lighter than the bino, and all of the sleptons are lighter than the second neutralino and lightest chargino.

Technically speaking, there is slightly more freedom in the Dirac scenario, because there is also a $U(1)_{B-L}$ symmetry available in Dirac neutrino scenarios. Since the effects of the PQ deformation are similar in Majorana and Dirac scenarios, we shall focus on Majorana scenarios.

The PQ deformation lowers the soft masses of the chiral matter fields, while raising the soft masses in the Higgs sector. For sufficiently large values of Δ_{PQ} , this induces a tachyonic mode in the spectrum, which imposes an upper bound on the value of Δ_{PQ} on the order of 200 – 400 GeV, the precise value of which depends on Λ . Let us also note that there is also an experimental upper bound on the size of Δ_{PQ} because of the present 100 GeV bound on the mass of the stau [79].

Summarizing, the parameter space of an F-theory GUT which we scan over is:

- Fixed messenger scale $M_{mess} \sim 10^{12}$ GeV

- For $N_{10} = 1 : 50$ TeV $\lesssim \Lambda(N_{10} = 1) \lesssim 95$ TeV
- For $N_{10} = 2 : 28$ TeV $\lesssim \Lambda(N_{10} = 2) \lesssim 53.2$ TeV
- $0 \leq \Delta_{PQ} \lesssim 200 - 400$ GeV

See figure 1 for a plot of the sparticle spectrum of a representative F-theory GUT with $N_{10} = 1$, $\Lambda = 50$ TeV at minimal and maximal PQ deformation, and figure 23 of Appendix C for the case of $N_{10} = 2$ and $\Lambda = 28$ TeV.

3 The LSP, NLSP and NNLSP

The collider phenomenology of a supersymmetric model strongly depends on which sparticle is the lightest superpartner (LSP), the next lightest superpartner (NLSP), and sometimes the next to next lightest superpartner (NNLSP). In this section, we study the spectrum of F-theory GUTs, and show that the LSP is always the gravitino, and in Majorana neutrino scenarios the NLSP is either the bino or the stau. In Dirac neutrino scenarios, we find that for small values of the PQ deformation, a right-handed sneutrino is also a possible NLSP, though in such cases the NNLSP which is either a bino or stau is still quasi-stable on the same timescale as the NLSP. To perform our numerical analysis of the spectrum we use the program `SOFTSUSY` [78].

The narrow window for supersymmetry breaking implies that the gravitino is the LSP, with mass:

$$m_{3/2} = \sqrt{\frac{4\pi}{3}} \frac{F}{M_{pl}} \sim 10 - 100 \text{ MeV}. \quad (19)$$

The gravitino is stable, and all of the other MSSM superpartners eventually decay to it, plus their Standard Model counterparts. In this class of models, such gravitinos provide a viable dark matter candidate [17], much as in the sweet spot model of supersymmetry breaking [80].

In many minimal gauge mediation models, the NLSP is a stau or a bino-like neutralino, and the situation in F-theory GUTs is no different. What is different in F-theory GUTs is that there is a specific range of values for the parameters of the model. Even without knowing the precise identity of the NLSP, the scale of supersymmetry breaking dictates that it will be quasi-stable, with a lifetime on the order of one second to an hour [12], so that it will appear stable to a collider detector.

Increasing the number of messengers or equivalently the dimension of the representation to which they belong tends to lower the masses of the scalars relative to the gauginos. For example, in a model with N_5 messengers in the $5 \oplus \bar{5}$, the scalar and gaugino masses at the

messenger scale are:

$$m_{\text{scalar}} = \sqrt{N_5} \cdot C_{\text{scalar}} \frac{\alpha}{4\pi} \Lambda \quad (20)$$

$$m_{\text{gaugino}} = N_5 \cdot C_{\text{gaugino}} \frac{\alpha}{4\pi} \Lambda, \quad (21)$$

where schematically, the C 's are constants fixed by the quadratic Casimirs of various representations, and the α 's are the fine structure constants of the gauge groups under which the sparticles are charged. This is especially important for the present class of models, where the messengers are in vector-like pairs of $10 \oplus \bar{10}$'s, the number of which we denote by N_{10} . The soft masses are proportional to the Dynkin index of the messengers. This means that each messenger pair in the $10 \oplus \bar{10}$ has the same effect as three in the $5 \oplus \bar{5}$, so that $3N_{10} = N_5$.

The rest of this section is organized as follows. Besides the discrete parameter N_{10} , the low energy content of a minimal F-theory GUT is controlled by the messenger scale, the characteristic scale of minimal gauge mediation Λ and the size of the PQ deformation Δ_{PQ} . We first show that near the value of the messenger scale favored by F-theory GUTs, small changes in M_{mess} can switch the relative orderings of the bino and stau mass. After this, we study the effects of the PQ deformation. This latter deformation leads to qualitatively distinct mass spectra in the case of $N_{10} = 1$ models, but leads to more subtle changes in the relative masses when $N_{10} = 2$. Next, we introduce some benchmark models, which crudely characterize these qualitatively different mass spectra. This is followed by a discussion of how shifts in the relative sparticle masses due to the PQ deformation affect decay topologies, which will be important later when we discuss candidate collider signals.

3.1 Masses and the Messenger Scale

We now discuss F-theory GUT scenarios at zero PQ deformation, but where we vary the messenger scale. For *low scale* gauge mediation models with $N_{10} = 1$, the stau is the NLSP. Increasing the messenger scale raises the mass of the scalars, because of the additional renormalization group evolution from the messenger to the weak scale. For example, in minimal gauge mediation models with $N_{10} = 1$, and $\Lambda \sim 50$ TeV, the bino becomes the NLSP for $M_{\text{mess}} \sim 10^{11}$ GeV. In minimal gauge mediation models with $N_{10} = 2$, however, the stau remains the NLSP until $M_{\text{mess}} \sim 10^{14}$ GeV.

Even when $N_{10} = 1$, the stau is the NLSP for a large region of F-theory GUT parameter space. Indeed, although the messenger scale tends to increase the mass of the stau relative to the bino, the PQ deformation lowers it back down. For example, in a Majorana neutrino scenario with $N_{10} = 1$, $M_{\text{mess}} \sim 10^{12}$ GeV, $\Lambda \sim 50$ TeV, the bino and stau become equal in mass around $\Delta_{PQ} \sim 90$ GeV. Figure 2 shows a plot detailing how M_{mess} and Δ_{PQ} determine

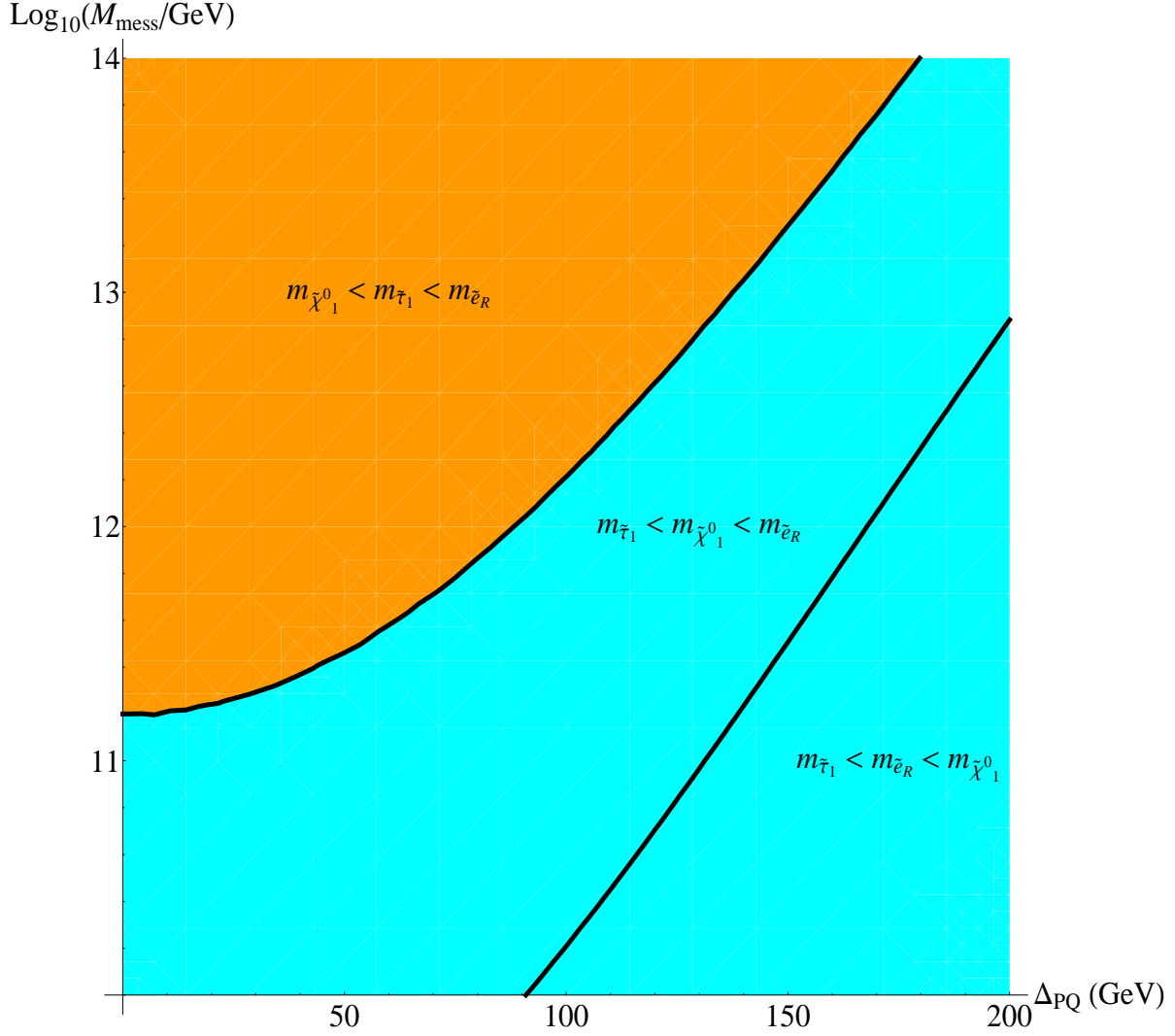


Figure 2: Contour plot indicating the relative masses of the bino, lightest stau and right-handed selectron as function of Δ_{PQ} and M_{mess} in the representative F-theory GUT scenario with $N_{10} = 1$ and $\Lambda = 50$ TeV. There are three qualitatively different regions separated by the two lines where the bino is equal in mass to either the stau (upper line) or selectron (lower line). Here we also indicate the bino NLSP (upper left orange region) and stau NLSP (lower right cyan region) regimes of parameter space.

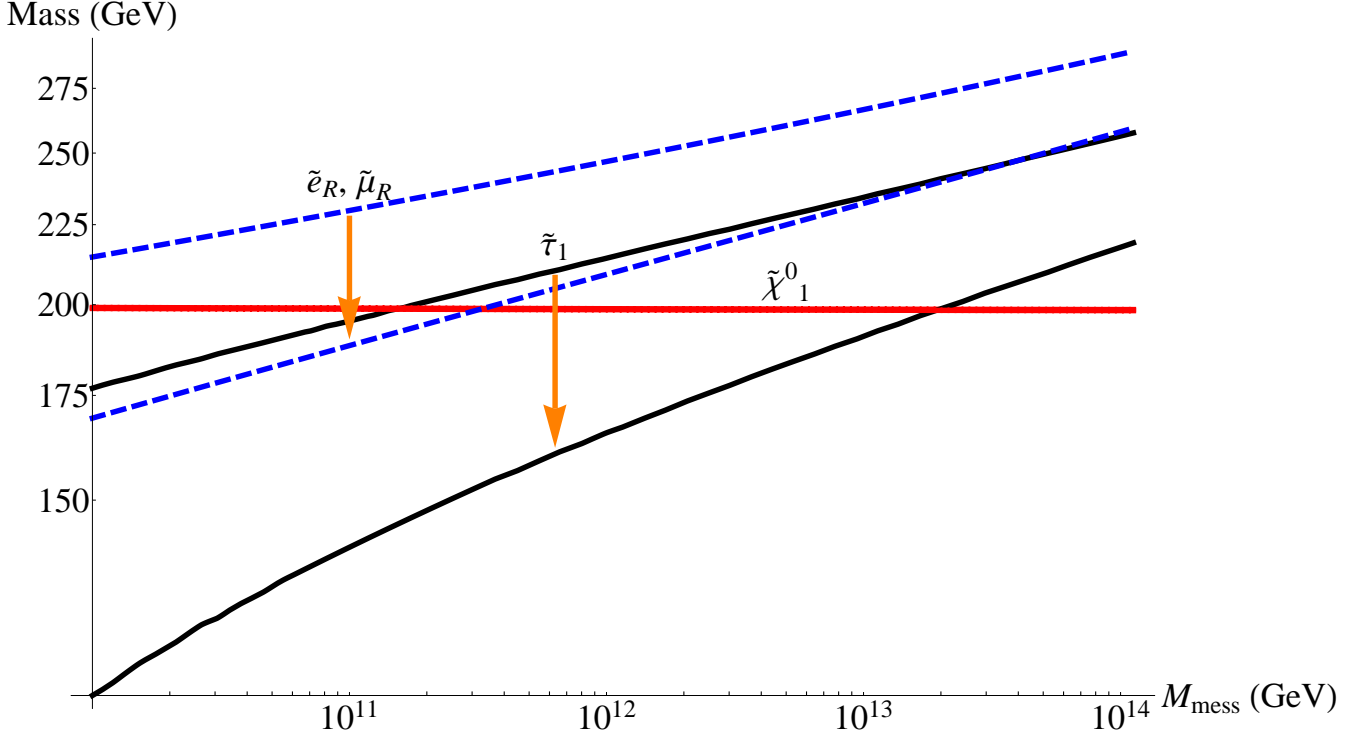


Figure 3: Plot of the four lightest sparticle masses as a function of messenger scale M_{mess} . Here $N_{10} = 1$, $\Lambda = 50$ TeV, and we have displayed the values for zero PQ deformation (upper lines) and $\Delta_{PQ} = 150$ GeV (lower lines). Note that the bino mass remains constant, both as a function of messenger scale and of PQ deformation.

the relative masses of the stau and bino. This also shows that for low enough messenger scales, and high enough PQ deformations, the right-handed selectron (and smuon, since they are degenerate in mass) can also become lighter than the bino.

Figure 3 shows the masses of the four lightest Standard Model superpartners as a function of M_{mess} and Δ_{PQ} for a Majorana scenario F-theory GUT with $N_{10} = 1$ and $\Lambda = 50$ TeV. See figure 22 of Appendix C for the analogous plot with $N_{10} = 2$, $\Lambda = 28$ TeV. Because the effects of the messenger scale induce only logarithmic changes in the masses of the scalar partners, in the remainder of this paper we shall fix M_{mess} to be:

$$M_{mess} = 10^{12} \text{ GeV}. \quad (22)$$

3.2 PQ Deformation of the Masses

In this subsection we study in greater detail the effects of the PQ deformation on the identity of the NLSP, and the other sparticle masses. As follows from the table of line (18),

the PQ deformation tends to lower the masses of all of the chiral matter superpartners relative to the gauginos. This effect is more pronounced for lower mass sparticles because the shift in the mass squared is:

$$m^2 = m_{(0)}^2 + q\Delta_{PQ}^2 \quad (23)$$

so that

$$m = m_{(0)} \left(1 + \frac{q}{2} \frac{\Delta_{PQ}^2}{m_{(0)}^2} + O\left(\frac{\Delta_{PQ}^4}{m_{(0)}^4}\right) \right). \quad (24)$$

Indeed, we find that the PQ deformation has a far greater effect on the masses of non-colored superpartners, so we focus on their masses in this subsection.

Fixing the messenger scale, we now examine how the relative masses of the sleptons shift as a function of Δ_{PQ} and Λ . Figure 4 shows the three qualitative crossing regions expected as one increases the value of the PQ deformation in F-theory GUTs with $N_{10} = 1$. The first crossover from a bino NLSP scenario to a stau NLSP scenario occurs at relatively low values of the PQ deformation. Moreover, by inspection of this plot, we observe that the value of Δ_{PQ} for which this transition occurs is roughly constant as a function of Λ , going from a value of $\Delta_{PQ} \sim 90$ GeV for $\Lambda \sim \Lambda_{\min}$ to $\Delta_{PQ} \sim 100$ GeV for $\Lambda \sim \Lambda_{\max}$. By inspection of the plot, there is a large range of parameter space where the stau is the NLSP, and a smaller sliver where the bino is the NLSP. Increasing Δ_{PQ} further causes the left-handed sleptons to become lighter than the second neutralino $\tilde{\chi}_2^0$ and lightest chargino $\tilde{\chi}_1^\pm$. This opens up new decay channels for these gauginos to left-handed sleptons, and significantly alters the decay topology. Further increasing Δ_{PQ} causes the right-handed selectron and smuon (which are mass degenerate) to become lighter than the bino. This alters the decay topology of these particles to three body decays mediated through an off-shell $\tilde{\chi}_1^0$. Figure 5 shows a plot of the non-colored sparticles as a function of Δ_{PQ} for models with $N_{10} = 1$ and $\Lambda = 50$ TeV.

In $N_{10} = 2$ scenarios, the stau is always the NLSP. Moreover, the right-handed selectron and smuon are also lighter than the bino, and all of the sleptons are lighter than the lightest chargino and second neutralino. As a consequence, there are no qualitatively different crossing regions for the relative masses as a function of Δ_{PQ} . On the other hand, the relative masses of the sparticles still depend on Δ_{PQ} , so that there will be some changes in the branching fractions. Figure 24 of Appendix C shows a plot of the non-colored sparticles as a function of Δ_{PQ} for models with $N_{10} = 2$ and $\Lambda = 28$ TeV.

3.3 Benchmark Models

In the previous sections we have studied how the mass spectrum depends on the parameters of an F-theory GUT. In the stau NLSP regime of $N_{10} = 1$ models, we have seen that there

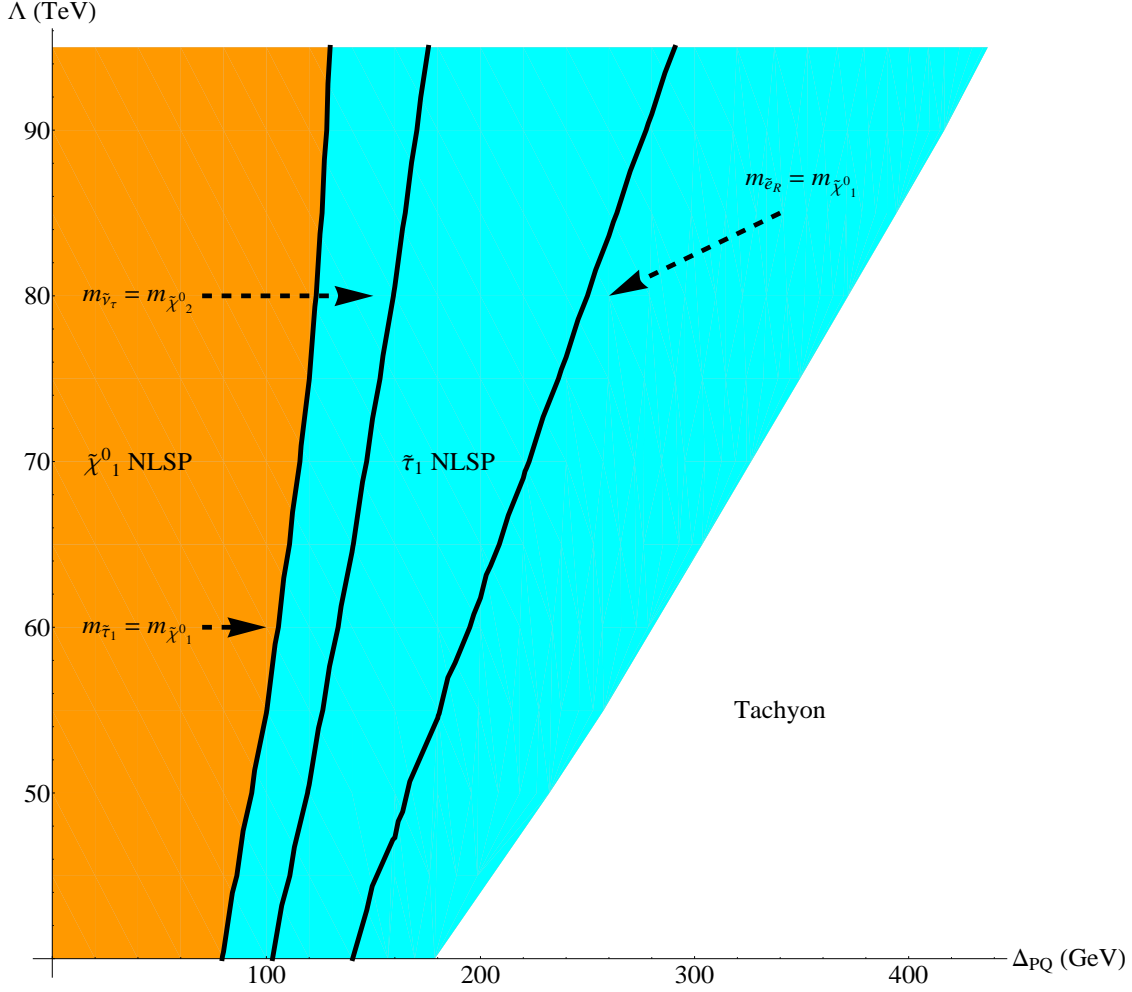


Figure 4: As a function of Δ_{PQ} and Λ , the masses of the sleptons will change relative to the gauginos. For F-theory GUTs with $N_{10} = 1$ messengers, as Δ_{PQ} increases, there are three qualitative crossing regions where the stau becomes lighter than the bino, all sleptons become lighter than the second neutralino and lightest chargino, and the right-handed selectron and smuon become lighter than the bino. In the plot, the orange region to the left denotes the range of parameter space where the bino is the NLSP, and the cyan region to the right indicates the region of the stau NLSP.

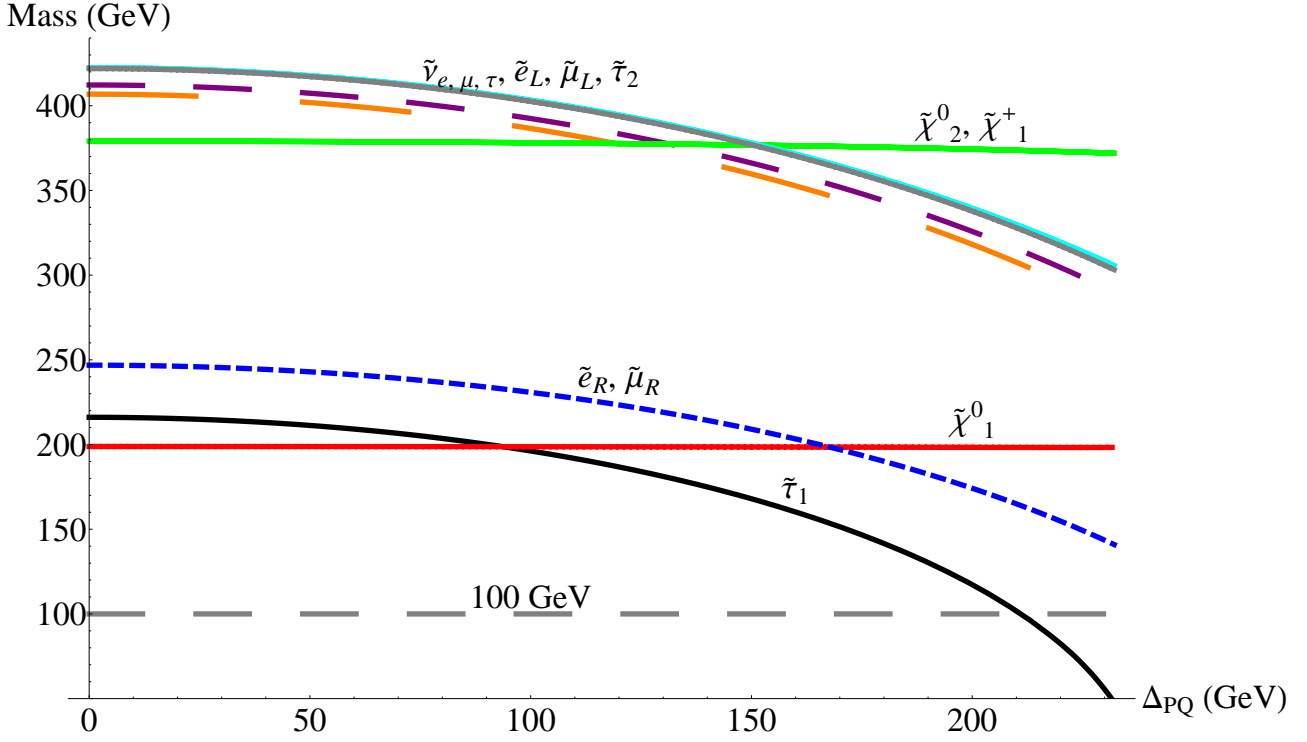


Figure 5: Mass spectrum of the sleptons and lightest chargino and two lightest neutralinos with $N_{10} = 1$, $\Lambda = 50$ TeV as a function of Δ_{PQ} . At values of $\Delta_{PQ} \sim 90$ GeV, the stau becomes the NLSP. At somewhat larger values of the PQ deformation, the sneutrinos become lighter than $\tilde{\chi}_2^0$ and at larger values, the right-handed selectron and smuon become lighter than the bino. The dashed grey line at 100 GeV denotes the present experimental bound on the mass of a quasi-stable stau.

are three qualitatively different orderings of the slepton masses relative to the electro-weak gauginos. For $N_{10} = 2$ models, there is less variation in the mass spectrum, so that the primary qualitative differences are well represented by models with minimal and maximal PQ deformation.

We now introduce representative “benchmark models” which reflect this behavior. Since the Dirac and Majorana neutrino scenarios are similar, we shall focus on the latter possibility. The benchmark models we consider are:

$$\text{Maj}_{\text{LO}}^{(1)} = (N_{10} = 1, \Lambda = 50 \text{ TeV}, \Delta_{PQ} = 0 \text{ GeV}) \quad (25)$$

$$\text{Maj}_{\text{MID}}^{(1)} = (N_{10} = 1, \Lambda = 50 \text{ TeV}, \Delta_{PQ} = 140 \text{ GeV}) \quad (26)$$

$$\text{Maj}_{\text{HI}}^{(1)} = (N_{10} = 1, \Lambda = 50 \text{ TeV}, \Delta_{PQ} = 209 \text{ GeV}) \quad (27)$$

$$\text{Maj}_{\text{LO}}^{(2)} = (N_{10} = 2, \Lambda = 28 \text{ TeV}, \Delta_{PQ} = 0 \text{ GeV}) \quad (28)$$

$$\text{Maj}_{\text{HI}}^{(2)} = (N_{10} = 2, \Lambda = 28 \text{ TeV}, \Delta_{PQ} = 175 \text{ GeV}). \quad (29)$$

3.4 PQ Deformation of the Branching Fractions

Shifting the relative masses of the sparticles also changes their branching fractions. In this section we study how the PQ deformation alters the branching fractions for particles which we expect to be produced by parton collisions. This includes gluinos and squarks, as well as second neutralinos and lightest charginos.

Because the masses of the squarks are so high, the branching fractions for the squarks and gluinos are effectively constant as a function of Δ_{PQ} . By contrast, the PQ deformation has a significant effect on the non-colored sparticles, primarily because they are much lighter. To illustrate the effects of the PQ deformation, we first show the relative branching fractions of a few channels for Majorana neutrino scenarios for $N_{10} = 1$ and 2, at minimal and nearly maximal PQ deformation for the benchmark models introduced in the previous subsection. With respect to these models, we compare the dominant decay channels and branching fractions of the gluino, lightest stop, lightest chargino and second neutralino. We use SDECAY [81] to compute the branching fractions numerically.

First consider the decays of the gluino. Since the PQ deformation has only a small effect on the colored sparticles, there is only a few percent shift in the branching fractions:

Channel	$\text{Maj}_{\text{LO}}^{(1)}$	$\text{Maj}_{\text{HI}}^{(1)}$	$\text{Maj}_{\text{LO}}^{(2)}$	$\text{Maj}_{\text{HI}}^{(2)}$
$\tilde{g} \rightarrow \tilde{t}_1^\mp t^\pm$	40%	33%	22%	21%
$\tilde{g} \rightarrow \tilde{q}_R^\mp q^\pm$	27%	33%	36%	37%
$\tilde{g} \rightarrow \tilde{b}_1^\mp b^\pm$	21%	21%	16%	16%
$\tilde{g} \rightarrow \tilde{b}_2^\mp b^\pm$	10%	12%	11%	11%

(30)

where here q refers to a first or second generation squark. Here we have omitted the decays to left-handed squarks, which only become relevant for the $N_{10} = 2$ case. Note that in going from $N_{10} = 1$ to $N_{10} = 2$ messengers, there is also a shift away from decays to stops and sbottoms in favor of first and second generation squarks. Nevertheless, the large branching fraction to stops in all cases suggest the presence of a large number of four top events, which should be relatively easy to see with low integrated luminosity [82].

Next consider the branching fractions of the stop. We similarly find that there is little shift for the two values of N_{10} and as a function of Δ_{PQ} :

Channel	Maj _{LO} ⁽¹⁾	Maj _{HI} ⁽¹⁾	Maj _{LO} ⁽²⁾	Maj _{HI} ⁽²⁾
$\tilde{t}_1^+ \rightarrow \tilde{\chi}_{1,2,3,4}^0 t^\pm$	46%	47%	47%	47%
$\tilde{t}_1^+ \rightarrow \tilde{\chi}_2^+ b^-$	31%	31%	29%	28%
$\tilde{t}_1^+ \rightarrow \tilde{\chi}_1^+ b^-$	22%	23%	25%	25%

(31)

The branching fractions of the lightest chargino and second lightest neutralino exhibit stronger dependence on the PQ deformation. For example, the branching fractions of the lightest chargino are:

Channel	Maj _{LO} ⁽¹⁾	Maj _{HI} ⁽¹⁾	Maj _{LO} ⁽²⁾	Maj _{HI} ⁽²⁾
$\tilde{\chi}_1^+ \rightarrow \tilde{\tau}_1^+ \nu_\tau$	82%	23%	25%	11%
$\tilde{\chi}_1^+ \rightarrow \tilde{\chi}_1^0 W^+$	18%	3%	5%	2%
$\tilde{\chi}_1^+ \rightarrow \tilde{\nu}_l l^+$	0%	30%	29%	33%
$\tilde{\chi}_1^+ \rightarrow \tilde{\nu}_\tau \tau^+$	0%	19%	18%	19%
$\tilde{\chi}_1^+ \rightarrow \tilde{l}_L \nu_l$	0%	18%	17%	25%
$\tilde{\chi}_1^+ \rightarrow \tilde{\tau}_2^+ \nu_\tau$	0%	7%	7%	10%

(32)

where here l denotes a first or second generation lepton. Similar Δ_{PQ} and N_{10} dependence is also present in the branching fractions of the second neutralino:

Channel	Maj _{LO} ⁽¹⁾	Maj _{HI} ⁽¹⁾	Maj _{LO} ⁽²⁾	Maj _{HI} ⁽²⁾
$\tilde{\chi}_2^0 \rightarrow \tilde{\tau}_1^\pm \tau^\mp$	80%	26%	29%	12%
$\tilde{\chi}_2^0 \rightarrow \tilde{\chi}_1^0 h$	15%	3%	5%	1%
$\tilde{\chi}_2^0 \rightarrow \tilde{\chi}_1^0 Z$	2%	0%	0%	0%
$\tilde{\chi}_2^0 \rightarrow \tilde{\nu}_l^* \nu_l$ or $\tilde{\nu}_l \bar{\nu}_l$	0%	27%	26%	30%
$\tilde{\chi}_2^0 \rightarrow \tilde{l}_L^\pm l^\mp$	2%	19%	16%	28%
$\tilde{\chi}_2^0 \rightarrow \tilde{\nu}_\tau^* \nu_\tau$ or $\tilde{\nu}_\tau \bar{\nu}_\tau$	0%	17%	16%	17%
$\tilde{\chi}_2^0 \rightarrow \tilde{\tau}_2^\pm \tau^\mp$	0%	8%	7%	11%

(33)

Scanning over the Δ_{PQ} dependence of the branching fractions for the second neutralino

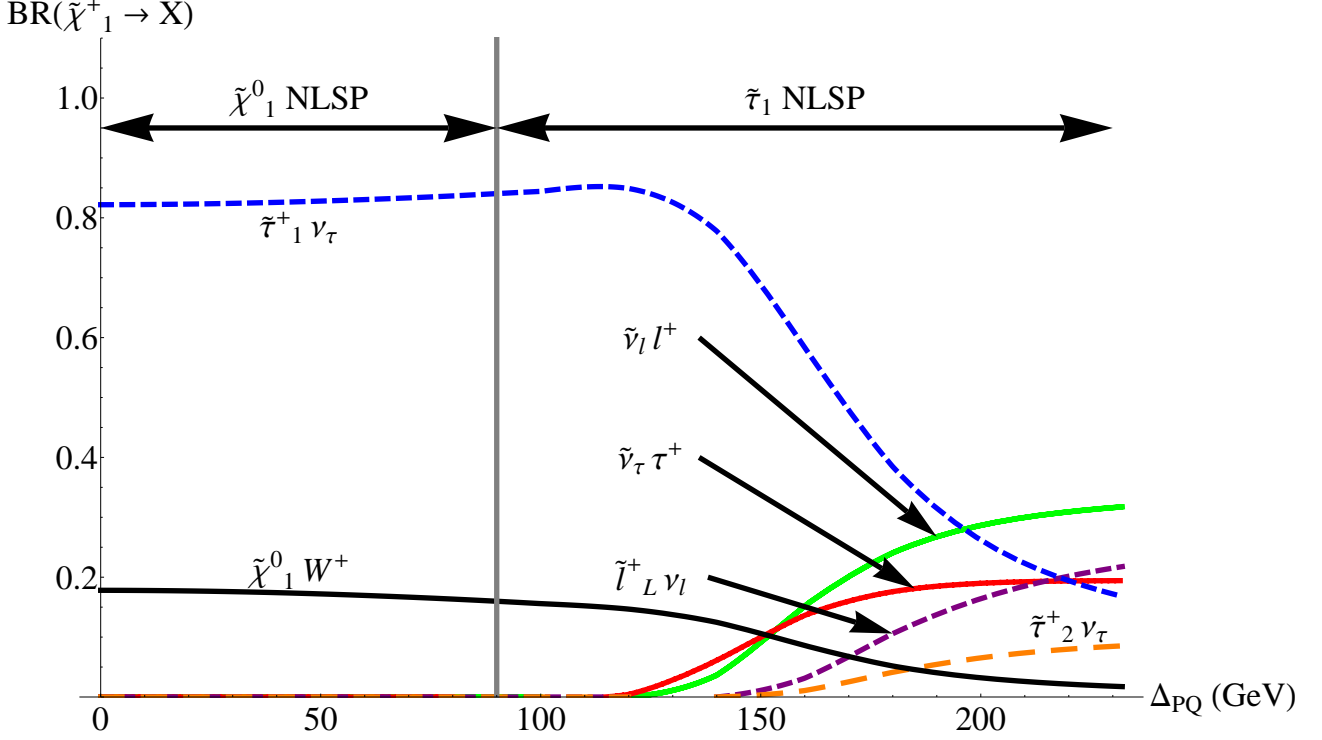


Figure 6: Dominant branching fractions of the lightest chargino as a function of Δ_{PQ} with $N_{10} = 1$ and $\Lambda = 50$ TeV. As the mass of the sneutrinos becomes lower than the chargino, additional decay channels open up.

and lightest chargino reveals that significant shifts occur for $N_{10} = 1$ F-theory GUTs when the sneutrinos become lighter than the chargino and second neutralino. Figures 6 and 7 show the respective changes in the branching fractions for the lightest chargino and second neutralino. Figures 25 and 26 in Appendix C show that for $N_{10} = 2$, there is less of a dramatic shift in the branching fractions, in accord with the fact that all sleptons are already lighter than $\tilde{\chi}_2^0$ and $\tilde{\chi}_1^\pm$.

Increasing Δ_{PQ} also increases the number of leptons present in the most likely decay chains. By inspection of all of the branching fractions, we see that as Δ_{PQ} increases, the first and second generation sleptons become light enough to become decay products for the lightest chargino and second neutralino. This decreases the branching fractions $\tilde{\chi}_2^0 \rightarrow \tilde{\tau}_1^\pm \tau^\mp$ and $\tilde{\chi}_1^+ \rightarrow \tilde{\tau}_1^+ \nu_\tau$, meaning the expected decays will tend to have additional leptons.

3.5 Right-Handed Sneutrino NLSP and Dirac Neutrinos

In the above discussion we have assumed that the NLSP corresponds to a superpartner of a Standard Model particle. This is appropriate in Majorana neutrino scenarios, where

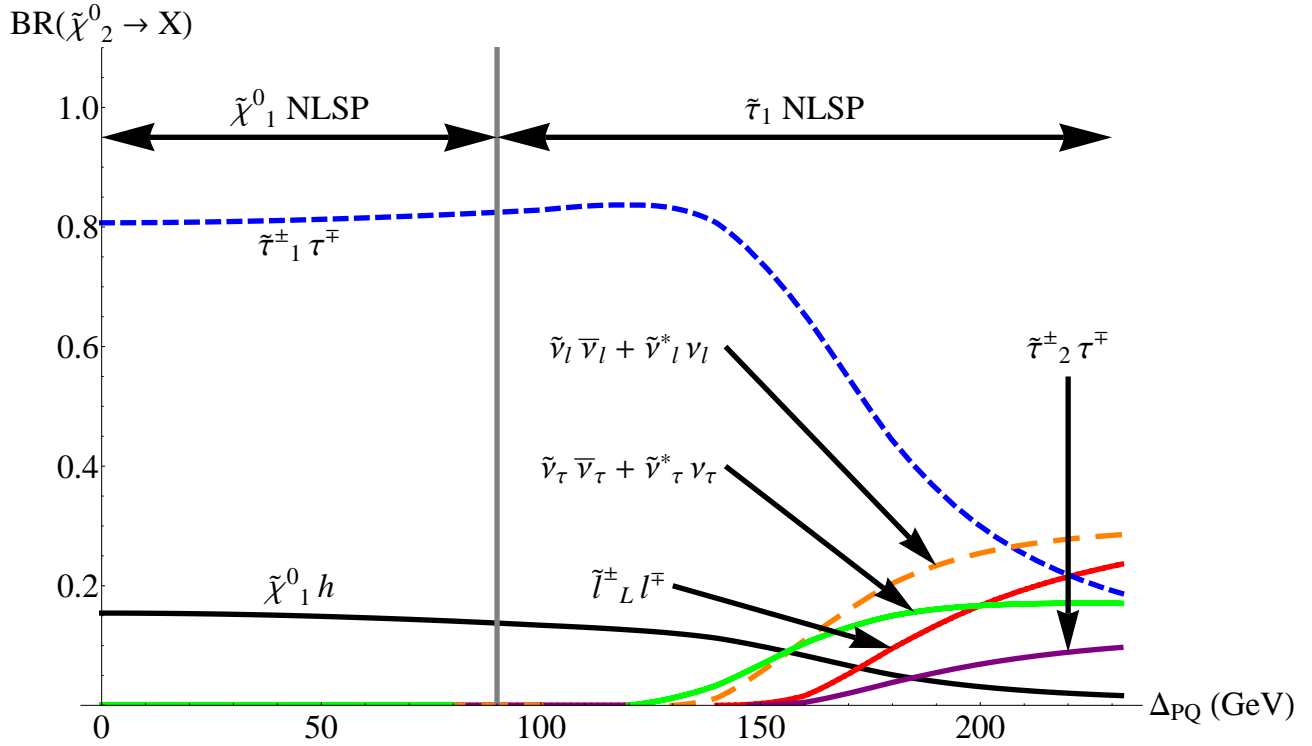


Figure 7: Dominant branching fractions of the second neutralino as a function of Δ_{PQ} with $N_{10} = 1$ and $\Lambda = 50$ TeV. As the mass of the sneutrinos becomes lower than the second neutralino, additional decay channels open up.

there are no additional light fermions beyond those already accounted for in the Standard Model. In F-theory GUT Dirac neutrino scenarios [24], however, the Dirac mass is induced through the higher-dimension operator:

$$\int d^4\theta \frac{H_d^\dagger L N_R}{\Lambda_{UV}} \rightarrow \frac{F_{H_d}^\dagger}{\Lambda_{UV}} \int d^2\theta N_L N_R \quad (34)$$

once H_d develops a supersymmetry breaking vev on the order of the weak scale. This type of F-term also induces an extremely small contribution to the mass of the right-handed sneutrino states, on the order of 0.05 eV. In certain ranges of parameter space, the $\tilde{\nu}_R$'s can correspond to the NLSP. In this case, the NNLSP is the stau or bino. Even so, this is rather inconsequential for collider phenomenology because of the highly suppressed interactions of the sneutrino with the MSSM.

First consider the contributions to the mass of the sneutrino, all of which are correlated with supersymmetry breaking. Contributions from Planck suppressed operators will generate a mass term on the order of the gravitino. Assuming this is the only contribution, this suggests the possibility that the $\tilde{\nu}_R$ could be the LSP, or at least very close in mass to the gravitino.

Typically, however, the PQ deformation will generate larger mass terms. Indeed, since N_R has PQ charge $q(N_R) = 3$, there is a positive contribution of $+3\Delta_{PQ}^2$ to the sneutrino mass squared. In the typical range of F-theory GUT parameter space where Δ_{PQ} is on the order of 100 GeV, $\tilde{\nu}_R$ is simply a heavy superpartner which is effectively decoupled from the MSSM.

In principle, contributions from a $U(1)_{B-L}$ gauge boson can also contribute to the mass of the sneutrino, though this depends on assumptions about this sector of the model. For simplicity, we shall assume in this paper that the $B - L$ gauge boson is heavier than the PQ gauge boson, but for the sake of argument, we now discuss what happens if we assume it interacts non-trivially with the supersymmetry breaking sector. Even when the $B - L$ gauge boson has similar mass to the PQ gauge boson, it will have almost no effect on the sparticle spectrum. This is because the X field is not charged under $U(1)_{B-L}$ [32], and so the analogue of the PQ deformation is necessarily suppressed by additional loops. When this gauge boson is lighter than the supersymmetry breaking scale, it can in principle induce additional contributions, much as in ordinary gauge mediation. In such scenarios, the mass of the sneutrino will then depend on the gauge coupling of $U(1)_{B-L}$. Since all of the sleptons have the same magnitude $U(1)_{B-L}$ charge, the right-handed sneutrino will have mass lower than all of the other sleptons, and in particular the stau. Note, however, that the gauginos are not charged under $U(1)_{B-L}$, so in principle either the bino or the right-handed sneutrino would in this case be the NLSP.

Nevertheless, the effects of a right-handed sneutrino NLSP are fairly inconsequential for

the purposes of a collider study since the decay rate of other sparticles to the NLSP is at most comparable to the decay to the gravitino \tilde{G} . Indeed, the decay rate for a sparticle $\tilde{\psi}$ to decay to a gravitino plus its Standard Model counterpart ψ is

$$\Gamma(\tilde{\psi} \rightarrow \tilde{G} + \psi) \sim \frac{m^5}{F^2}, \quad (35)$$

with m the mass of $\tilde{\psi}$. On the other hand, the decay channel provided by the right-handed sneutrino is suppressed by the scale Λ_{UV} , and so assuming no additional loop suppression, will lead to a decay rate on the order of:

$$\Gamma(\tilde{\psi} \rightarrow \tilde{\nu}_R + \dots) \sim \frac{m^3}{\Lambda_{UV}^2}. \quad (36)$$

In the context of an F-theory GUT where F/Λ_{UV} is also on the order of the weak scale, it follows that decays to the right-handed sneutrino are at most comparable to decays to a gravitino. This implies that the NNLSP will still be quasi-stable. By abuse of terminology, we shall therefore refer to the NNLSP in such situations as the NLSP, since there is little distinction between these possibilities for collider studies.

4 Event Generation of Long-Lived Staus

In the previous sections we found that over much of the parameter space of minimal F-theory GUTs with E_8 point unification, the stau is a quasi-stable particle on timescales probed by a collider detector. In the remainder of this paper we focus exclusively on Majorana neutrino F-theory GUT scenarios with a stau NLSP, and explore how associated stau signatures depend on the parameters of minimal F-theory GUTs. In addition to scanning over the parameters of F-theory GUTs, we also briefly comment on how the center-of-mass energy \sqrt{s} affects the expected cross sections and distributions. Since the energy scales of operation 7 TeV and 14 TeV are expected to be of particular relevance, we shall often focus on these cases.

We have performed a Monte Carlo simulation of supersymmetric event production for F-theory GUTs at the LHC using `PYTHIA` [83], with basic detector effects included for various objects (see Appendix A for more details). The mass spectra and decay information are generated using `SOFTSUSY` [78], `SDECAY` [81] and `BRIDGE` [84], and this output is passed to `PYTHIA` in Susy Les Houches Accord format [85]. In subsection 4.1, we present the expected cross sections of F-theory GUTs as a function of the parameters Λ , Δ_{PQ} , as well as the center-of-mass energy \sqrt{s} . After the initial production of a supersymmetric event, the resulting sparticles will undergo a sequence of decays so that the final state contains an even number of staus (due to R-parity) which can be accompanied by Standard Model

particles. In subsection 4.2 we explain how we shall identify staus, taking into account some crude features of detectors.

4.1 Production Cross Sections

The number of expected supersymmetric events is determined by the production cross section of supersymmetric particles generated by parton collisions. Figure 8 shows the dominant leading order cross sections of an F-theory GUT with $N_{10} = 1$ and $\Lambda \sim 50$ TeV as a function of the center-of-mass energy \sqrt{s} of the LHC. See figure 28 of Appendix C for a similar plot for $N_{10} = 2$ and $\Lambda \sim 28$ TeV F-theory GUTs. Figure 9 shows that the production of colored objects strongly increases by roughly two to three orders of magnitude in passing from $\sqrt{s} \sim 5$ TeV to $\sqrt{s} \sim 14$ TeV. This is primarily because the mass of the gluinos and squarks are all above a TeV, so that the required energy transfer from partons must be at least of the same order of magnitude. Note, however, that even for smaller values of \sqrt{s} , there is also significant production of non-colored sparticles such as lightest charginos, second neutralinos, and Drell-Yan produced lightest staus.

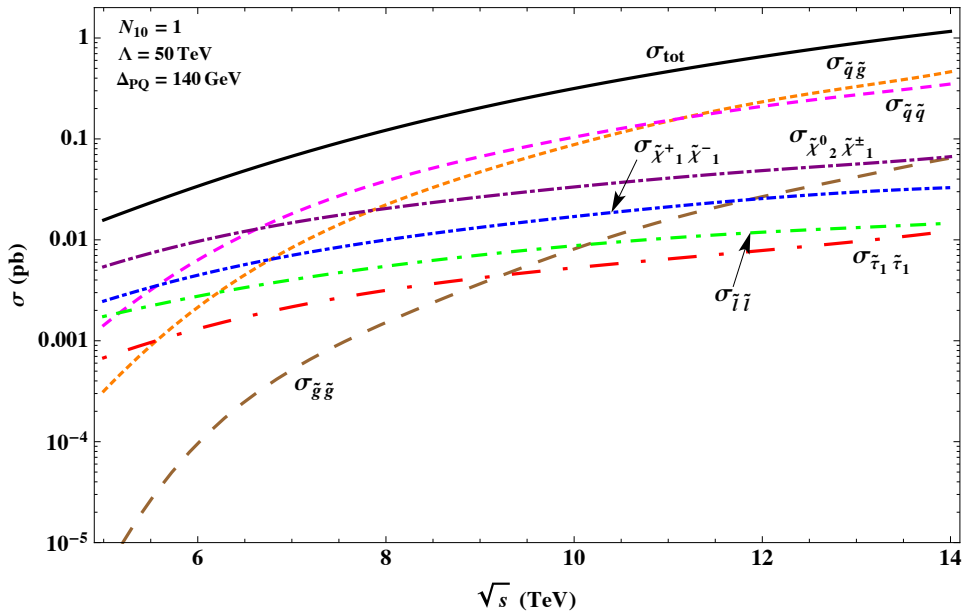


Figure 8: Plot of the leading order cross sections of various production channels as functions of center-of-mass energy \sqrt{s} for the benchmark $\text{Maj}_{\text{MID}}^{(1)}$ scenario.

As a function of Δ_{PQ} , there is little change in the cross section of most channels. This is to be expected, because the percentage change in the mass of the squarks as a function of Δ_{PQ} is small, and for the gauginos such as the gluino and lightest charginos and second neutralinos, the PQ deformation vanishes. The two notable exceptions to this are the Drell-Yan production of lightest staus and sleptons. This is because the mass of the lightest

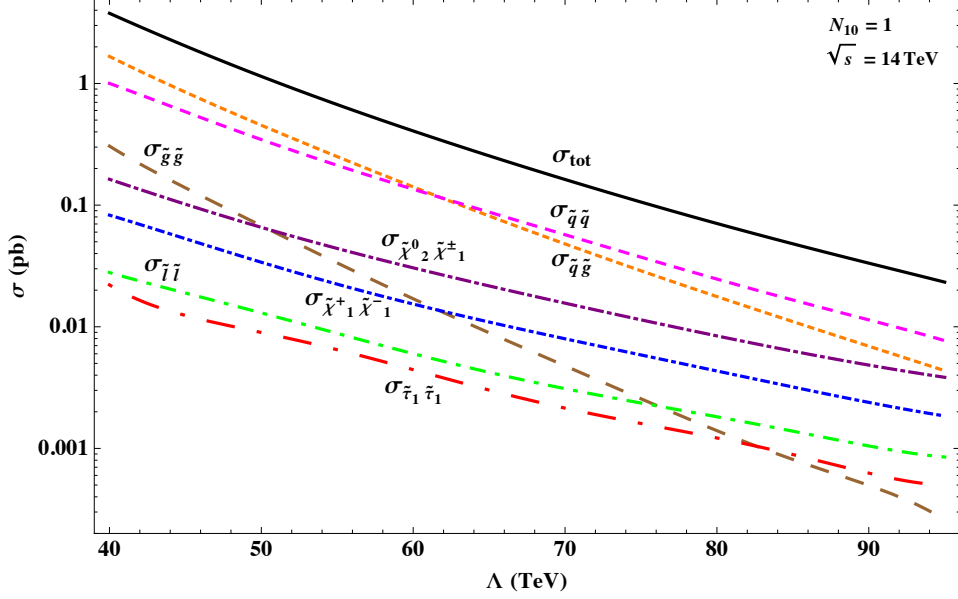


Figure 9: Plot of the leading order cross sections of various production channels for F-theory GUTs with $N_{10} = 1$ as a function of Λ with a minimal value of Δ_{PQ} such that the stau is the NLSP. Aside from Drell-Yan production of staus and sleptons, these cross sections are independent of Δ_{PQ} (see figure 10).

sleptons more strongly depends on Δ_{PQ} , which in turn alters the expected production cross section. Figure 10 illustrates that for an F-theory GUT with $N_{10} = 1$ and $\Lambda = 50$ TeV and as a function of Δ_{PQ} , Drell-Yan production of staus increases from 0.01 pb at moderate values of $\Delta_{PQ} \sim 100$ GeV to roughly an order of magnitude more at $\Delta_{PQ} \sim 200$ GeV, allowing it to become comparable to the production cross section of second neutralinos and lightest charginos. Figure 29 of Appendix C shows a similar plot for the case $N_{10} = 2$ and $\Lambda \sim 28$ TeV.

Next consider the dependence of the cross sections on the parameter Λ . In figure 9 we plot the leading order production cross sections in $N_{10} = 1$ models where a minimal value of Δ_{PQ} is chosen such that the stau is the NLSP. The production cross section for gluinos is initially larger than that of the non-colored sparticles, but then becomes smaller at larger values of Λ . See figure 29 of Appendix C for a similar plot of the case with $N_{10} = 2$ and $\Lambda = 28$ TeV for vanishing Δ_{PQ} . A related issue is that as a function of Λ , the production cross sections have different slopes. This is because the parton distribution function (pdf) for the gluons and sea quarks are different as a function of the momentum transfer fraction x . In particular, it is known that the gluon pdf significantly decreases at large x . Thus, as the sparticles increase in mass, the resulting momentum transfer from partons must be that much larger, leading to a pronounced decrease in sparticles produced from gluon collisions rather than quark collisions. At a theoretical level, increasing Λ also tends to lead to more

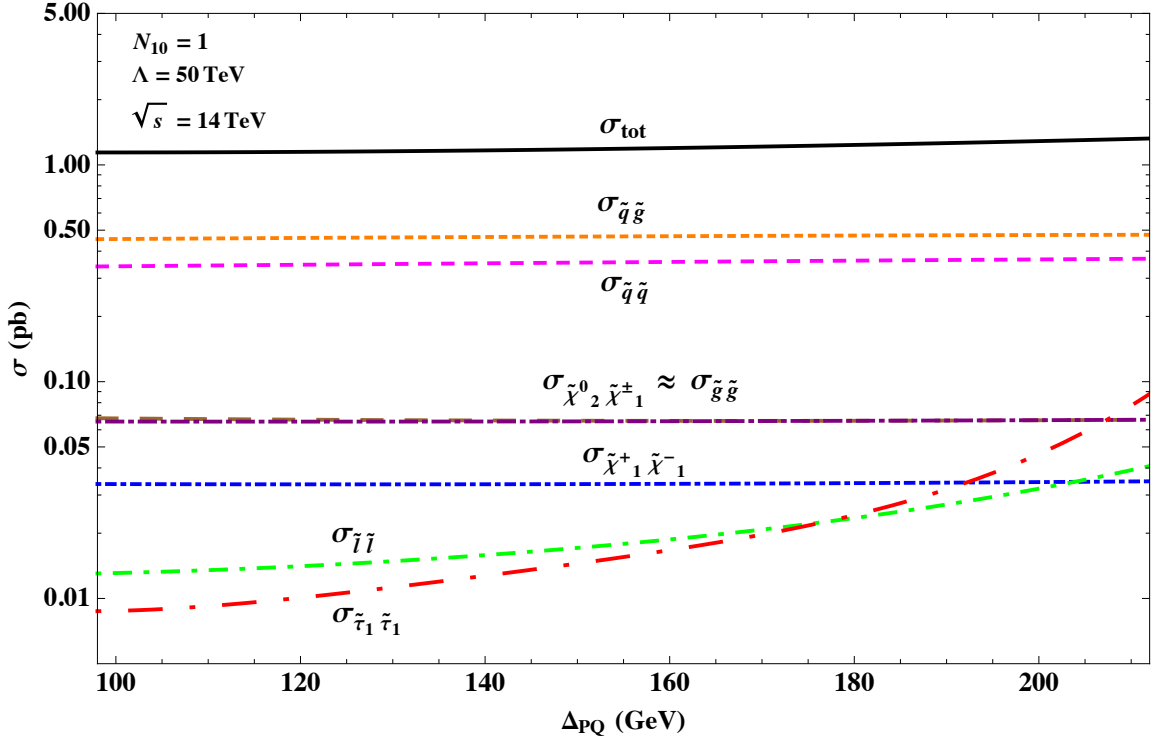


Figure 10: Plot of the leading order cross sections of the dominant production channels as functions of Δ_{PQ} for $N_{10} = 1$ and $\Lambda = 50 \text{ TeV}$.

fine-tuning in the Higgs sector. In other words, the more motivated possibility of lower Λ is also the one most accessible to the LHC, and this is the case we shall typically focus on.

4.2 Candidate Staus

After the production of a supersymmetric particle, it will undergo a sequence of cascade decays down to the quasi-stable stau NLSP. As opposed to many supersymmetric scenarios with either a quasi-stable bino or wino, which register as missing transverse energy, a stau will leave a more prominent signal, because it is electromagnetically charged.

Though a complete detector simulation is beyond the scope of the present paper, the detector resolutions σ_β and σ_p for the velocity $\beta \equiv v/c$ and momentum p of candidate staus are [60] (see also [86]):

$$\frac{\sigma_\beta}{\beta} = 0.028\beta, \quad \frac{\sigma_p}{p} = \frac{k_1 p}{\text{GeV}} \oplus k_2 \sqrt{1 + \frac{m_\tau^2}{p^2}} \oplus \frac{k_3 \text{ GeV}}{p} \quad (37)$$

where $k_1 = 0.0118\%$, $k_2 = 2\%$ and $k_3 = 89\%$. Since staus are quasi-stable, and have the same charge as muons, many will pass the level one (L1) and level 2 (L2) muon triggers, and will initially register as muons, provided they have high enough velocity. Indeed, standard data collection and reconstruction of charged tracks in the inner tracking chamber and muon detection system will record many muon events, of which some will actually correspond to staus.

The staus generated by cascade decays from heavier particles will typically have large velocities. On the other hand, nearly all muons will have large β . The Standard Model background for stau candidates mainly comes from muons whose velocity β is inaccurately measured. The typical Standard Model processes involving muons are dominantly the single boson production $W/Z + jets$, as well as top and bottom pair production $t\bar{t}$ and $b\bar{b}$. With the cut $\beta < 0.91$ on stau candidates, a rejection rate of ~ 1000 can be achieved on background muons.² In order to differentiate muons from staus, we shall therefore impose the selection cuts for candidate staus:

- $0.67 < \beta < 0.91$
- $p_T > 20 \text{ GeV}$, $|\eta| < 2.5$.

Let us comment on the selection cut for β . As already mentioned, the upper bound on β is necessary to reduce contamination from actual muons. The lower bound reflects the requirement that candidate staus which move too slowly will not be properly identified

²Using fast-moving staus is also possible, see [87] for a recent study.

with the correct bunch crossing. At the ATLAS detector, for example, the muon trigger efficiency drops rapidly for slow moving particles with velocity $\beta < 0.8$ in the barrel, and $\beta < 0.7$ in the endcap of the detector [88]. In principle, the bound $\beta > 0.67$ can be relaxed to 0.6 [88], though the detector efficiency is very low. Lowering the cut in this way requires that slow-moving staus can be reconstructed through an offline analysis using the monitored drift tube (MDT) data. In section 5 we shall discuss how inclusive stau signals depend on this lower bound. For $\beta > 0.8$, the efficiency is very close to 100%. The cuts on p_T and η are included because this is the acceptance range for the detector.

Figure 11 shows a plot of the β distribution of staus for the benchmark $\text{Maj}_{\text{MID}}^{(1)}$ scenario for 10,000 supersymmetric events at $\sqrt{s} = 7$ TeV and 14 TeV with the selection cuts on p_T and $|\eta|$ imposed. This plot illustrates that the β distribution is strongly peaked near $\beta \sim 1$, and is much lower at smaller values of β near the lower bound of 0.67. Another interesting feature of this plot is that increasing the center-of-mass energy from $\sqrt{s} = 7$ TeV to 14 TeV tends to push up the number of high β staus. This means that once the selection cut on β is imposed, the acceptance of staus will drop slightly for the 14 TeV case. Of course, this is counterbalanced by the fact that the overall number of supersymmetric events is expected to be higher at $\sqrt{s} = 14$ TeV. Said differently, because the distributions have roughly the same shape for 10,000 events each, the much higher number of supersymmetric events expected at $\sqrt{s} = 14$ TeV will increase the signal, and the discovery potential.

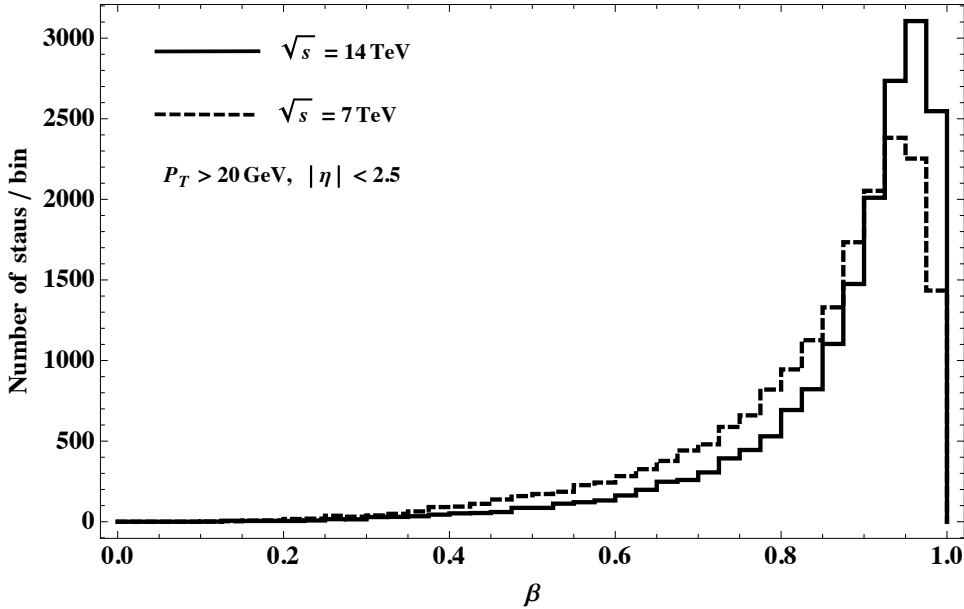


Figure 11: β distribution of candidate staus generated with 10,000 supersymmetric events for the benchmark $\text{Maj}_{\text{MID}}^{(1)}$ scenario at center-of-mass energies $\sqrt{s} = 7$ TeV and 14 TeV.

Not all staus, however, will pass the muon trigger system. For slow enough staus, the

timing of a “muon event” may not correlate with the bunch crossing of the collider beam, and will therefore not pass the initial trigger system, and must instead be detected through a dedicated offline analysis. Though the direct detection of slow-moving staus is therefore more challenging, their low velocity will allow some of them to become stopped in or near the detector, providing a means to measure additional properties of the stau. We shall return to the prospects for such stopped stau scenarios later in section 6. For this reason, in the next section we focus on scenarios where candidate staus pass the muon trigger. Indeed, because such staus are produced through the decay of heavier sparticles, a large fraction of them will have sufficiently high velocity to pass the L1 and L2 muon triggers.

5 Search Channels

We now discuss potential search channels for stau NLSP scenarios in F-theory GUTs. In many supersymmetric extensions of the Standard Model, a common signature consists of searching for cascade decays which terminate with a large missing transverse energy carried by either the LSP or quasi-stable NLSP, accompanied by some number of Standard Model states. Here, this extra energy carried by the analogous quasi-stable supersymmetric state is more visible, since all cascade decays terminate with the stau NLSP.

The characteristics of a long-lived charged particle passing through the detector would already provide a striking deviation from the Standard Model. Combined with other evidence, such as a determination of the spin of the particle, this would provide evidence in favor of a stau NLSP scenario. It is therefore important to determine how many such stau events to expect at the LHC, and how the number of events depends on the parameters of F-theory GUTs. The background from Standard Model processes is quite low in such scenarios, and is mainly due to improperly measuring the velocity of muons. We shall return to specific selection cuts which can be used in various search channels, and how these can be used to further reduce Standard Model (SM) background.

One of the most promising discovery channels for staus is based on summing over all possible candidate events in inclusive channels which contain one or two staus.³ We study how the parameters Λ and Δ_{PQ} of an F-theory GUT, as well as the parameters of the LHC such as the integrated luminosity and center-of-mass energy affect the discovery potential of finding staus at the LHC. We find that though the total cross section strongly depends on Λ , there is little dependence on Δ_{PQ} . This means in particular that such search channels can be used as a means to constrain the value of Λ . After this has been done, other search channels can then be used as a means to constrain Δ_{PQ} .

More refined information about the parameter dependence of F-theory GUTs can be

³The reason we also consider one stau events is that the other stau expected based on R-parity may not pass the selection cut imposed to differentiate staus from muons.

extracted from exclusive channels which require a specific combination of particles beyond the ubiquitous staus. Indeed, one particularly clean signature consists of just one or two staus, and nothing else. Such signatures can arise from Drell-Yan pair production of lightest staus, or alternatively lightest charginos. In the latter case, some missing energy will also be carried away by neutrinos. Since such signatures are most directly sensitive to the mass of the stau, they provide an especially clean means to track the dependence on Δ_{PQ} . Other exclusive channels with low background are based on stau events with some number of additional leptons.

Even when we cannot distinguish the stau from a muon, the corresponding events with additional leptons are difficult to mimic with Standard Model processes. Such events correspond to leptons with the same charge which we refer to as same-sign leptons, as well as events with three or more leptons.

5.1 Inclusive Stau Channels

In this subsection we discuss inclusive stau channels obtained by summing over all signals containing one or two staus. The inclusive ≥ 1 stau signal has the largest cross section and therefore provides the best channel for a discovery. Even though all supersymmetric events will contain two staus because of R-parity, imposing selection cuts used to isolate a signal will lead to some loss of signal. In particular, some two stau events may instead register as one stau events, or may not register at all. Letting σ_{tot}^{SUSY} denote the total production cross section of supersymmetric events, we define the acceptance $\epsilon_{1,2\tilde{\tau}}$ of one and two stau events as the ratio of the observed cross section of one and two stau events $\sigma_{1\tilde{\tau}}^{obs}$ and $\sigma_{2\tilde{\tau}}^{obs}$ to σ_{tot}^{SUSY} :

$$\epsilon_{i\tilde{\tau}} \equiv \frac{\sigma_{i,2\tilde{\tau}}^{obs}}{\sigma_{tot}^{SUSY}} \quad (38)$$

for $i = 1, 2$. In the remainder of this subsection, we analyze how sensitive the observed cross sections are to the choice of β cut imposed, and then discuss the sensitivity of this cross section to the parameters Λ and Δ_{PQ} . After this, we discuss the prospects for discovery in this channel after further selection cuts are imposed.

5.1.1 β_{min} and Cross Sections

As mentioned in section 4, the number of expected staus depends on the choice of selection cuts, and in particular, the lower bound β_{min} on the velocity β . To a certain extent, this lower bound depends on how well slow-moving staus can be identified by an offline analysis. To gauge how much loss of signal to expect, we compute how $\sigma_{1\tilde{\tau}}^{obs}$ and $\sigma_{2\tilde{\tau}}^{obs}$ depend on β_{min} . In figure 12 we plot this dependence for the benchmark $\text{Maj}_{\text{MID}}^{(1)}$ model, where we also show the acceptances $\epsilon_{1\tilde{\tau}}$ and $\epsilon_{2\tilde{\tau}}$. This plot illustrates that for $\sqrt{s} = 14$ TeV, the cross section

of one stau events $\sigma_{1\tilde{\tau}}^{obs}$ is always a few times larger than that for two stau events $\sigma_{2\tilde{\tau}}^{obs}$. This is primarily because a large portion of staus have velocity $\beta > 0.91$, and are therefore eliminated by the selection cut.

Figure 12 also illustrates that there is little dropoff in the value of $\sigma_{1\tilde{\tau}}^{obs}$ or $\sigma_{2\tilde{\tau}}^{obs}$ as a function of β_{min} until β_{min} becomes comparable to 0.7, which is around the value of the selection cut taken anyway. One curious feature of this plot is that in the case where $\sqrt{s} = 7$ TeV, the one stau cross section $\sigma_{1\tilde{\tau}}^{obs}$ is almost the same as $\sigma_{2\tilde{\tau}}^{obs}$ when β_{min} is small, but then increases as β_{min} increases up to ~ 0.7 . This occurs because as the cut becomes more stringent, some of the previously accepted two stau events will now be rejected, and will instead be recognized as single stau events. Comparing the total acceptance at $\sqrt{s} = 7$ TeV and 14 TeV, note that although the total cross section at 7 TeV is lower, the acceptance is higher. This is again because the stau velocity tends to be smaller at the lower center-of-mass energy, meaning that fewer events are rejected based on the selection cut $\beta < 0.91$.

5.1.2 Λ and Δ_{PQ} Dependence

Having seen that in the case of representative benchmark models that there is little change in the observed cross section as we change the lower bound on the selection cut $\beta_{min} < \beta$, we now fix the value of this cut at $\beta_{min} = 0.67$, as in section 4. In this subsection we focus on how the production cross sections depend on the F-theory GUT parameters N_{10} , Λ and Δ_{PQ} . Figure 9 shows that as we increase the parameter Λ , we find that the total production cross section σ_{tot} decreases. This is to be expected because increasing Λ also increases the mass of all of the sparticles. Indeed, even though increasing Δ_{PQ} will tend to lower the mass of the sleptons and in particular the stau, note that in such a situation, the mass splitting between the heavier sparticles and stau will become more pronounced. This in turn means that staus generated by a cascade decay will tend to be more energetic, having higher velocity, and will therefore not pass the selection cut on β as easily.

Figure 13 shows that at least for these inclusive stau signals, the dependence on the PQ deformation Δ_{PQ} is quite mild. This is mainly because the bulk of produced staus are generated from decays of colored sparticles which have masses largely independent of this deformation. If stau signals are observed, this inclusive channel can then be used as an effective means to constrain the parameter Λ , once a fit to the F-theory GUT parameters has been performed.

5.1.3 Discovering Staus

Imposing additional selection cuts on inclusive stau channels can further eliminate contamination from background muons produced through Standard Model processes, leading to a cleaner signal and a better chance of discovery. In addition to the basic cut $\beta < 0.91$

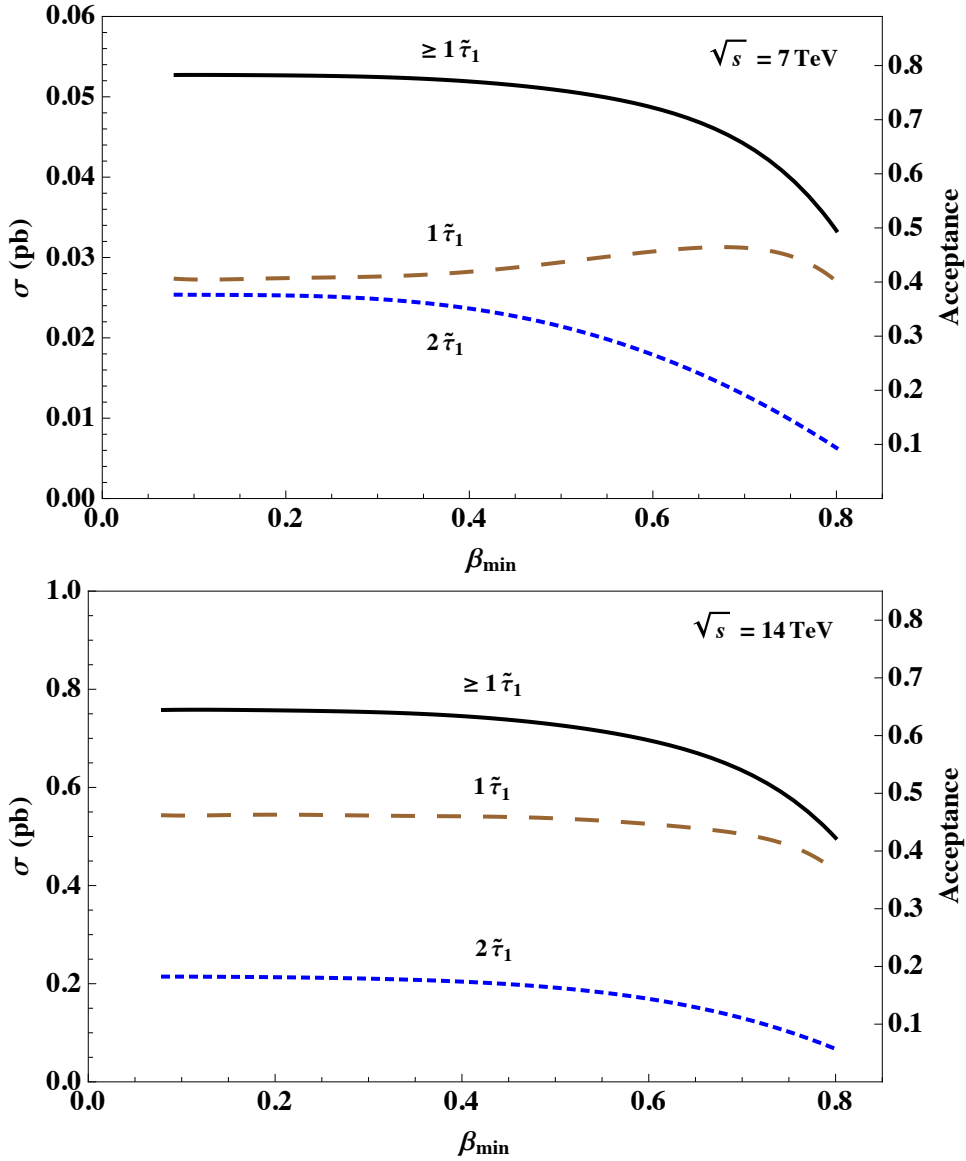


Figure 12: Observed cross sections and acceptances for events with one and two stau candidate events as functions of the lower velocity cut β_{\min} for the benchmark model $\text{Maj}_{\text{MID}}^{(1)}$ defined in subsection 3.3. The acceptance is by definition proportional to the observed cross section (see equation (38)). Also displayed is the total number of one and two stau candidate events. The upper and lower panels are for $\sqrt{s} = 7 \text{ TeV}$ and 14 TeV respectively.

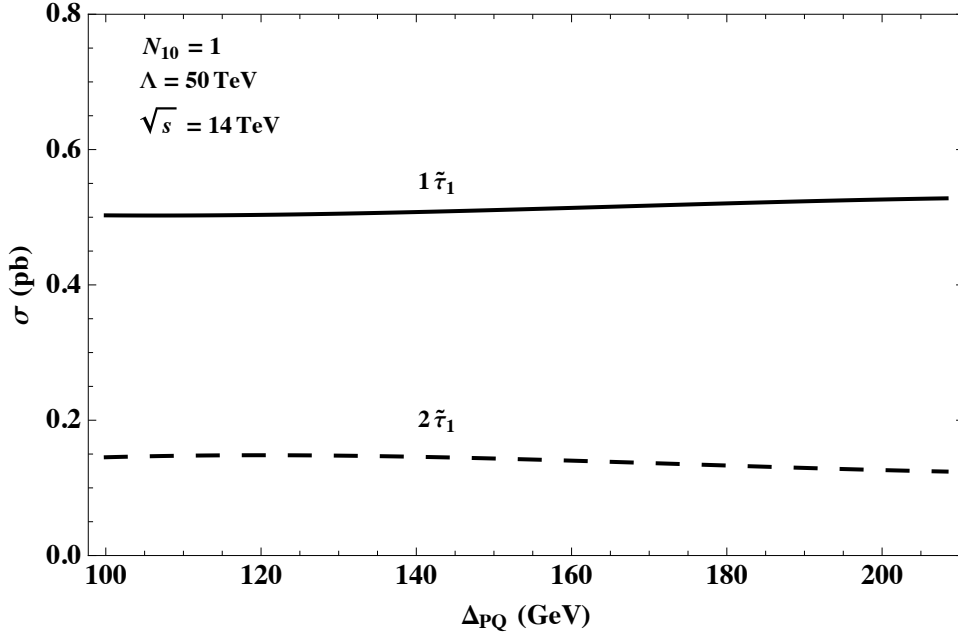


Figure 13: Plots of the observed cross sections of inclusive one and two stau signatures at $\sqrt{s} = 14$ TeV as a function of Δ_{PQ} for stau NLSP F-theory GUT scenarios with $N_{10} = 1$ and $\Lambda = 50$ TeV.

mentioned in subsection 4.2 which we use to avoid contamination from muons, we shall also include the event selection cuts in [60, 61]:⁴

- At least one hadronic jet with $p_T > 50$ GeV and a calorimetric $E_T^{miss} > 50$ GeV (trigger requirement);
- $m_{eff} > 800$ GeV,

where m_{eff} is the total invariant mass of the event constructed starting from the transverse momentum of the high p_T jets and muons (or muon-like particles)

$$m_{eff} = \sum_{i=1}^{\min(4, N_{jet})} p_T^{jet, i} + \sum_{i=1}^{\min(2, N_{\mu})} p_T^{\mu, i}. \quad (39)$$

The Standard Model background after all these cuts is estimated to be $\sigma_{SM}^{bkgn} \lesssim 1$ fb and has only a mild effect on the signal acceptance [60, 61]. Note that since this cut requires

⁴Though we do not include it here, additional discrimination from background muons can be achieved as in [60, 61] by requiring $p > m_{\tilde{\tau}_1} \frac{\beta - 0.05}{\sqrt{1 - (\beta - 0.05)^2}}$, where $m_{\tilde{\tau}_1}$ is obtained from the stau mass measurement (see section 7). This cut significantly increases the level of muon rejection, but only affects candidate stau events at the level of a few percent.

at least one hadronic jet, it will reject events generated by Drell-Yan production of staus and charginos. In practice, this means that such signals can be treated as independent constraints on the parameter space of F-theory GUTs.

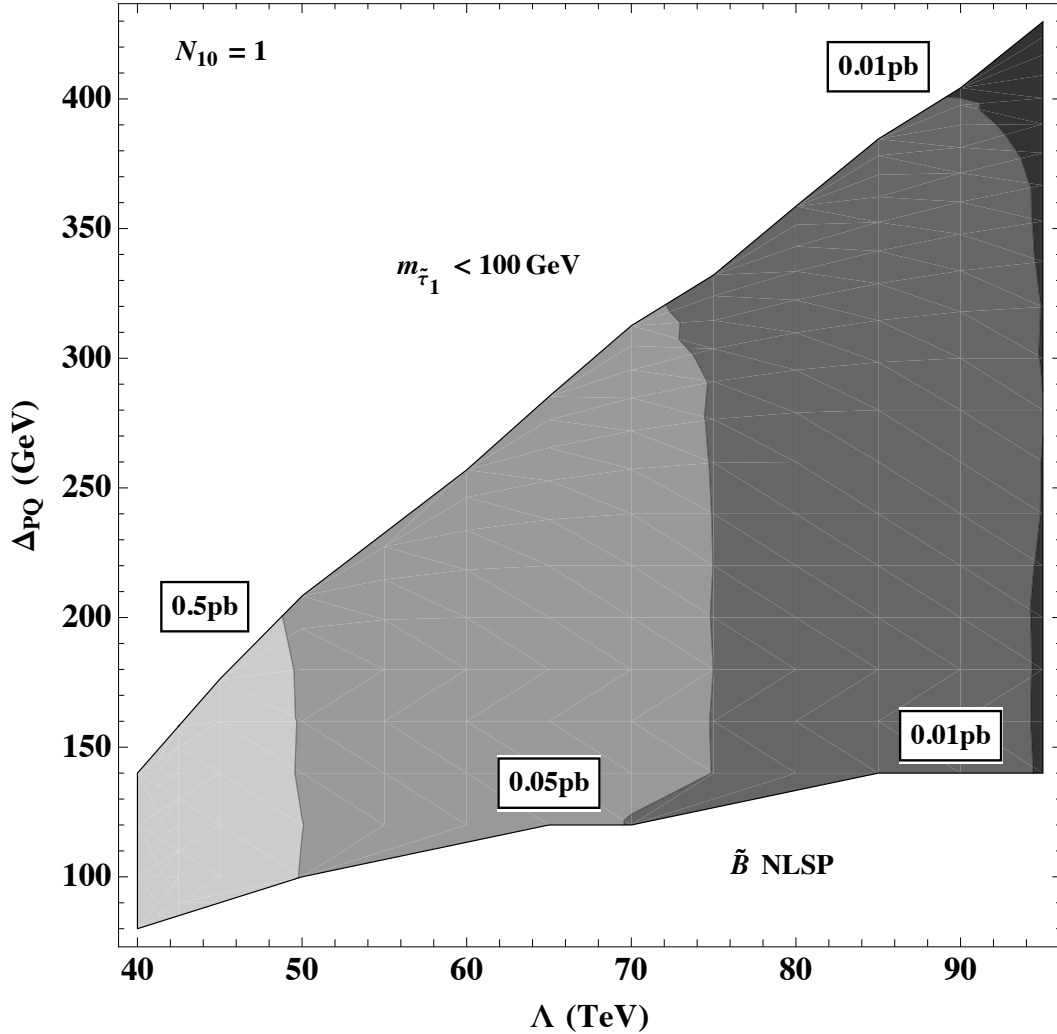


Figure 14: Contour plot of the inclusive $\geq 1\tilde{\tau}_1$ signal in parameter space Λ and Δ_{PQ} for $\sqrt{s} = 14$ TeV and $N_{10} = 1$ messengers. The three contours correspond to the value of the cross section at 0.5 pb, 0.05 pb, and 0.01 pb. To detect five inclusive one or two stau events, this amounts to an integrated luminosity of respectively 10 pb^{-1} , 100 pb^{-1} and 0.5 fb^{-1} .

The estimated upper bound of $\sigma_{SM}^{bkgnd} \lesssim 1$ fb means that even for 1 fb^{-1} of integrated luminosity, we can expect around one Standard Model event. Assuming one Standard Model event as background, a 5σ level discovery would then correspond to roughly seeing five times as many candidate stau events. To gauge the necessary integrated luminosity required to claim discovery, we have computed the inclusive cross section at $\sqrt{s} = 14$ TeV of one and two stau candidate events as a function of N_{10} , Λ , and Δ_{PQ} by imposing the

further selection cut mentioned above. In figure 14 we plot for $N_{10} = 1$ models the resulting contours for cross sections of 0.5 pb, 0.05 pb, and 0.01 pb. See figure 27 of Appendix C for the analogous plot for $N_{10} = 2$ models. To detect five inclusive one or two stau events, this amounts to an integrated luminosity of respectively 10 pb⁻¹, 100 pb⁻¹ and 0.5 fb⁻¹. Note that this in some sense overestimates the number of Standard Model background events, which upon allowing for fractions of an event for each integrated luminosity is roughly 0.01, 0.1 and 0.5.

At lower center-of-mass energies $\sqrt{s} \sim 7$ TeV, the total production cross section is smaller, so the prospects for discovery are lower. Even so, for large enough integrated luminosities, it may still be possible to discover such stau events. Indeed, returning to figures 8 and 12, we see that the total cross section of inclusive stau events at 7 TeV is lower by a factor of 10 compared with the cross section at 14 TeV, so that the required integrated luminosity for discovery is roughly a factor of 10 higher compared with what is required in the 14 TeV plots of figure 14 and figure 27 of Appendix C. For example with a few hundreds of pb⁻¹ data delivered at 7 TeV, we can expect to discover staus with $\Lambda = 50$ TeV for $N_{10} = 1$ or $\Lambda = 28$ TeV for $N_{10} = 2$. Depending on how long the LHC operates at 7 TeV, higher values of Λ may also be within reach.

5.2 Exclusive Two Stau Channel

Additional information about the parameter dependence of F-theory GUTs can also be extracted by examining more specialized channels. In particular, in subsection 5.1.3 we imposed a selection cut on inclusive stau signatures requiring at least one hadronic jet. This excludes, however, signatures such as Drell-Yan production of staus and charginos, which can lead to two opposite sign staus. In the case of Drell-Yan produced charginos, the decay of the charginos will also generate neutrinos which will leave the detector as missing energy. Because the stau mass depends strongly on Δ_{PQ} , this correlates the expected cross section with Δ_{PQ} . Moreover, with the additional information on the measured stau mass (see section 7), the stau production cross section can also be used to determine the spin of the stau [89]. Though the specifics of the event selection are different, this same channel has been used in Tevatron searches for long-lived charged particles [90, 91].

In this subsection we consider events with only two staus, and no additional (detectable) Standard Model states. More explicitly, we require there is at least one stau candidate which passes the cut on β and η introduced in subsection 4.2, and which passes the slightly more stringent cut that $p_T > 100$ GeV for any stau candidate. For candidate events in which only one stau passes this cut, we shall still require that an additional “lepton” has $p_T > 100$ GeV. To exclude the presence of final states with additional particles, we also veto events with jets satisfying $p_T > 20$ GeV and $|\eta| < 3$ and extra leptons satisfying $p_T > 5$ GeV and $|\eta| < 2.5$. To further distinguish between staus generated by Drell-Yan production of

staus and charginos, it is also helpful to impose the cut $E_T^{miss} < 10$ GeV which eliminates staus created from charginos which decay to a highly energetic neutrino plus a stau. In the following we consider exclusive two stau events with and without this cut.

We now study the dependence of the resulting exclusive two stau events as a function of Δ_{PQ} , fixing a particular representative value of $\Lambda = 50$ TeV for $N_{10} = 1$ and $\Lambda = 28$ TeV for $N_{10} = 2$ F-theory GUTs. In figure 15 we plot this dependence. First consider the case of $N_{10} = 1$ F-theory GUTs. When the further cut $E_T^{miss} < 10$ GeV is not imposed, there is a two-fold degeneracy in the expected cross section. This is because the two contributions from Drell-Yan produced staus and charginos behave differently under shifts of the PQ deformation. Whereas the PQ deformation decreases the mass of the stau, and thus leads to a monotonically increasing contribution from Drell-Yan produced staus, for Drell-Yan produced charginos, the overall production cross section of charginos is independent of Δ_{PQ} , but as seen in section 3, the subsequent branching fraction of charginos to a stau and neutrino decreases at larger Δ_{PQ} , as new decay channels become available. This has the effect of lowering the contribution to this channel. In tandem with the contribution from Drell-Yan produced staus, the net effect is to produce a small dip in the cross section as a function of Δ_{PQ} . Note, however, that once the further cut $E_T^{miss} < 10$ GeV is included, the cross section is again a monotonically increasing function of Δ_{PQ} , as expected.

Next consider the case of $N_{10} = 2$ F-theory GUT models. In section 3 we found that the change in the chargino branching fraction is much milder in such scenarios, essentially because no new decay channels open up as Δ_{PQ} is changed. As a consequence, even without imposing a further $E_T^{miss} < 10$ GeV cut, we see that the exclusive two stau channel is a monotonically increasing function of Δ_{PQ} . Imposing this cut leads to a shift of about 0.005 pb in the overall cross section, which is largely independent of Δ_{PQ} .

Since the stau is the sparticle with mass most sensitive to the PQ deformation, it is especially interesting to use the expected number of events to extract more detailed information on the PQ dependence. Imposing the further selection cut $E_T^{miss} < 10$ GeV, we note that in figure 15, the overall cross section ranges from roughly 0.005 pb at low Δ_{PQ} in the $N_{10} = 2$ scenario, to about 0.02 pb in both $N_{10} = 1$ and $N_{10} = 2$ scenarios. For 10 fb^{-1} of integrated luminosity, this translates to 50 – 200 expected events.

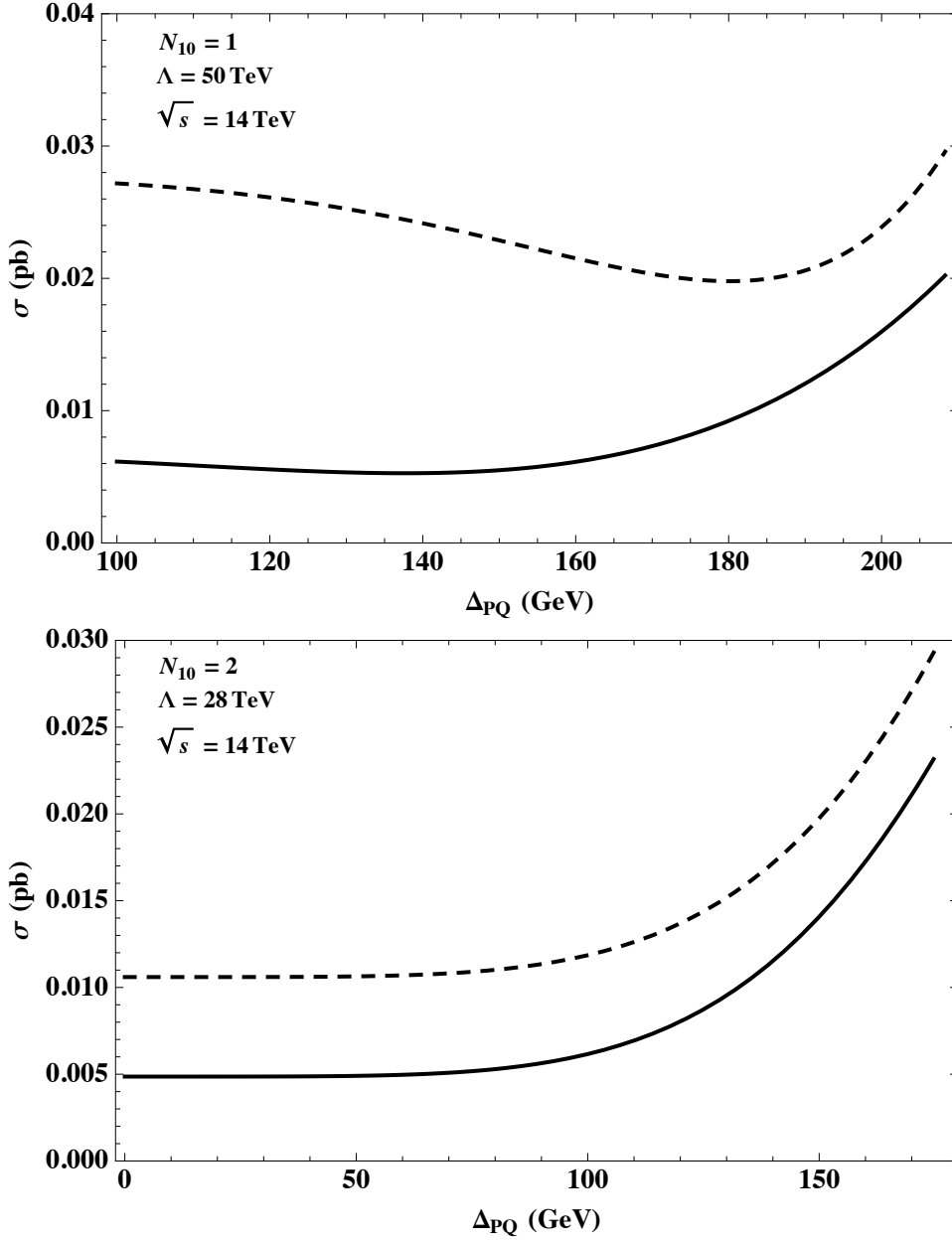


Figure 15: Cross sections of exclusive events with only two staus as functions of Δ_{PQ} in stau NLSP F-theory GUTs. The upper panel is for $N_{10} = 1$ and $\Lambda = 50$ TeV, while the lower one is for $N_{10} = 2$ and $\Lambda = 28$ TeV. The upper dashed line corresponds to the signal without a cut on E_T^{miss} , while the lower solid line corresponds to the signal with $E_T^{miss} < 10$ GeV.

5.3 Two Stau Plus Lepton(s) Channels

In this subsection we study two stau events which include one or two leptons. Such final states typically originate from the decay of the second neutralino and lightest chargino as in the decay processes:

$$\begin{aligned}
\tilde{\chi}_2^0 &\rightarrow \tilde{l}^\pm + l^\mp \rightarrow \tilde{\tau}_1^\pm + \tau^\mp + l^+ + l^-, \\
&\tilde{\nu} + \nu \rightarrow \tilde{\tau}^\pm + (\tau^\mp \text{ or } l^\mp) + 2\nu, \\
&\tilde{\tau}_1^\pm + \tau^\mp \\
\tilde{\chi}_1^+ &\rightarrow \tilde{\tau}_1^+ + \nu_\tau, \\
&\tilde{\nu}_\tau + \tau^+ \rightarrow \tilde{\tau}_1^\pm + \tau^\mp + \tau^+ + \nu
\end{aligned}$$

where as usual in collider studies, we have distinguished the somewhat different τ and other leptonic final states (l 's). τ 's which decay leptonically to e and μ will contribute isolated leptons to the final state. Given the fact that the lepton efficiency is high, the relative size of different signatures with different number of leptons encodes the information about the branching fractions of chargino and neutralino decays, and therefore can be used to probe the size of Δ_{PQ} , as well as to serve in reconstructing the mass of the second neutralino and lightest chargino, a point we shall return to in section 7.

Here we consider the following signatures:

- $2 \tilde{\tau}_1 + (\geq 1l) + 0 \text{ jet}$
- $2 \tilde{\tau}_1 + (\geq 1l)$
- $2 \tilde{\tau}_1 + (\geq 2l)$

where the $2\tilde{\tau}$ events are selected as in the previous subsection, and “0 jet” refers to events which are vetoed if they contain a jet with $p_T > 20$ GeV and $|\eta| < 3$. For these channels, the background is again suppressed by the strong stau selection cuts, as well as by requiring additional leptons. The dependence of these signals on Δ_{PQ} is shown in figure 16 for F-theory GUTs with $N_{10} = 1$ and $\Lambda = 50$ TeV, as well as $N_{10} = 2$ and $\Lambda = 28$ TeV. By inspection, we see that the inclusive stau signals with leptons and jets have large cross section as expected and increase monotonically with Δ_{PQ} .

By contrast, the stau signal with leptons but no jet has relatively small cross section. This is also expected because such signals are produced entirely by electro-weak processes, and so are not connected with the decay of a squark or gluino, which have much higher production cross sections when compared with charginos and neutralinos. In addition, note that this signal has very little dependence on Δ_{PQ} , which is to be expected because the gaugino masses are independent of Δ_{PQ} .

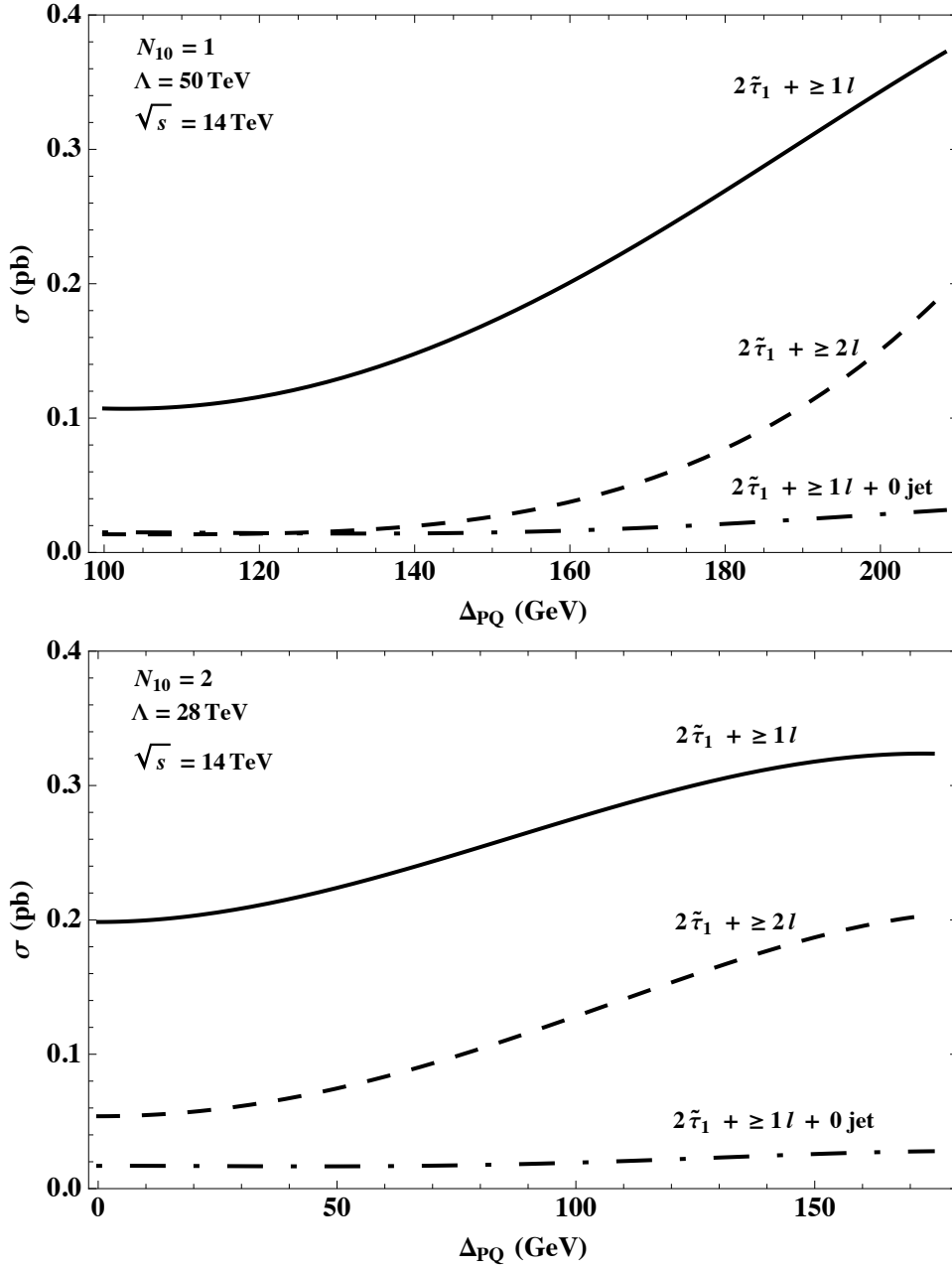


Figure 16: Plots of the cross sections of candidate events with two staus and ≥ 1 lepton + 0 jets, ≥ 1 lepton and ≥ 2 leptons as functions of Δ_{PQ} in the stau NLSP regime of F-theory GUTs with $N_{10} = 1$ and $\Lambda = 50$ TeV (upper panel) and $N_{10} = 2$ and $\Lambda = 28$ TeV (lower panel).

5.4 Inclusive Lepton Signals

In the above analysis we have focussed on signatures which aim to distinguish staus from muons. Even when such staus cannot be distinguished from muons, they can still generate signatures with low Standard Model background. Since Standard Model processes copiously produce leptons, such signatures require either the presence of multiple leptons, or specific charge combinations of leptons combined with a large p_T cut.

In this subsection we study inclusive lepton signals where we do not explicitly attempt to differentiate staus from muons. In other words, we now consider any stau as a “muon” if it satisfies:

- $\beta > 0.67$
- $p_T > 20 \text{ GeV}$, $|\eta| < 2.5$

With respect to these cuts which allow fast-moving staus, the inclusive lepton signatures we consider are:

- SS: A pair of same-sign isolated leptons.
- $3l$: Three isolated lepton candidates.
- $4l+$: Four or more isolated lepton candidates.

In order to reduce background, we also require these signal events to have:

- At least two hard leptons with $p_T > 100 \text{ GeV}$
- At least two hard jets with $p_T > 150 \text{ GeV}$.

Since staus passing the “muon” cut should always have $p_T \gtrsim 100 \text{ GeV}$, the p_T cut on the two hardest leptons only mildly affect the signals, but can significantly reduce Standard Model background. For the SS signal, the Standard Model background is negligible. For the $3l$ signal, the primary source of Standard Model background is from WZ and $t\bar{t}$ production. We reduce the WZ background by requiring that no pair of charged leptons reconstructs to an invariant mass $m_Z \pm 10 \text{ GeV}$. The $t\bar{t}$ background is potentially large if the muon from a b quark decay is isolated. To suppress it, we require two hard leptons with $p_T > 100 \text{ GeV}$ to reduce the acceptance of leptons from W decay, and additionally require two hard jets with $p_T > 150 \text{ GeV}$. Alternatively, if one is interested in the signal from electro-weakino or slepton productions, one can also use a jet veto to suppress the $t\bar{t}$ background, which we will not discuss here. For the $4l+$ signal, the Standard Model background is pre-dominantly from ZZ production. We reduce this background using the same type of cut as in the $3l$ signal.

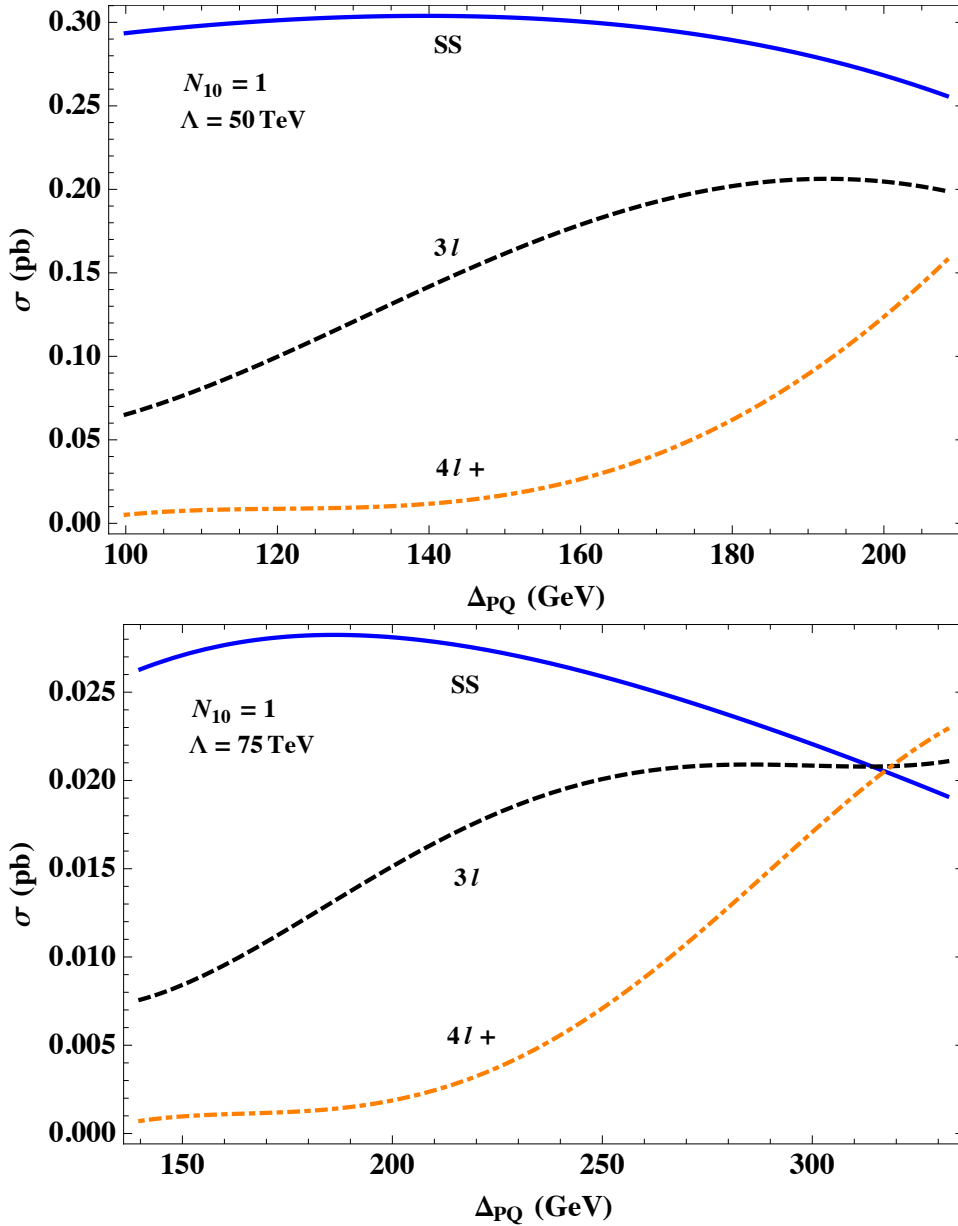


Figure 17: Plots of the cross sections of inclusive lepton events in which fast-moving staus are identified as leptons for two F-theory GUT scenarios with $N_{10} = 1$ at $\Lambda = 50$ TeV (upper panel) and $\Lambda = 75$ TeV (lower panel). The same-sign lepton (SS) tri-lepton ($3l$) and at least four lepton ($4l+$) signals respectively correspond to roughly increasing and decreasing functions of Δ_{PQ} .

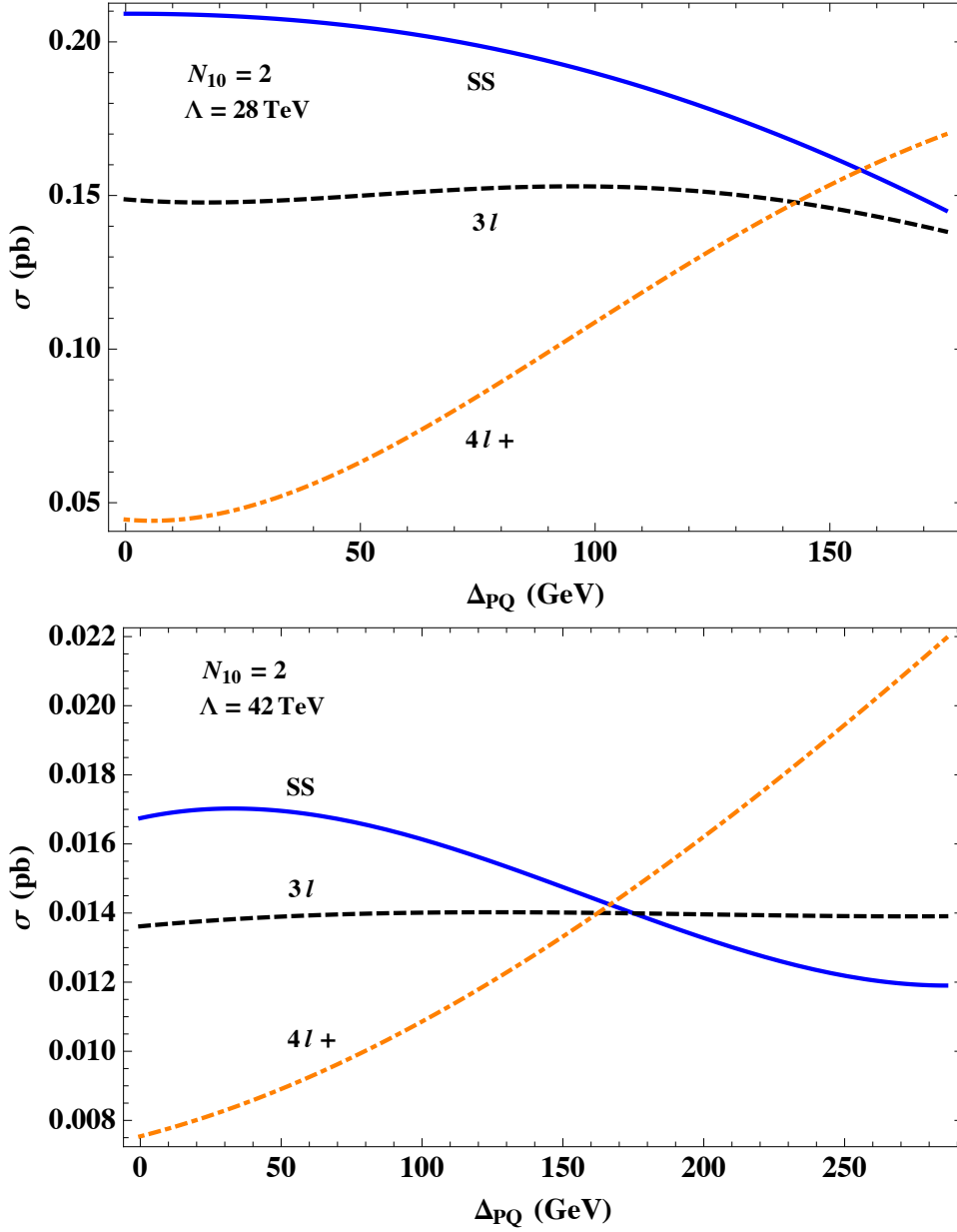


Figure 18: Plots of the cross sections of inclusive lepton events in which fast-moving staus are identified as leptons for two F-theory GUT scenarios with $N_{10} = 2$ at $\Lambda = 28$ TeV (upper panel) and $\Lambda = 42$ TeV (lower panel). The same-sign lepton (SS) tri-lepton ($3l$) and at least four lepton ($4l+$) signals respectively correspond to roughly increasing, constant, and decreasing functions of Δ_{PQ} .

Let us now discuss the primary origin of these signatures and our theoretical expectations for the corresponding dependence on the PQ deformation. For the same-sign (SS) isolated lepton signal, gluinos and squarks can decay to pairs of same sign lightest charginos $\tilde{\chi}_1^\pm \tilde{\chi}_1^\pm$ and pairs of second lightest neutralinos $\tilde{\chi}_2^0 \tilde{\chi}_2^0$. The subsequent decay of the lightest chargino for example via $\tilde{\chi}_1^\pm \rightarrow \tilde{\tau}_1^\pm + \nu_\tau$ and the second neutralino for example via $\tilde{\chi}_2^0 \rightarrow \tilde{\tau}_1^\pm + \tau^\mp$ with the τ decaying hadronically, will generate SS lepton signals.

As can be seen from figures 17 and 18, the SS signal is roughly a decreasing function of Δ_{PQ} . To see how this comes about, note that in the case of same sign staus generated by lightest chargino and second neutralino decays, as Δ_{PQ} increases, the branching fraction to states without additional charged leptons decreases. Note that increasing the value of Δ_{PQ} simply diverts these decays through channels which generate additional charged leptons in the final state.

Tri-lepton ($3l$) and four or more lepton ($4l+$) signatures correspond to processes involving two fast-moving staus, as well as additional e or μ leptons, and can be generated in a variety of different cascade decays. For example, focussing on the contribution from a single branch of a cascade decay, the $3l$ signal can be generated by decays involving $\tilde{\chi}_1^+ \rightarrow \tilde{l} + \nu$, $\tilde{\chi}_1^+ \rightarrow \tilde{\nu} + l$, $\tilde{\chi}_2^0 \rightarrow \tilde{\tau}_1^\pm + \tau^\mp$ or other channels where $\tilde{\chi}_2^0$ decays to a stau and some taus. Note that we can get contributions to the $3l$ and $4l+$ signatures depending on whether the taus in the final state decay hadronically or leptonically. Figure 17 shows that for $N_{10} = 1$, both of these signals are roughly increasing functions of Δ_{PQ} . As Δ_{PQ} increases, the masses of \tilde{e}_L , $\tilde{\mu}_L$, $\tilde{\tau}_2$, $\tilde{\nu}_e$, $\tilde{\nu}_\mu$ and $\tilde{\nu}_\tau$ decrease and eventually drop below the mass of $\tilde{\chi}_2^0$ and $\tilde{\chi}_1^\pm$, while \tilde{e}_R and $\tilde{\mu}_R$ both become lighter than $\tilde{\chi}_1^0$.⁵ Consequently, the branching ratios of $\tilde{\chi}_2^0$ and $\tilde{\chi}_1^\pm$ into these states increases. Since these states typically decay to $\tilde{\tau}_1$ with additional leptons, the increase of Δ_{PQ} also increases the $3l$ and $4l+$ signals.

In the case of $N_{10} = 2$ models, figure 18 shows that the $3l$ signal is roughly constant, while the increase in $4l+$ signatures becomes more prominent than for $N_{10} = 1$. The difference in the $N_{10} = 1$ and $N_{10} = 2$ cases is due to a subtle tradeoff in the increase and decrease of the branching fractions of heavier sparticle states. For example, the branching fraction of $\tilde{\chi}_1^+$'s via $\tilde{\chi}_1^+ \rightarrow \tilde{l} + \nu$ increases as Δ_{PQ} increases, while the branching fraction of $\tilde{\chi}_2^0 \rightarrow \tilde{\tau}_1^\pm + \tau^\mp$ decreases. For $N_{10} = 1$, the net contribution from these effects leads to an increase in the overall number of $3l$ signals, while for $N_{10} = 2$, the positive and negative contributions to this branching fraction more exactly balance out, leading to a constant Δ_{PQ} dependence.

⁵Note that in the case of $N_{10} = 2$ F-theory GUTs, this statement already holds for vanishing PQ deformation.

6 Stopped Staus

Up to this point, we have treated the stau NLSP as stable on timescales probed by colliders. In this section we study the prospects for F-theory GUT stau NLSPs to become stopped in or near the detector, and to decay at some later time to a tau and a gravitino. Searching for stopped staus through their decay products would provide additional evidence that the quasi-stable massive charged particle is in fact a stau. When the origin of the stopped stau can be reconstructed, observing its decay would provide a measurement of its lifetime, and consequently the scale of supersymmetry breaking [86, 92–95].

An analysis including all details of the ATLAS and CMS detectors, and in particular the ways that they are situated in their respective caverns is beyond the scope of the present paper. To extract the main physical features of stopped stau scenarios, we consider an idealization where after the initial production of staus, these particles enter a large spherical ball of either iron or carbon. Using the overall production cross section of staus as well as the associated velocity distribution obtained in section 4, we simulate 100 fb^{-1} of LHC data and compute the total number of stopped staus $N(R)$ contained within a distance R from the collision point. Here we focus on candidate staus with $p_T > 20 \text{ GeV}$ and $|\eta| < 2.5$. As expected, we see that integrating over an ever larger ball leads to more stopped staus. Though small, the number of such stopped staus is not completely negligible. In figure 19 we show a plot of $N(R)$ for stopping in iron and carbon for the $\text{Maj}_{\text{MID}}^{(1)}$ scenario. In this plot, we see that the expected number of stopped stau events is on the order of a few thousand after passing through ~ 5 meters of either iron or carbon. More generally, increasing Λ tends to decrease the total production cross section of staus, and thus the total number of staus which could become stopped.

The effects of the PQ deformation on the number of stopped staus is more subtle. Fixing the mass of the other sparticles while lowering the mass of the stau will cause the staus which are produced through a decay chain to be more energetic, which in turn skews the velocity distribution to faster moving staus. Though this does reduce the total number of slow-moving staus, the stopping length of the stau depends linearly on its mass. In other words, though there are fewer slow-moving staus, they are more easily stopped. We find that when both effects are taken into account, the effective number of stopped staus at a given distance from the collision point increases as the stau mass decreases. For example, comparing the benchmark $\text{Maj}_{\text{MID}}^{(1)}$ scenario with $\Delta_{PQ} = 140 \text{ GeV}$ to the benchmark $\text{Maj}_{\text{HI}}^{(1)}$ scenario with $\Delta_{PQ} = 209 \text{ GeV}$, we find the number of stopped staus at a given distance is larger in the $\text{Maj}_{\text{HI}}^{(1)}$ model by a factor of ~ 1.3 .

We now discuss how such stopped staus could in practice be observed. First consider the case of staus stuck in the rock surrounding the detector. In this case, a full reconstruction of the timing of the stau decay with that of the initial production can likely not be achieved, but the observation of the decay product, given by a leptonically decaying tau could still

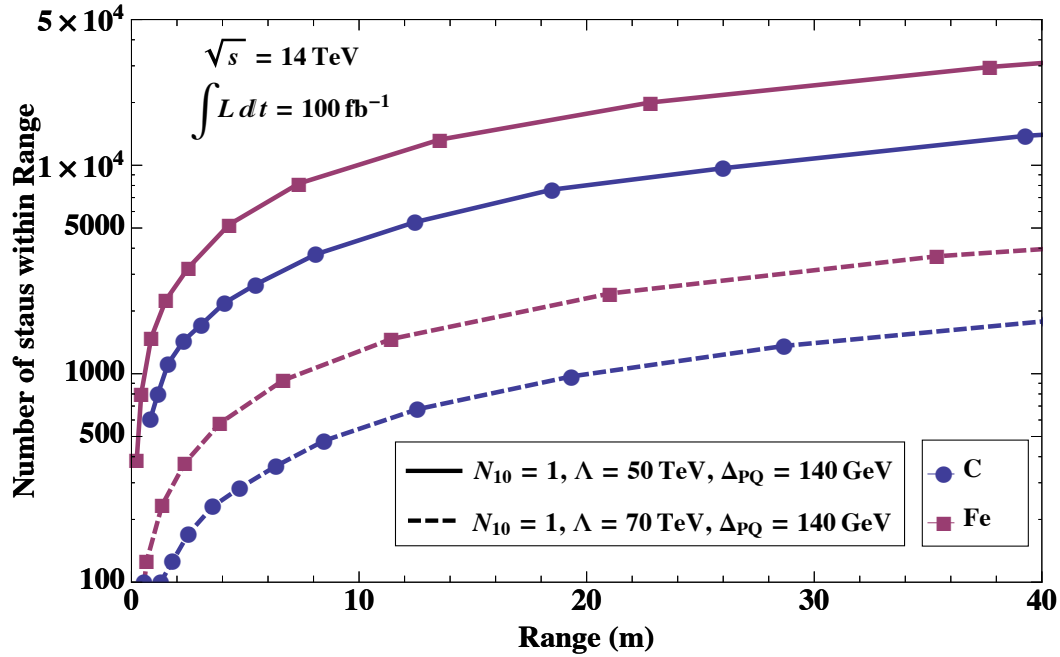


Figure 19: Plot of the number of stopped staus expected from 100 fb^{-1} of simulated LHC data in two F-theory GUT scenarios as a function of distance from the collision point in an idealization where surrounding the collision point there is a large ball of either carbon (C) or iron (Fe). As we integrate over larger distances, the number of stopped staus necessarily increases.

be observed. The decay of a tau to a muon can be measured by the muon chamber, and in some cases also the inner tracking chamber.

The primary source of Standard Model background for such muon events is from cosmic rays. Such cosmic rays enter from the sky above, and so will correspond to muons passing *downwards* through the detector. By contrast, there are no cosmic rays passing through the other side of the Earth, so that contamination from *upwards* moving cosmic rays will be negligible. Hence, we focus on the prospects for detecting upwards moving muons from stau decays. The number of such upward moving muons is estimated to be $\sim 0.7\%$ of the total number of stopped staus [86]. Assuming the number of stopped staus can be estimated by the number of staus with $\beta < 0.5$, we can expect $\mathcal{O}(50)$ events in the benchmark $\text{Maj}_{\text{MID}}^{(1)}$ scenario. We note that this is an order of magnitude estimate, and should be improved with a more realistic simulation.

Even for upwards moving muons, however, there is still a non-negligible background from atmospheric neutrinos which pass through the Earth. When these neutrinos (and anti-neutrinos) strike nuclei underneath the detector, they can generate a conversion $\nu \rightarrow \mu$, with roughly equal likelihood for generating μ^+ and μ^- . Using the results of the MACRO experiment [96], the number of such upward-going muons passing through a $20\text{m} \times 20\text{m}$ detector is expected to be ~ 80 events/year. Using the same selection cuts on upward passing muons as in [96], it was found there that the muon energy distribution from this background has a broad peak around 50 GeV. The kinematic upper bound on the energy of a muon generated by the decay $\tilde{\tau}_1 \rightarrow \tilde{G}\nu_\tau\nu_\mu\mu$ will have energy $E_\mu < m_{\tilde{\tau}_1}/2 \sim 50 - 100$ GeV, which is itself on the tail of the distribution of this three-body process. This means that of the roughly 80 background muons, less than half actually constitute background for stau decays. Further, though this background is not completely negligible, the signal can still be statistically significant if the velocity and direction of the background is reliably calculated. In addition, the tracking information of a stau event can be helpful in identifying these events [86]. This is because the momentum and the direction of the slow-moving staus can be recorded during their escape from the detector. This information can be used to infer the trajectory along which a slow-moving stau could be stopped. Looking for muons coming from a particular direction, this would provide a means to significantly reduce the background of such events.

Staus can also become stuck in the detector. For tau leptons which decay hadronically, the optimal location for a stau to be stopped would be in the hadronic calorimeter of either the ATLAS or CMS detector. This type of search is similar in spirit to looking for stopped gluinos in split supersymmetry models [97]. From figure 19 we see there are ~ 3000 (resp. 5000) staus stopped in 2 meters (resp. 4 meters) of iron out from the collision point for the low Λ model. This implies that a similar number of staus should be stopped in the calorimeter. Let us first consider the case that those staus stopped inside

the hadronic calorimeter (HCAL) decay hadronically via the tau decay product of the stau. This possibility is interesting since the tau jet is typically narrow, and therefore can deposit all its energy in one or very few calorimeter cells. For a 200 GeV mass stau, the tau jet will have energy ~ 100 GeV. In this case, the hadronic calorimeter would light up, but no track would be seen in the tracking chamber, and no energy would be deposited in the electromagnetic calorimeter (ECAL). This is in contrast to QCD jets which would leave tracks as well as have energy deposited in both the ECAL and HCAL. This would seem to indicate that QCD background can be reduced significantly. Even so, given the large number of QCD events, any leakage to the signal could be dangerous, which must be studied in detail separately. Cosmic rays are another potential source of background. However, most of the cosmic rays are muons and can be detected in the muon chamber. If they are neutral particles, they are likely to be stopped by the outer material of the detector. Stopped staus stuck in the HCAL can also decay into muons, although the chances are smaller at around 10%. If the muon goes outward from the hadronic calorimeter, the muon can only be detected in the muon chamber when there is no activity in other parts of the detector. Standard Model objects cannot mimic this type of process, and so hardware fluctuations or malfunctions would appear to provide the main source of background.

Stopped staus can in principle also be used to deduce the scale of supersymmetry breaking [86, 93–95]. Recall that the decay rate of the stau NLSP to a gravitino and tau $\Gamma_{\tilde{\tau}_1}$ is given in terms of the scale of supersymmetry breaking $\sqrt{F_0}$ felt by the gravitino and the mass of the stau through the relation (see for example [74]):

$$\Gamma_{\tilde{\tau}_1} = \left(\frac{m_{\tilde{\tau}_1}}{100 \text{ GeV}} \right)^5 \left(\frac{100 \text{ TeV}}{\sqrt{F_0}} \right)^4 \cdot (2 \times 10^{-3} \text{ eV}). \quad (40)$$

Measuring the scale $\sqrt{F_0}$ would then allow us to also determine the mass of the gravitino. Let us note that although here we have distinguished between $\sqrt{F_0}$ and the scale of supersymmetry breaking \sqrt{F} felt by the messengers, in the context of F-theory GUTs it is most natural to set $F = F_0$. In F-theory GUTs, $F \sim 10^{17} \text{ GeV}^2$, and the lifetime of the NLSP is on the order of one second to an hour [12].

Methods to measure the lifetime of the stopped stau typically rely on being able to transport the material in which the stau is stopped to a remote location, where its decay can then be carefully studied. For example, in [93, 95] it was proposed that a “stopper detector” be added which could surround the ordinary detector, and in [94] it was proposed to use a large water tank as a collector for stopped staus. Staus which become lodged in the neighboring cavern rock could in principle also be removed [86]. Both methods work best for staus which are stable on the order of at least a day to a week. In the context of F-theory GUTs, however, where the stau lifetime is far less than a day, such detection methods do not appear as practical. Other methods have been proposed for detecting quasi-stable staus

which decay on shorter timescales, as for example in [98].⁶ For example, in the related context of stopped gluino scenarios [97], it was proposed that if a pair of gluinos become stopped in the detector or neighboring cavern, correlating the time separation between the decays of these pairs would then provide another means to extract the lifetime, and could in principle be adapted to the case of stopped stau scenarios.

Though a full study is beyond the scope of the present paper, we now speculate on potential ways to measure the lifetime of staus in the context of F-theory GUTs. The primary challenge in extracting the lifetime of the stau stems from correlating the initial production of the stau with its final decay. Although staus typically decay out of time with the bunch crossing of the original production event, the information on the stau (for example information of tracking and energy deposit in both the HCAL and ECAL) may already be recorded in the data if the production event is hard enough (e.g. with hard jets or leptons) to be triggered on. In fortuitous circumstances, the direction and velocity of the stau could then be reconstructed from an off-line analysis from the energy deposit dE/dx in the calorimeters and monitored drift tube data for staus stopped in the muon chamber. In such cases, it would then be possible to deduce where such a stau would possibly be stopped. For example, if the stau stopped in the middle of the CMS muon chamber⁷, the tracking apparatus would detect a muon track traversing and then ending in some section of the muon chamber, and it would become possible to estimate the position of the candidate stopped stau. If at some later time a muon was emitted in the vicinity of the stopped stau, and provided there is no other activity in that part of the detector, this would likely correspond to a signal for a stopped stau. The time difference between the decay event and production event would then provide a measure of the lifetime of the long-lived stau. For staus stuck in the HCAL a similar type of correlation analysis may also be available. Given the tantalizing prospect of obtaining direct access to the scale of supersymmetry breaking, it would seem important to investigate this issue further.

7 Mass Spectra and Distinguishing Look-Alikes

Our focus in much of this paper has been on signatures of stau NLSP F-theory GUTs. Assuming evidence has been found for such a scenario, it is important to study what classes of models reproduce the same observables. This broader question based on the LHC

⁶Though not the case studied here, for staus which decay with an average time of $10^{-8} - 10^{-5}$ seconds, it is possible to exploit the fact that there is a distribution of timescales for the decay of the stau, so that some staus will decay inside the detector [60]. For F-theory GUTs, this method is not available because the stau has a lifetime of one second to an hour.

⁷Compared to ATLAS, the CMS muon tracking system has a far higher density of iron, making it much more likely that a stau can become trapped there. We thank members of the CMS group for discussions on this point.

inverse problem has been studied from different vantagepoints for example in [99, 100]. One approach to this problem is based on the general footprint method [101, 102], which directly compares the collider observables of different classes of models to determine possible differences. This method has been applied to F-theory GUT models with a bino NLSP in [12] to compare particular classes of well-motivated supersymmetry breaking scenarios.

In this section we consider a simplified version of this problem by studying possible degeneracies in the mass spectrum of F-theory GUTs with other models with an MSSM-like spectrum. More precisely, we study how mass measurements extracted from stau NLSP scenarios can be used to distinguish between F-theory GUTs and minimal gauge mediated supersymmetry breaking (mGMSB) models. To this end, we first review how to extract details of the sparticle mass spectrum in stau NLSP scenarios which are similar to F-theory GUTs. Next, we use the high precision of these mass measurements as a means to distinguish between F-theory GUTs and mGMSB models.

7.1 Mass Reconstruction with Staus

Following [62] and [63], we now discuss how quasi-stable stau scenarios allow one to deduce much of the sparticle mass spectrum. We can extract the mass of the stau through the relation:

$$m_{\tilde{\tau}_1} = \frac{p}{\beta\gamma} \quad (41)$$

where β is measured with the time-of-flight in the precision muon chambers, and p is reconstructed through a measurement of p_T and η [88]. Due to the uncertainty in the measurement of p and β , the reconstructed mass distribution will show a broadening around the correct mass. From the resolution of p given in equation (37) of section 4, we see that the uncertainty in p is proportional to p^2 for large stau momentum. This illustrates that the mass reconstruction is more accurate at low momenta and velocities. Since the relative number of low velocity staus is lower compared with the number of high velocity staus, increasing the total number of such events requires a relatively large integrated luminosity. It was shown in [62] that the stau mass can be determined up to an uncertainty of ~ 0.02 GeV using 30 fb^{-1} of integrated luminosity.

Reasonable estimates of the stau mass can also be obtained for lower integrated luminosity. For example, at $\sqrt{s} = 14 \text{ TeV}$ and $\sim 500 \text{ pb}^{-1}$ of simulated LHC data, figure 8 of section 4 illustrates that for the $\text{Maj}_{\text{MID}}^{(1)}$ benchmark model, the total cross section for supersymmetric production of events is $\sim 1 \text{ pb}$, indicating there will be about 500 supersymmetric events with staus. In this case, we find that the best fit of the stau mass is $m_{\tilde{\tau}}^{\text{fit}} = 175.59 \pm 0.47 \text{ GeV}$ using a Gaussian fit (see figure 20). In the analysis, we selected staus with velocity $0.6 < \beta < 0.91$. With 100 pb^{-1} data, we find only 69 event stau candidates remain, but the fit of the stau mass is almost as good as the previous case, with the

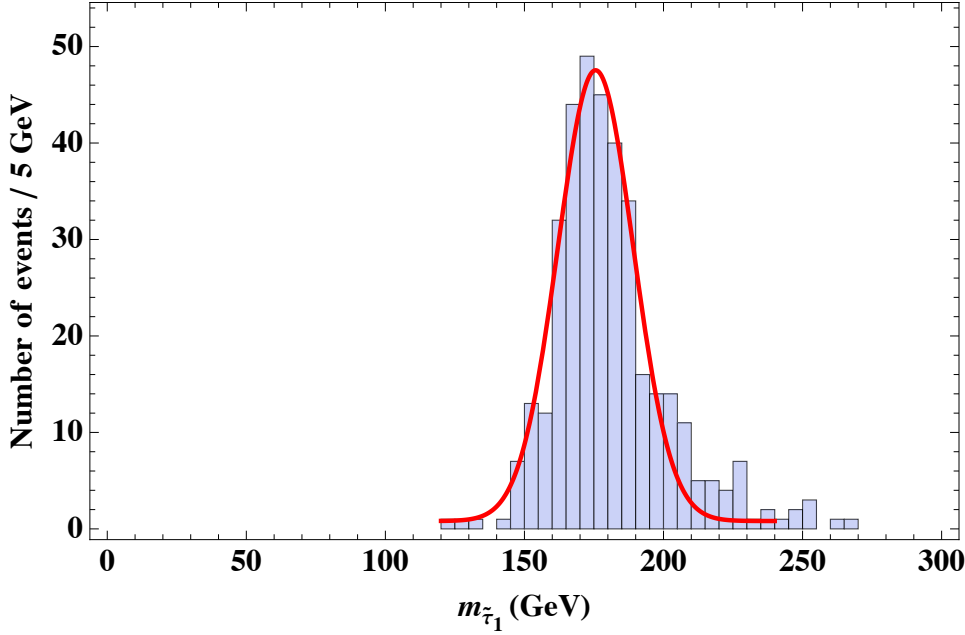


Figure 20: Distribution of the reconstructed stau mass for the benchmark model $\text{Maj}_{\text{MID}}^{(1)}$ defined in subsection 3.3. 500 events are generated and staus are selected with velocity $0.6 < \beta < 0.91$. The Gaussian fit gives $m_{\tilde{\tau}}^{\text{fit}} = 175.59 \pm 0.47$ GeV, while the actual stau mass is 175 GeV.

error bar increased slightly to 0.63 GeV.

The presence of quasi-stable staus in the final state provides a convenient means to reconstruct the masses of other particles further up a decay chain. For example, the mass of $\tilde{\chi}_1^0$ can be reconstructed by exploiting the fact that over the entire parameter space of stau NLSP F-theory GUT scenarios, there is a significant branching fraction to $\tilde{\chi}_1^0 \rightarrow \tilde{\tau}_1^\pm \tau$. By selecting final states which contain opposite sign staus and two opposite sign τ 's, we can reconstruct the resonance associated to the invariant mass of a pair of $\tilde{\tau}_1^\pm \tau^\mp$ to a $\tilde{\chi}_1^0$. Note that a similar resonance will also occur for $\tilde{\chi}_2^0$, providing a means to reconstruct the mass of this particle as well. In [62] this type of strategy was employed to work backwards up cascade decays to deduce the masses of many particles. In particular, the “ ε model” considered in [62] has a similar mass spectrum to that of the $\text{Maj}_{\text{MID}}^{(1)}$ benchmark model (though different enough to be distinguishable!), and so rather than perform a complete analysis of our case, we shall simply use the same precision estimates based on 30 fb^{-1} of integrated luminosity at $\sqrt{s} = 14$ TeV:

$$\begin{aligned}
\Delta m_{\tilde{\tau}_1} &= 0.021 \text{ GeV}, \quad \Delta m_{\tilde{\nu}_\tau} = 1.2 \text{ GeV}, \quad \Delta m_{\tilde{l}_L} = 2.0 \text{ GeV} \\
\Delta m_{\tilde{\chi}_1^0} &= 0.9 \text{ GeV}, \quad \Delta m_{\tilde{\chi}_2^0} = 2.0 \text{ GeV}, \\
\Delta m_{\tilde{q}_R} &= 2.8 \text{ GeV}, \quad \Delta m_{\tilde{q}_L} = 3.7 \text{ GeV}, \quad \Delta m_{\tilde{b}_1} = 57.7 \text{ GeV}.
\end{aligned} \tag{42}$$

Note that for all of the non-colored sparticles, the accuracy is within the range of 2 GeV or less. In addition, the mass difference for first and second generation squarks are both less than 4 GeV. The reason for the larger uncertainty in the sbottom mass is that events from \tilde{b}_1 and \tilde{b}_2 are mixed together since both of them can decay to $b\tilde{\chi}_1^0$ [62]. The result only serves as an estimate of the combination of \tilde{b}_1 and \tilde{b}_2 masses.

To distinguish between models which can mimic the spectrum of F-theory GUTs, we will also find it convenient to reconstruct the mass of the first and second generation right-handed sleptons \tilde{l}_R . In this case, the decay chain of interest depends on the relative masses of $\tilde{\chi}_1^0$ and \tilde{l}_R . Indeed, we have seen that for $N_{10} = 1$ scenarios at moderate PQ deformation $m_{\tilde{l}_R} > m_{\tilde{\chi}_1^0}$, whereas at larger PQ deformation for $N_{10} = 1$ and for all values of Δ_{PQ} in $N_{10} = 2$ scenarios, we instead have $m_{\tilde{l}_R} < m_{\tilde{\chi}_1^0}$. The latter case has been studied in detail in [63] where it was found that with 100 fb^{-1} of integrated luminosity at $\sqrt{s} = 14 \text{ TeV}$, $\Delta m_{\tilde{l}_R} \sim 1 \text{ GeV}$.

Let us now return to scenarios where $m_{\tilde{l}_R} > m_{\tilde{\chi}_1^0}$ so that right-handed sleptons dominantly decay via

$$\tilde{l}_R \rightarrow \tilde{\chi}_1^0 l \rightarrow \tilde{\tau}_1^\pm \tau^\mp l. \quad (43)$$

Since the actual production of right-handed sleptons is somewhat low in models such as the $\text{Maj}_{\text{MID}}^{(1)}$ benchmark model, generating a sufficient number of events requires a large integrated luminosity, in part because heavier sparticles rarely decay to \tilde{l}_R , and because the direct production cross section $\sigma_{\tilde{l}_R^+ \tilde{l}_R^-} = 1.3 \times 10^{-2} \text{ pb}$ is relatively small. To demonstrate the reconstruction of the right-handed slepton mass can be done with small enough uncertainty, we perform an analysis with 100 fb^{-1} integrated luminosity of simulated data for the benchmark model $\text{Maj}_{\text{MID}}^{(1)}$. First, we selected events with at least one stau candidate, one tau jet and no jets. Then the invariant mass $M_{inv}(\tilde{\tau}_1^\pm \tau^\mp)$ of any opposite-sign tau-stau pair is calculated.⁸ Only if there is one invariant mass within 5 GeV around the true mass of $\tilde{\chi}_1^0$, the event is selected. Finally, we take all possible combinations of leptons in the event with the tau-stau pair, and the invariant mass of the lepton-tau-stau system is calculated, giving rise to the distribution in figure 21. Fitting the peaks with a Gaussian plus a constant background

$$A \exp \left[-\frac{1}{\sigma^2} (M_{inv}(\tilde{\tau}_1^\pm \tau^\mp l) - M^{peak})^2 \right] + B \quad (44)$$

with A , B , σ and M^{peak} fitting parameters, we find that the peak position is $215.8 \pm 0.6 \text{ GeV}$. This is in good agreement with the actual \tilde{l}_R mass 214.3 GeV . Of course, we should also include uncertainties which propagate from the mass measurement of $\tilde{\tau}_1$ and $\tilde{\chi}_1^0$. Since these uncertainties are typically $\lesssim 1 \text{ GeV}$, including them does not significantly affect the overall uncertainty in the mass measurement of \tilde{l}_R .

⁸Here we assume that the tau four momentum can be fully constructed. In practice, a calibration of the tau momentum can be done as in [62].

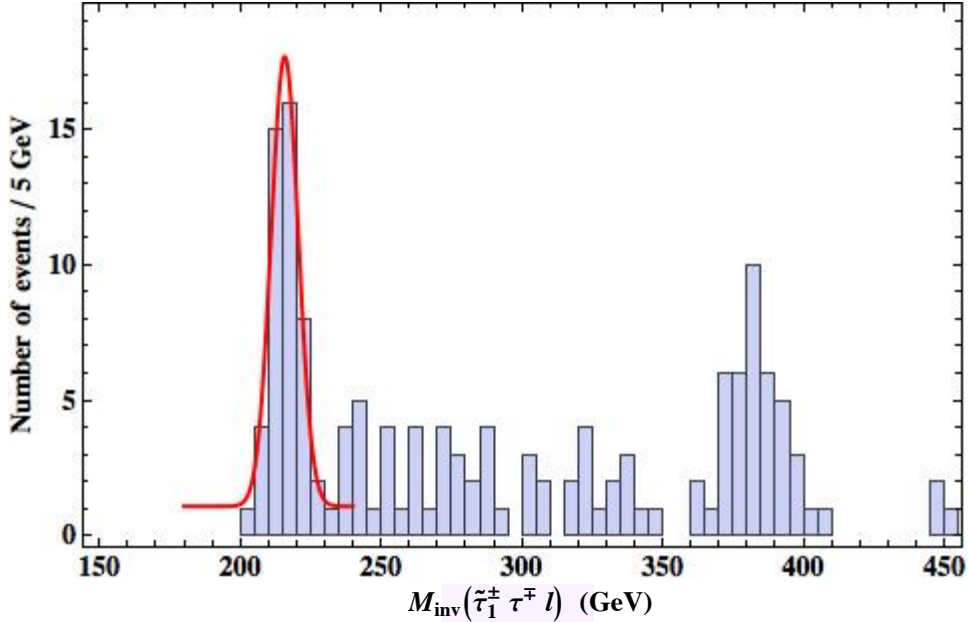


Figure 21: Plot of the lepton-tau-stau invariant mass in the benchmark $\text{Maj}_{\text{MID}}^{(1)}$ model using the event selections discussed below equation (44). The peak at ~ 215 GeV corresponds to the resonance from decays of the right-handed selectron \tilde{e}_R and smuon $\tilde{\mu}_R$. The somewhat lower and broader peak at ~ 380 GeV corresponds to the resonance from decays of the left-handed selectron \tilde{e}_L and smuon $\tilde{\mu}_L$.

Let us note that in the above we have quoted results from the literature which typically utilize integrated luminosities on the order of $30 - 100 \text{ fb}^{-1}$. We have also seen that cruder mass reconstructions can be performed at lower integrated luminosity. It would be interesting to study the overall expected mass resolution of such stau NLSP scenarios as a function of integrated luminosity. Further detailed information on mass measurements would also be readily available with the ILC.

7.2 Comparison with Minimal Gauge Mediation

Measuring the masses of the sparticles provides a very precise way to potentially distinguish models with similar spectra. Indeed, fitting to an F-theory GUT model leads to a quite specific range of possible values for N_{10} and Λ . Moreover, because the PQ charge assignments are different in the Majorana and Dirac neutrino scenarios (see section 2), measuring the masses of the sleptons and fitting to the rest of the spectrum would allow us to distinguish between these two possibilities. This would then provide even more precise information on both the size of Δ_{PQ} , as well as the PQ charge assignments of the sparticles.

In this subsection we consider minimal gauge mediated supersymmetry breaking (mGMSB)

models such that the lightest bosonic and fermionic superpartners respectively given by a quasi-stable $\tilde{\tau}_1$ and $\tilde{\chi}_1^0$ have the same mass as their F-theory counterparts. We analyze to what extent such look-alikes can mimic the rest of an F-theory GUT spectrum. In minimal gauge mediation, the available parameters which can be varied are the supersymmetry breaking scale \sqrt{F} in the messenger sector, the analogous scale $\sqrt{F_0}$ which generates the mass of the gravitino,⁹ the messenger scale M_{mess} , the effective number of messengers in the $5 \oplus \bar{5} N_5$, and $\tan\beta$. Here we assume that the mass of the messengers are determined through the supersymmetry breaking vev of a single GUT singlet. The parameters F and M_{mess} fix the characteristic scale $\Lambda = F/M_{mess}$. Parameters such as μ and $B\mu$ are determined by the condition that proper electroweak symmetry breaking is achieved for a given value of $\tan\beta$. Let us note that a much broader range of sparticle masses can be achieved in more general gauge mediation setups. See for example [103, 104] for recent discussion.

As a first step in identifying potential mGMSB look-alikes, we must require that the stau is the NLSP, and that it is quasi-stable on timescales probed by the LHC. Assuming that $\sqrt{F} \sim \sqrt{F_0}$, equation (40) now implies that $\sqrt{F} \gtrsim 10^6$ GeV. In particular, this implies that the ratio $F/M_{mess}^2 = \Lambda^2/F \lesssim 0.01$. Hence, we can reliably use an approximation for the mGMSB candidate look-alike in which all soft masses at the messenger scale are proportional to Λ . Later in this subsection we shall consider a potential look-alike where we drop this assumption and allow lower messenger scale models, but we will again see that this candidate does not effectively mimic F-theory GUTs.

In quasi-stable mGMSB models with $\sqrt{F} \sim \sqrt{F_0}$, the primary deviation between F-theory GUTs and minimal gauge mediation models comes from the specific scale of supersymmetry breaking, and the effects of the PQ deformation on the soft scalar masses. As a first step towards finding potential look-alikes, we focus on the masses of sparticles where the effects of the PQ deformation are largely unimportant, in particular the gauginos and the first and second generation squarks. Assuming that we have measured enough of the gaugino masses, we therefore require:¹⁰

$$3N_{10}^{(F)}\Lambda^{(F)} \simeq N_5^{(m)}\Lambda^{(m)}, \quad (45)$$

where the superscript “ F ” denotes the F-theory model and “ m ” is for the “mimic”. Next consider the masses of the squarks. There is little left-right mixing for the first two generations of left and right-handed squarks, and so we focus on this case here. As for all scalar

⁹As noted previously, in the context of F-theory GUTs, it is most natural to set $F = F_0$.

¹⁰Note that in general, there will be some mixing between the neutral $SU(2)_L \times U(1)_Y$ gauginos and the neutral Higgsinos, and the charged gauginos and the charged Higgsinos. This can in principle complicate the identification of the gaugino mass measurement, though in the present class of models, this is a small effect which we shall ignore.

partners in mGMSB models, the masses of the squarks at the messenger scale are:

$$m_{\tilde{q}} = \frac{\alpha}{4\pi} C_{\tilde{q}} \sqrt{N_5^{(m)}} \Lambda^{(m)}, \quad (46)$$

where we have again schematically indicated the dependence on the various fine structure constants and quadratic Casimirs of representations through α and $C_{\tilde{q}}$. The possible ways that an F-theory GUT could reproduce the same squark masses but with a different number of messengers and Λ is by turning on Δ_{PQ} , and adjusting the messenger scale. As we have already seen in section 3, the effects of the PQ deformation are far milder for heavy squarks. In particular, the overall shift in the mass of the squarks is on the order of $\Delta_{PQ}^2/m_{\tilde{q}} \sim O(100 \text{ GeV})^2/O(1 \text{ TeV}) \sim O(10) \text{ GeV}$, which is a very slight shift. Varying the messenger scale M_{mess} produces logarithmic contribution to the mass-squared, and in minimal gauge mediation models, only shifts the squark masses by an effect which is at most on the order of $O(100) \text{ GeV}$. This yields the additional constraint:

$$\frac{\alpha}{4\pi} C_{\tilde{q}} \sqrt{3N_{10}^{(F)}} \Lambda^{(F)} = \frac{\alpha}{4\pi} C_{\tilde{q}} \sqrt{N_5^{(m)}} \Lambda^{(m)} + O(100) \text{ GeV}. \quad (47)$$

Since the squark masses are on the order of a TeV, we conclude that the messenger number and Λ must agree:

$$3N_{10}^{(F)} = N_5^{(m)}, \quad \Lambda^{(F)} \sim \Lambda^{(m)}. \quad (48)$$

Fixing the parameters N_5 and Λ to agree with the F-theory GUT model allows it to mimic the masses of the gauginos and the first and second generation squarks. We now discuss whether it is possible to adjust the values of the remaining parameters M_{mess} and $\tan\beta$ to exactly match the rest of the spectrum. In the class of models we are considering, the effects of $\tan\beta$ affect the third generation of squarks and sleptons by inducing more mixing between left and right-handed sparticles. To isolate the effects of M_{mess} , we therefore focus on the masses of the left and right-handed sleptons \tilde{e}_L and \tilde{e}_R . Our strategy will be to compare the needed Messenger scale for the two soft mass relations in the presence of the PQ deformation. We find that at most one of these masses can be matched by adjusting $M_{mess}^{(m)}$.

To arrive at this result, we now study in more precise terms the masses of the left and right-handed selectrons as a function of the messenger scale. Letting $\mathcal{M}^2(t)$ denote the soft masses of a minimal gauge mediation model with N_5 effective messengers and characteristic scale Λ evaluated at a renormalization group (RG) time $t = \log(M_{mess}^2/Q^2)$, the condition for the selectrons of the F-theory GUT and look-alike to have the same masses is:

$$\mathcal{M}_i^2(t^{(m)}) = \mathcal{M}_i^2(t^{(F)}) + q_i \cdot \Delta_{PQ}^2, \quad (49)$$

Table 1: Mass spectra of F-theory benchmark model $\text{Maj}_{\text{MID}}^{(1)}$ and some candidate mGMSB look-alike models with $N_5 = 3$ messengers. All masses are in GeV, and we have taken the top mass to be 172.4 GeV in our calculation.

parameter	$\text{Maj}_{\text{MID}}^{(1)}$	mGMSB1	mGMSB2
M_{mess}	10^{12}	10^{12}	2×10^9
\sqrt{F}	2.2×10^8	2.2×10^8	10^7
$\tan \beta$	24.05	34.7	24.5
$m_{\tilde{g}}$	1112	1113	1116
$m_{\tilde{\chi}_1^0}$	198.6	199.0	199.3
$m_{\tilde{\chi}_2^0}$	377.1	379.4	378.0
$m_{\tilde{\chi}_1^\pm}$	380.3	382.3	381.2
$m_{\tilde{u}_L}$	1106	1112	1102
$m_{\tilde{u}_R}$	1059	1066	1063
$m_{\tilde{t}_1}$	857.6	866.7	898.1
$m_{\tilde{t}_2}$	1050	1047	1059
$m_{\tilde{b}_1}$	997.2	982.2	1014
$m_{\tilde{b}_2}$	1032	1032	1046
$m_{\tilde{e}_L, \tilde{\mu}_L}$	383.0	421.7	382.2
$m_{\tilde{\nu}_e, \tilde{\nu}_\mu}$	372.5	412.1	371.6
$m_{\tilde{e}_R, \tilde{\mu}_R}$	214.3	246.9	204.9
$m_{\tilde{\tau}_1}$	175.0	174.8	174.7
$m_{\tilde{\nu}_\tau}$	366.1	400.4	367.7
$m_{\tilde{\tau}_2}$	384.0	422.3	385.1
m_h	114.3	114.3	113.8
m_A	693.1	614.2	623.4

where $t^{(F)}$ and $t^{(m)}$ respectively correspond to the RG time evolution from the messenger scale to the weak scale for the F-theory GUT and the mimic. Here we are implicitly using the fact that the Yukawas of the first two generations are small, so that the PQ deformation can be treated as an additive shift for $\tilde{l} = \tilde{e}_R$ and \tilde{e}_L . Eliminating Δ_{PQ} from this system of equations, we therefore find the condition:

$$\frac{q_{\tilde{e}_L}}{q_{\tilde{e}_R}} = \frac{\mathcal{M}_{\tilde{e}_L}^2(t^{(F)}) - \mathcal{M}_{\tilde{e}_L}^2(t^{(m)})}{\mathcal{M}_{\tilde{e}_R}^2(t^{(F)}) - \mathcal{M}_{\tilde{e}_R}^2(t^{(m)})}. \quad (50)$$

In Appendix B we compute the leading order behavior of the righthand side of this equation,

the end result of which is:

$$\frac{q_{\tilde{e}_L}}{q_{\tilde{e}_R}} \simeq \frac{1 + N_5}{1 + 5N_5/33} \times \frac{9}{220} \times \left(\frac{\alpha_2}{\alpha_1}\right)^3. \quad (51)$$

In our conventions the weak scale values of the couplings α_i are $\alpha_1 \sim 1/100$ and $\alpha_2 \sim 1/30$ which implies:

$$\frac{q_{\tilde{e}_L}}{q_{\tilde{e}_R}} \sim 1.5 \times \frac{1 + N_5}{1 + 5N_5/33}, \quad (52)$$

which for $N_5 = 3$ and 6 yields the condition:

$$N_5 = 3 \implies \frac{q_{\tilde{e}_L}}{q_{\tilde{e}_R}} \sim 4, \quad (53)$$

$$N_5 = 6 \implies \frac{q_{\tilde{e}_L}}{q_{\tilde{e}_R}} \sim 6. \quad (54)$$

In other words, since the actual ratio of q 's is 2 for Majorana scenarios, and 1 for Dirac scenarios, a candidate look-alike cannot be found where the masses exactly agree. For example, in an F-theory GUT Majorana scenario with $N_{10} = 1$, this would lead to a mismatch by a factor of 2 in the q 's.

In principle, uncertainties in the mass measurement could still allow a candidate look-alike to remain compatible with an F-theory GUT, up to experimental error. In the present context, we can view this as reflecting an uncertainty in determining the ratio of the q 's. Since the mimics of $N_{10} = 1$ Majorana scenarios lead to a smaller deviation from the actual ratio of the q 's, we focus on this case. Rescaling q by the factor of 2 discussed below equation (54) translates to a shift in the mass squared of order $2 \times \Delta_{PQ}^2$. We now ask whether this type of shift could be explained by an uncertainty in the mass measurement. Using the relation:

$$m^{actual} \simeq m^{observed} \pm \Delta m \quad (55)$$

and squaring, we obtain:

$$(m^{actual})^2 \simeq (m^{observed})^2 \pm 2 \times m \times \Delta m. \quad (56)$$

In other words F-theory GUTs which can be mimicked have Δ_{PQ} which satisfies the upper bound:

$$2 \times \Delta_{PQ}^2 \lesssim 2 \times m \times \Delta m. \quad (57)$$

In typical F-theory GUTs, the masses of the right-handed sleptons satisfy $m \sim 300$ GeV. Combined with the uncertainty in the mass measurement $\Delta m \lesssim 2$ GeV reviewed in the previous subsection, we find:

$$\Delta_{PQ} \lesssim 30 \text{ GeV}, \quad (58)$$

Table 2: Mass spectra of F-theory benchmark model $\text{Maj}_{\text{HI}}^{(1)}$ and some candidate mGMSB look-alike models with $N_5 = 3$ messengers. All masses are in GeV, and we have taken the top mass to be 172.4 GeV in our calculation.

parameter	$\text{Maj}_{\text{HI}}^{(1)}$	mGMSB3	mGMSB4
M_{mess}	10^{12}	10^8	3×10^5
\sqrt{F}	2.2×10^8	2.2×10^6	1.22×10^5
$\tan \beta$	24.9	40.2	40.7
$m_{\tilde{g}}$	1110	1118	1128
$m_{\tilde{\chi}_1^0}$	198.3	199.7	200.0
$m_{\tilde{\chi}_2^0}$	373.8	376.1	350.9
$m_{\tilde{\chi}_1^\pm}$	377.5	378.7	350.3
$m_{\tilde{u}_L}$	1098	1098	1091
$m_{\tilde{u}_R}$	1050	1062	1062
$m_{\tilde{t}_1}$	846.1	916.3	968.4
$m_{\tilde{t}_2}$	1041	1049	1062
$m_{\tilde{b}_1}$	979.8	986.3	1008
$m_{\tilde{b}_2}$	1019	1037	1052
$m_{\tilde{e}_L, \tilde{\mu}_L}$	329.7	363.7	330.0
$m_{\tilde{\nu}_e, \tilde{\nu}_\mu}$	317.4	352.9	318.4
$m_{\tilde{e}_R, \tilde{\mu}_R}$	166.6	188.9	163.3
$m_{\tilde{\tau}_1}$	104.6	104.5	104.7
$m_{\tilde{\nu}_\tau}$	309.5	345.2	314.5
$m_{\tilde{\tau}_2}$	331.5	373.2	340.5
m_h	114.3	113.3	112.8
m_A	701.8	497.5	395.9

which should be viewed as an order of magnitude estimate. In other words, the high precision of the mass measurement translates into a tight upper bound on the size of the PQ deformation which can be mimicked.

To further support this general analysis, we now consider in greater detail potential look-alikes for the benchmark model $\text{Maj}_{\text{MID}}^{(1)}$. As a first example, consider mGMSB models with $M_{mess} = 10^{12}$ GeV, $\Lambda = 50$ TeV, and $N_5 = 3$. The only remaining parameter of an mGMSB model which we can vary is $\tan \beta$, which changes the amount of left-right mixing for staus, allowing the lightest stau to become degenerate in mass with the F-theory GUT value. By increasing $\tan \beta$ to 34.7, one can achieve a stau NLSP with mass very close to that of the F-theory GUT. The mass spectrum of this model (mGMSB1) is shown in Table 1. Though the gaugino and squark masses are within a few GeV, the slepton masses in

mGMSB1 deviate from the $\text{Maj}_{\text{MID}}^{(1)}$ values by as much as ~ 30 GeV. Returning to equation (42), we conclude that this difference is large enough to distinguish these two models with sufficient LHC data.

Next consider variations of the messenger scale M_{mess} . Table 1 displays the mass spectrum of an mGMSB model (mGMSB2) where the model parameters are the same as the benchmark $\text{Maj}_{\text{MID}}^{(1)}$ except $M_{\text{mess}} = 2 \times 10^9$ GeV and $\tan\beta = 24.5$. One can see that in addition to matching the gauginos and first and second generation squark masses, the left-handed slepton masses are also very close to the $\text{Maj}_{\text{MID}}^{(1)}$ model. The notable differences are the right-handed slepton mass and the third-generation squarks, as well as the Higgs masses. The difference in the third-generation squark masses is mainly due to the lower messenger scale which shortens the contribution from renormalization group flow effects.

For F-theory models with larger Δ_{PQ} , the deformation effects are larger. As we have seen, this makes it more difficult to find an mGMSB look-alike. As an example we consider the benchmark model $\text{Maj}_{\text{HI}}^{(1)}$ where $N_{10} = 1$, $\Lambda = 50$ TeV and $\Delta_{PQ} = 209$ GeV. Even when the messenger scale is as low as $\sim 10^8$ GeV in the model mGMSB3, table 2 shows that the slepton masses typically differ by as much as ~ 35 GeV, which can be resolved with the mass measurement procedure detailed above. For even lower messenger scale, the stau NLSP in mGMSB model would decay inside the detector, so long as we assume $F_0 = F$.

Even when we allow the possibility that $F_0 \neq F$ so that the stau decays outside the detector, we find that representative low scale messenger models do not correctly mimic the spectrum of the $\text{Maj}_{\text{HI}}^{(1)}$ scenario. An example of this type is shown as the model mGMSB4 in table 2. Let us note that when $F/M_{\text{mess}}^2 \sim O(1)$, the theoretical analysis presented earlier in this subsection and in Appendix C is no longer accurate. Table 2 shows that even though the slepton masses can be quite degenerate with the above mentioned F-theory model, the masses of $\tilde{\chi}_2^0$ and $\tilde{\chi}_1^\pm$ would be ~ 20 GeV lighter than the corresponding masses in the F-theory model. The reason for this is mainly due to the lowered messenger scale where the running of $m_{H_u}^2$ is reduced and therefore become less negative. From the relation

$$|\mu|^2 \approx -m_{H_u}^2 - \frac{1}{2}m_Z^2, \quad (59)$$

we can see the μ term decreases in this situation, and therefore the higgsino masses become closer to the gaugino masses. The increased mixing between gauginos and higgsinos decreases the physical masses of $\tilde{\chi}_2^0$ and $\tilde{\chi}_1^\pm$. This mismatch in the neutralino and chargino masses is by itself enough to resolve the potential degeneracy.

Our numerical analysis has mainly been based on two benchmark models with $N_{10} = 1$. The basic idea is similar for other models, as well as for $N_{10} = 2$ scenarios. Though beyond the scope of the present paper, it would be interesting to perform a more complete scan over other well-motivated look-alikes.

8 Conclusions

In this paper we have seen that over a broad range of parameter space in minimal F-theory GUTs, a quasi-stable stau is the NLSP. The consequences for collider physics are quite striking, since in stau NLSP scenarios, this particle will appear as a massive quasi-stable charged particle at the LHC. We have seen that with the center-of-mass energies and integrated luminosity expected at the LHC, signatures of this scenario can be discovered. We have also seen how the corresponding number of stau events correlates with the number of leptonic final states as a function of F-theory GUT parameters. Focussing on inclusive one and two stau events, it is possible to constrain the characteristic scale of gauge mediation Λ , and using more exclusive signatures such as Drell-Yan production of staus, it is possible to constrain the size of the stringy PQ deformation parameter present in F-theory GUTs. Slow-moving staus can also become stuck in or near the detector, and we have analyzed in an idealized situation the number of such events to expect. Finally, we have used the high precision expected in mass measurements in stau scenarios as a way to compare the spectra of F-theory GUTs with minimal gauge mediation models.

In the remainder of this section, we briefly speculate on some possible avenues of further investigation. In this work we have focussed on the potential for discovering quasi-stable stau NLSP F-theory GUT scenarios. Quasi-stable stau NLSPs are also a feature of other models with an MSSM-like spectrum, and we have seen that there are some measurable differences between minimal gauge mediation models and F-theory GUTs. Broadening the range of possible models both to more general gauge mediation models, and more general scenarios with a stau NLSP, it would be interesting to further study the level at which F-theory GUTs can be distinguished from other well-motivated possibilities.

We have seen that in the context of F-theory GUTs, staus can become stuck in or near the detector. This holds out the exciting prospect of measuring the scale of supersymmetry breaking. It would be interesting to further investigate with more realistic simulations how to use the ATLAS and CMS detectors to detect stopped staus, and measure their lifetimes.

Acknowledgements

We thank B.S. Acharya, J. Hubisz, G.L. Kane, M. Papucci, M. Perelstein, A. Pierce, G. Polesello, A. Rizzi, A. De Roeck and M. Spiropulu for helpful discussions. We also thank members of the ATLAS and CMS groups for comments. JJH and CV thank the CERN theory group for hospitality during part of this work. JJH thanks the Harvard high energy theory group for hospitality during part of this work. The work of JJH is supported by NSF grant PHY-0503584. The work of JS is supported by Syracuse University College of Arts and Sciences. The work of CV is supported by NSF grant PHY-0244281.

Appendix A: Simulation Details

We simulate SUSY events using PYTHIA [83]. The analysis is done based on the parton-level objects

- lepton: $p_T > 5$ GeV and $|\eta| < 2.5$ and the transverse energy deposited in a cone $\Delta R = 0.4$ around the lepton is less than 5 GeV. Note: staus which have large velocity $\beta > 0.91$ are also treated as muons.
- tau jet: $p_T > 20$ GeV and $|\eta| < 3.0$, with efficiency $\epsilon_\tau = 0.5$. leptonic decaying taus are identified as leptons based on the lepton cuts.
- jet: $p_T > 20$ GeV and $|\eta| < 3.0$.

We shall often augment these basic cuts by additional analysis cuts.

We include the detector resolution of the momentum and energy for muon, lepton and jet, which are parameterized as follows in the ATLAS detector [88]:

- For muon the momentum resolution is:

$$\frac{\sigma_{p_T}}{p_T} = \frac{ap_T}{\text{TeV}} \oplus \frac{b}{\sqrt{\sin \theta}} \quad (60)$$

Here we take $a = 36\%$ and $b = 1.3\%$,

- For electron the energy resolution is:

$$\frac{\sigma_E}{E} = \frac{a}{\sqrt{E/\text{GeV}}} \oplus b \quad (61)$$

Here we take $a = 10\%$ and $b = 0.4\%$,

- For jet, the energy resolution is similar to electron, but with $a = 80\%$ and $b = 15\%$.

Appendix B: Selectron Mass Comparison

In this Appendix we compare in more precise terms the masses of the left and right-handed selectrons in F-theory GUTs and minimal gauge mediated supersymmetry breaking. In minimal gauge mediation, the first and second generation soft masses squared at a renormalization group (RG) time $t = \log(M_{\text{mess}}^2/Q^2)$ are given by (see for example [74]):

$$\mathcal{M}^2(t) = 2 \sum_{r=1}^3 C_r k_r \left(\frac{\alpha_r(t)}{4\pi} \right)^2 N_5 \Lambda^2 \left[\left[1 - \frac{\alpha_r(t)}{4\pi} b_r t \right]^{-2} + \frac{N_5 k_r}{b_r} \left[\left[1 - \frac{\alpha_r(t)}{4\pi} b_r t \right]^{-2} - 1 \right] \right], \quad (62)$$

where we have dropped running effects due to the Yukawa couplings, which are small for the first two generations. In the above, r is an index labelling the three gauge groups, C_r is the quadratic Casimir associated to the representation of the scalar, $k_1 = 5/3$, $k_2 = k_3 = 1$ so that $\alpha_i(t)k_i$ unify at the GUT scale, and in this normalization $b_r = 11, 1, -3$ denote the beta functions for $r = 1, 2, 3$, respectively. Further, the renormalized fine structure constant satisfies:

$$\alpha_r(0) = \alpha_r(t) \left[1 - \frac{\alpha_r(t)}{4\pi} b_r t \right]^{-1}. \quad (63)$$

Here, $t = 0$ corresponds to the Messenger scale, and we shall be interested in evaluating both the F-theory GUT and candidate look-alike at the weak scale. Because of this, we can replace each $\alpha_r(t)$ by its weak scale value, which we denote by α_r . In this case, all of the difference from RG flow effects is captured by the terms in brackets containing $\alpha_r b_r t / 4\pi$. Letting $t^{(F)}$ and $t^{(m)}$ denote the respective values of the RG time for the F-theory GUT and the candidate look-alike, it follows that the right-handed selectrons and sleptons of a candidate mimic must satisfy the relations:

$$q_{\tilde{l}} \Delta_{PQ}^2 = 2 \sum_{r=1}^3 C_r^{(\tilde{l})} k_r \left(\frac{\alpha_r}{4\pi} \right)^2 N_5 \left(1 + \frac{N_5 k_r}{b_r} \right) \Lambda^2 \left[\left[1 - \frac{\alpha_r}{4\pi} b_r t^{(m)} \right]^{-2} - \left[1 - \frac{\alpha_r}{4\pi} b_r t^{(F)} \right]^{-2} \right]. \quad (64)$$

For the right-handed selectrons, the sum on r truncates to the term $r = 1$, and for the left-handed selectrons, the $r = 2$ term dominates. Taking the ratio of these two contributions, we find:

$$\frac{q_{\tilde{e}_L}}{q_{\tilde{e}_R}} = \frac{1 + N_5}{1 + 5N_5/33} \times \frac{k_2 C_2^{(\tilde{e}_L)}}{k_1 C_1^{(\tilde{e}_R)}} \times \left(\frac{\alpha_2}{\alpha_1} \right)^2 \frac{\left[\left[1 - \frac{\alpha_2}{4\pi} b_2 t^{(m)} \right]^{-2} - \left[1 - \frac{\alpha_2}{4\pi} b_2 t^{(F)} \right]^{-2} \right]}{\left[\left[1 - \frac{\alpha_1}{4\pi} b_1 t^{(m)} \right]^{-2} - \left[1 - \frac{\alpha_1}{4\pi} b_1 t^{(F)} \right]^{-2} \right]} \quad (65)$$

$$\simeq \frac{1 + N_5}{1 + 5N_5/33} \times \frac{C_2^{(\tilde{e}_L)}}{C_1^{(\tilde{e}_R)}} \times \frac{k_2 b_2}{k_1 b_1} \times \left(\frac{\alpha_2}{\alpha_1} \right)^3 \quad (66)$$

$$= \frac{1 + N_5}{1 + 5N_5/33} \times \frac{9}{220} \times \left(\frac{\alpha_2}{\alpha_1} \right)^3, \quad (67)$$

where in the second to last equality we have kept only the leading logarithms. Note that this final expression is independent of the logarithmic dependence on the messenger scale, as well as Λ .

Appendix C: Miscellaneous Plots

In this Appendix we collect additional plots of potential interest.

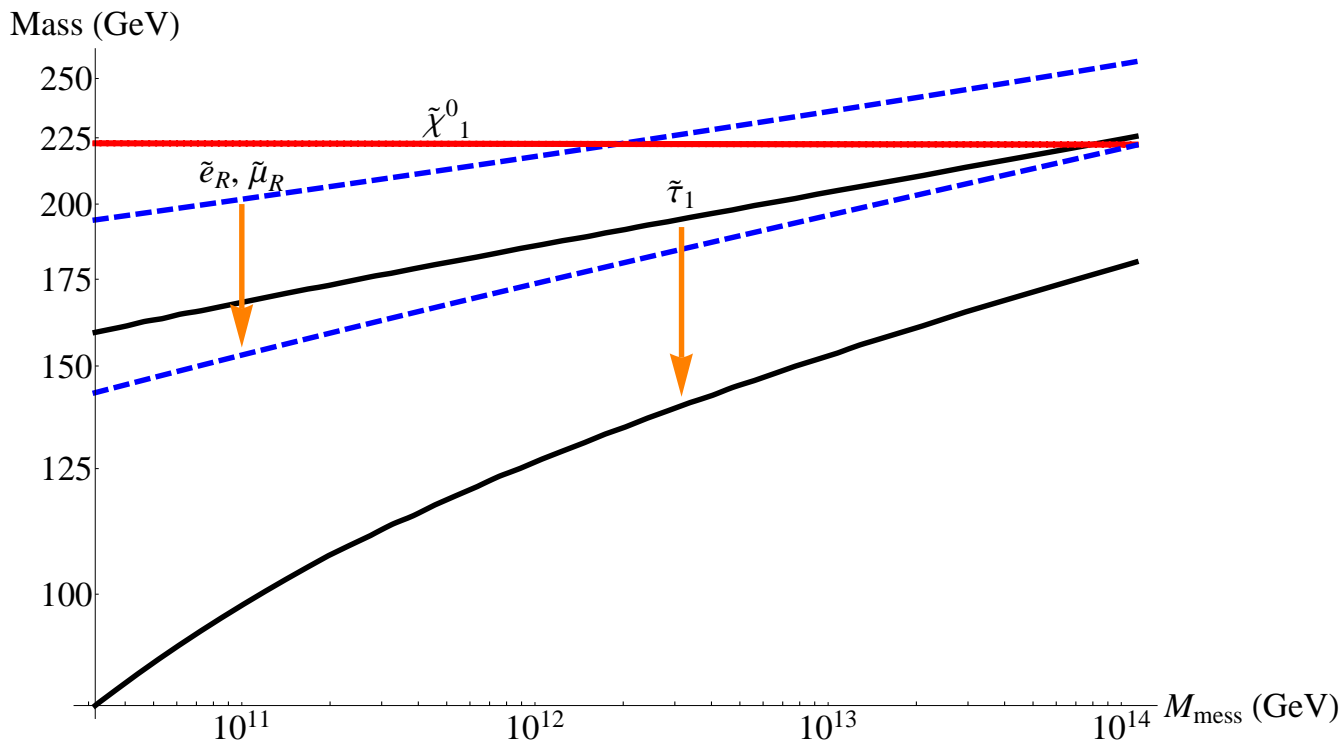


Figure 22: Plot of the four lightest sparticle masses as a function of messenger scale M_{mess} . Here $N_{10} = 2$, $\Lambda = 28$ TeV, and we have displayed the values for zero PQ deformation (upper lines) and $\Delta_{PQ} = 150$ GeV (lower lines). Note that the bino mass remains constant, both as a function of messenger scale and of PQ deformation.

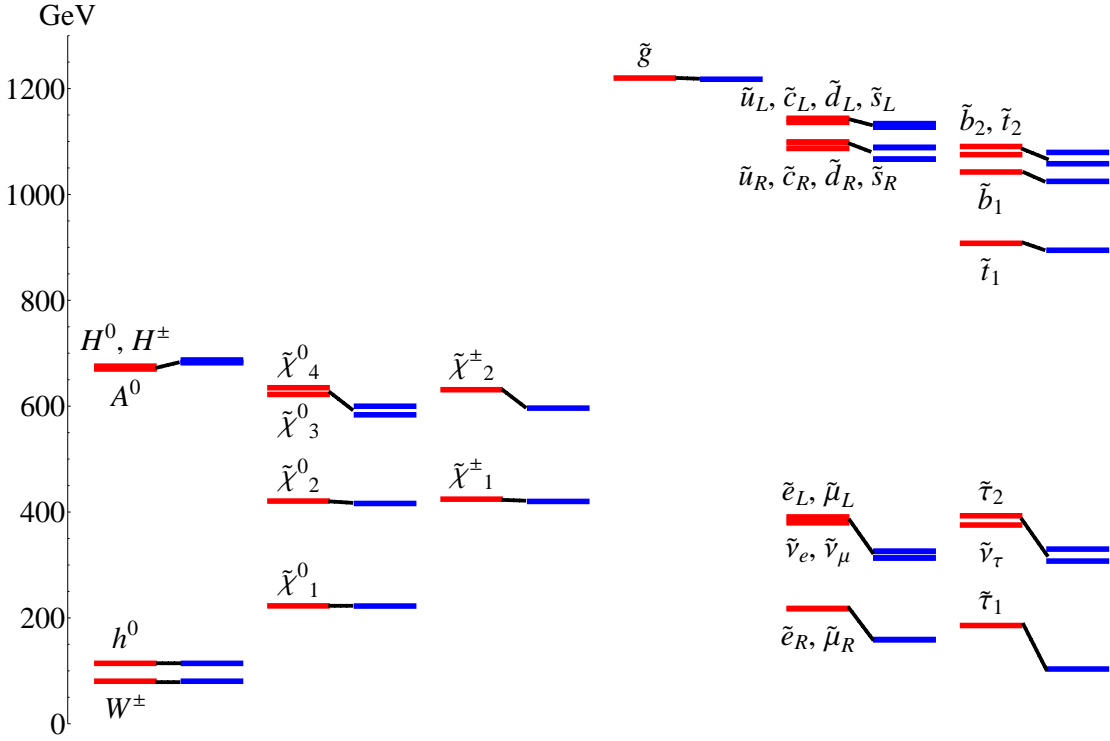


Figure 23: Spectrum of an F-theory GUT Majorana neutrino scenario with $N_{10} = 2$, $\Lambda = 28$ TeV for minimal (red left columns) and maximal (blue right columns) PQ deformation. As opposed to the case of $N_{10} = 1$ models, for larger numbers of messengers the stau is always the NLSP for F-theory GUTs.

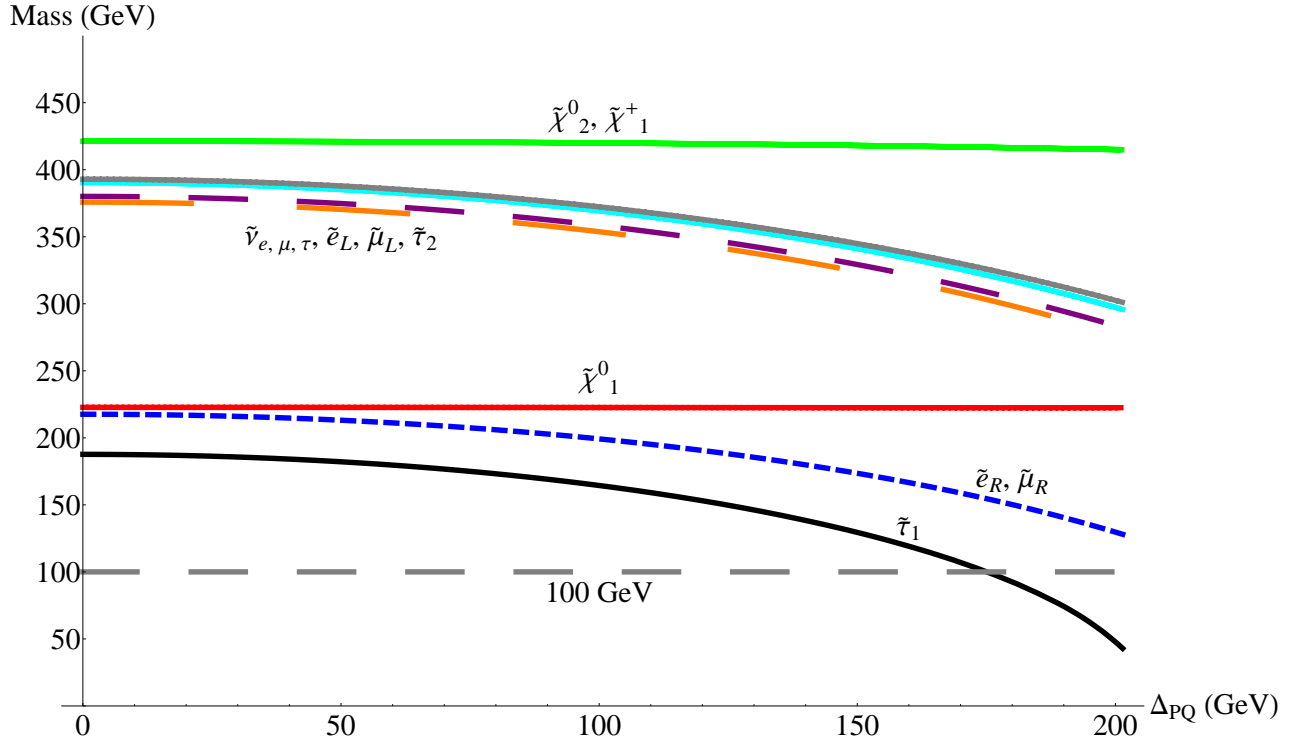


Figure 24: Mass spectrum of the sleptons, lightest chargino and two lightest neutralinos with $N_{10} = 2$, $\Lambda = 28$ TeV as a function of Δ_{PQ} . The dashed grey line at 100 GeV denotes the present experimental bound on the mass of a quasi-stable stau.

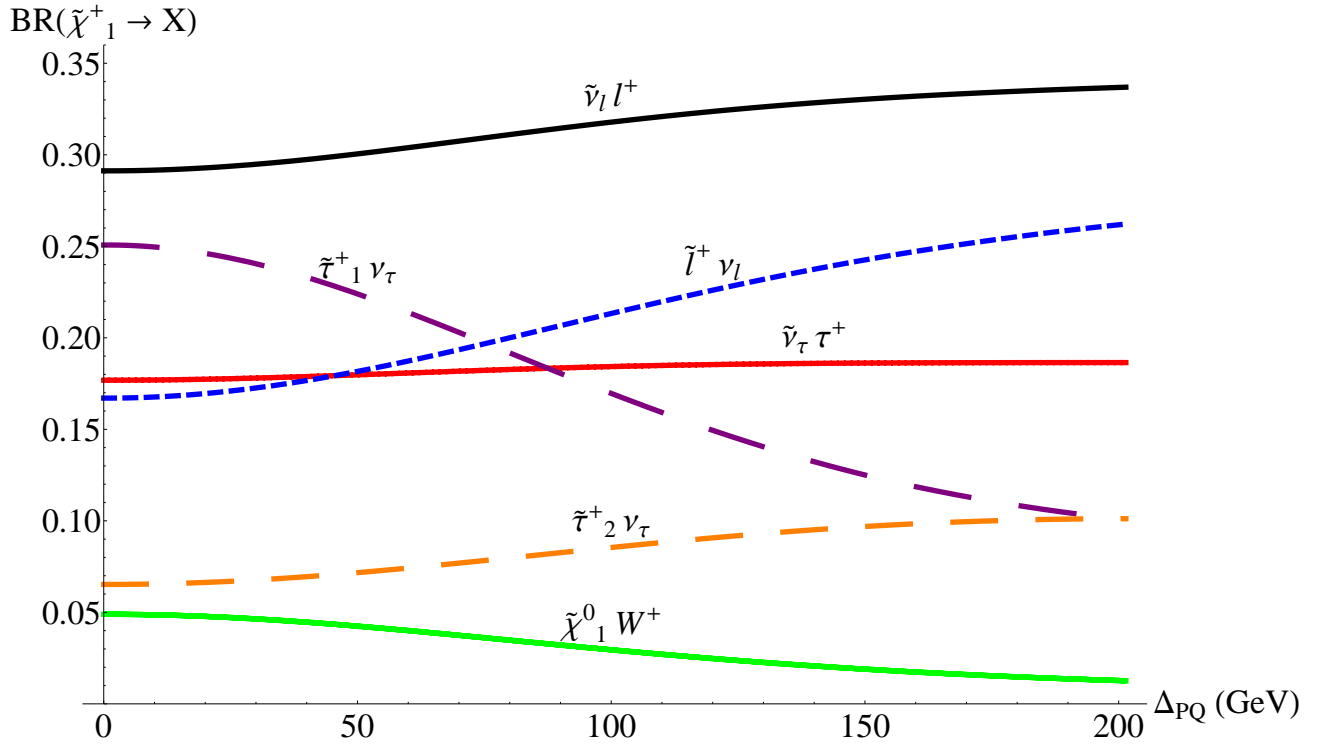


Figure 25: Dominant branching fractions of $\tilde{\chi}_1^\pm$ as a function of Δ_{PQ} with $N_{10} = 2$ and $\Lambda = 28$ TeV. As opposed to the case $N_{10} = 1$, the overall Δ_{PQ} dependence is smaller. In addition, the decay channel to sneutrinos is available even for $\Delta_{PQ} = 0$.

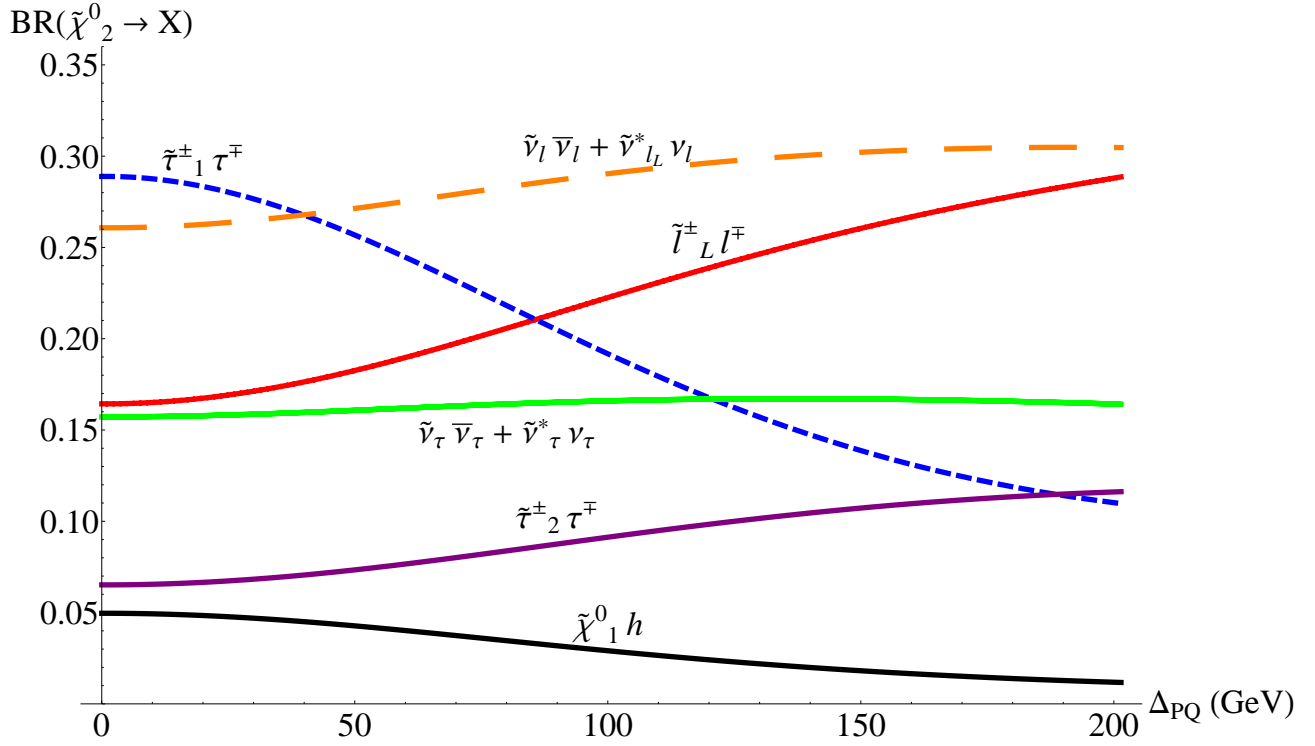


Figure 26: Dominant branching fractions of $\tilde{\chi}_2^0$ as a function of Δ_{PQ} with $N_{10} = 2$ and $\Lambda = 28$ TeV. As opposed to the case $N_{10} = 1$, the overall Δ_{PQ} dependence is smaller. In addition, the decay channel to sneutrinos is available even for $\Delta_{PQ} = 0$.

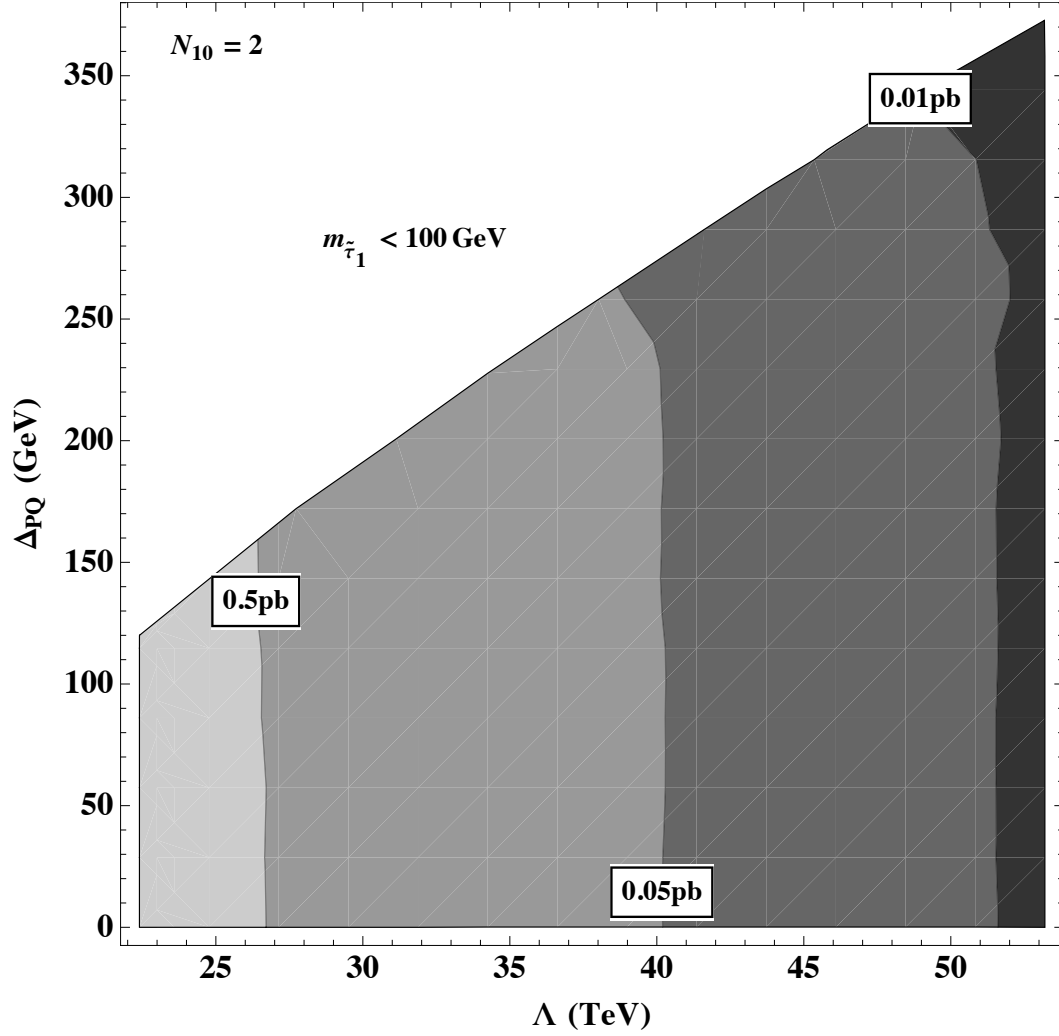


Figure 27: Contour plot of the inclusive $\geq 1\tilde{\tau}_1$ signal in parameter space Λ and Δ_{PQ} for $\sqrt{s} = 14 \text{ TeV}$ and $N_{10} = 2$ messengers. The three contours correspond to the value of the cross section at 0.5 pb, 0.05 pb, and 0.01 pb. To detect five inclusive one or two stau events, this amounts to an integrated luminosity of respectively 10 pb^{-1} , 100 pb^{-1} and 0.5 fb^{-1} .

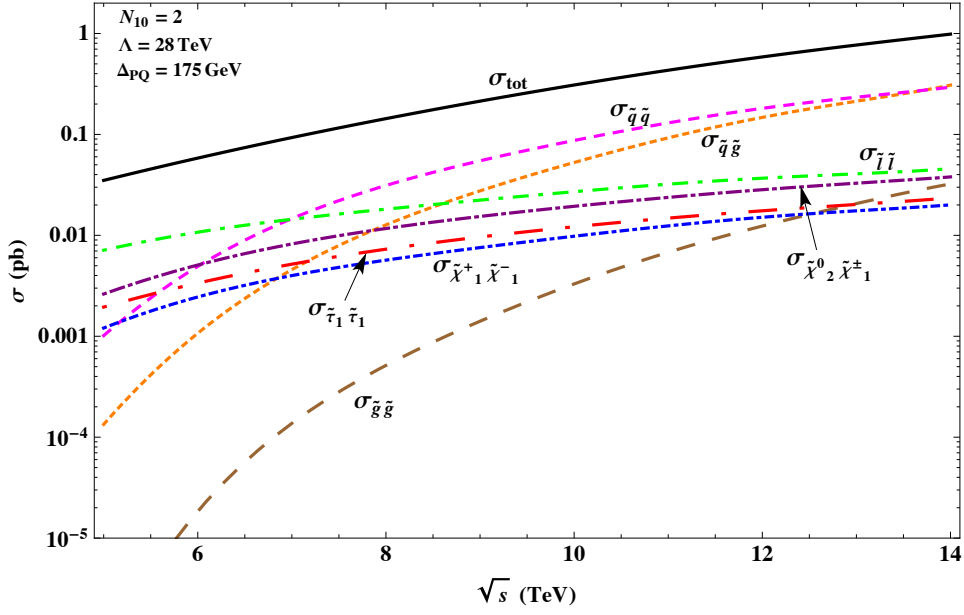


Figure 28: Plot of the leading order cross sections of various production channels as functions of center-of-mass energy \sqrt{s} for the benchmark $\text{Maj}_{\text{HII}}^{(2)}$ scenario.

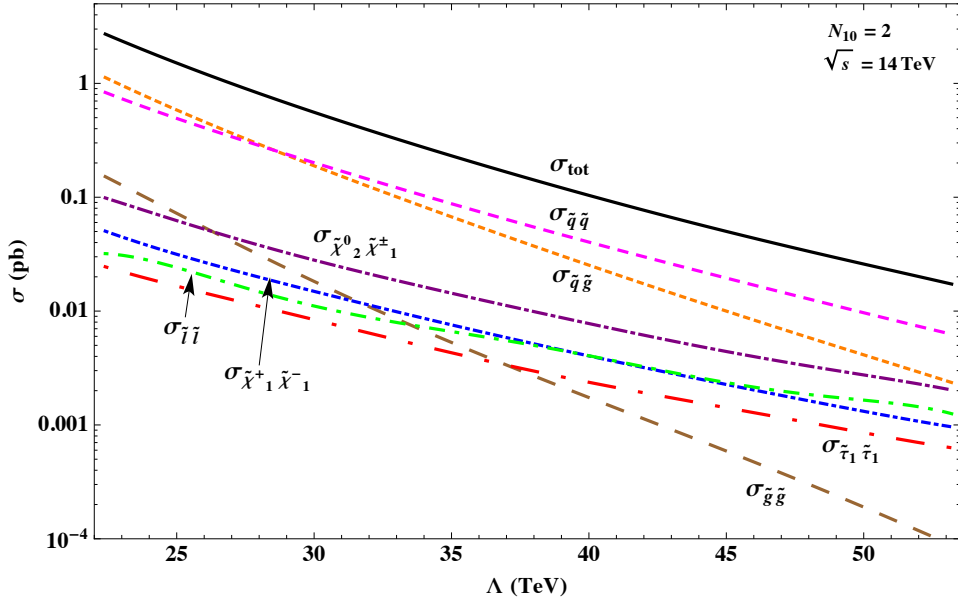


Figure 29: Plot of the leading order cross sections of various production channels for F-theory GUTs with $N_{10} = 2$ as a function of Λ at $\Delta_{PQ} = 0$.

References

- [1] R. Donagi and M. Wijnholt, “Model Building with F-theory,” [arXiv:0802.2969](#) [[hep-th](#)].
- [2] C. Beasley, J. J. Heckman, and C. Vafa, “GUTs and Exceptional Branes in F-theory - I,” *JHEP* **01** (2009) 058, [arXiv:0802.3391](#) [[hep-th](#)].
- [3] H. Hayashi, R. Tatar, Y. Toda, T. Watari, and M. Yamazaki, “New Aspects of Heterotic–F Theory Duality,” [arXiv:0805.1057](#) [[hep-th](#)].
- [4] L. Aparicio, D. G. Cerdeño, and L. E. Ibáñez, “Modulus-dominated SUSY-breaking soft terms in F-theory and their test at LHC,” *JHEP* **07** (2008) 099, [arXiv:0805.2943](#) [[hep-ph](#)].
- [5] E. I. Buchbinder, “Dynamically SUSY Breaking SQCD on F-Theory Seven-Branes,” [arXiv:0805.3157](#) [[hep-th](#)].
- [6] C. Beasley, J. J. Heckman, and C. Vafa, “GUTs and Exceptional Branes in F-theory - II: Experimental Predictions,” *JHEP* **01** (2009) 059, [arXiv:0806.0102](#) [[hep-th](#)].
- [7] J. J. Heckman, J. Marsano, N. Saulina, S. Schäfer-Nameki, and C. Vafa, “Instantons and SUSY breaking in F-theory,” [arXiv:0808.1286](#) [[hep-th](#)].
- [8] J. Marsano, N. Saulina, and S. Schäfer-Nameki, “Gauge Mediation in F-Theory GUT Models,” [arXiv:0808.1571](#) [[hep-th](#)].
- [9] J. J. Heckman and C. Vafa, “F-theory, GUTs, and the Weak Scale,” [arXiv:0809.1098](#) [[hep-th](#)].
- [10] R. Donagi and M. Wijnholt, “Breaking GUT Groups in F-Theory,” [arXiv:0808.2223](#) [[hep-th](#)].
- [11] J. Marsano, N. Saulina, and S. Schäfer-Nameki, “An Instanton Toolbox for F-Theory Model Building,” [arXiv:0808.2450](#) [[hep-th](#)].
- [12] J. J. Heckman and C. Vafa, “From F-theory GUTs to the LHC,” [arXiv:0809.3452](#) [[hep-ph](#)].
- [13] A. Font and L. E. Ibáñez, “Yukawa Structure from U(1) Fluxes in F-theory Grand Unification,” *JHEP* **02** (2009) 016, [arXiv:0811.2157](#) [[hep-th](#)].
- [14] J. J. Heckman and C. Vafa, “Flavor Hierarchy From F-theory,” [arXiv:0811.2417](#) [[hep-th](#)].

- [15] R. Blumenhagen, V. Braun, T. W. Grimm, and T. Weigand, “GUTs in Type IIB Orientifold Compactifications,” [arXiv:0811.2936 \[hep-th\]](#).
- [16] R. Blumenhagen, “Gauge Coupling Unification in F-Theory Grand Unified Theories,” *Phys. Rev. Lett.* **102** (2009) 071601, [arXiv:0812.0248 \[hep-th\]](#).
- [17] J. J. Heckman, A. Tavanfar, and C. Vafa, “Cosmology of F-theory GUTs,” [arXiv:0812.3155 \[hep-th\]](#).
- [18] J. L. Bourjaily, “Local Models in F-Theory and M-Theory with Three Generations,” [arXiv:0901.3785 \[hep-th\]](#).
- [19] H. Hayashi, T. Kawano, R. Tatar, and T. Watari, “Codimension-3 Singularities and Yukawa Couplings in F-theory,” [arXiv:0901.4941 \[hep-th\]](#).
- [20] B. Andreas and G. Curio, “From Local to Global in F-Theory Model Building,” [arXiv:0902.4143 \[hep-th\]](#).
- [21] C.-M. Chen and Y.-C. Chung, “A Note on Local GUT Models in F-Theory,” [arXiv:0903.3009 \[hep-th\]](#).
- [22] J. J. Heckman, G. L. Kane, J. Shao, and C. Vafa, “The Footprint of F-theory at the LHC,” [arXiv:0903.3609 \[hep-ph\]](#).
- [23] R. Donagi and M. Wijnholt, “Higgs Bundles and UV Completion in F-Theory,” [arXiv:0904.1218 \[hep-th\]](#).
- [24] V. Bouchard, J. J. Heckman, J. Seo, and C. Vafa, “F-theory and Neutrinos: Kaluza-Klein Dilution of Flavor Hierarchy,” [arXiv:0904.1419 \[hep-ph\]](#).
- [25] L. Randall and D. Simmons-Duffin, “Quark and Lepton Flavor Physics from F-Theory,” [arXiv:0904.1584 \[hep-ph\]](#).
- [26] J. J. Heckman and C. Vafa, “CP Violation and F-theory GUTs,” [arXiv:0904.3101 \[hep-th\]](#).
- [27] J. L. Bourjaily, “Effective Field Theories for Local Models in F-Theory and M-Theory,” [arXiv:0905.0142 \[hep-th\]](#).
- [28] R. Tatar, Y. Tsuchiya, and T. Watari, “Right-handed Neutrinos in F-theory Compactifications,” [arXiv:0905.2289 \[hep-th\]](#).
- [29] J. Jiang, T. Li, D. V. Nanopoulos, and D. Xie, “Flipped $SU(5) \times U(1)_X$ Models from F-Theory,” [arXiv:0905.3394 \[hep-th\]](#).

- [30] A. Collinucci, “New F-theory lifts II: Permutation orientifolds and enhanced singularities,” [arXiv:0906.0003 \[hep-th\]](#).
- [31] R. Blumenhagen, T. W. Grimm, B. Jurke, and T. Weigand, “F-theory Uplifts and GUTs,” [arXiv:0906.0013 \[hep-th\]](#).
- [32] J. J. Heckman, A. Tavanfar, and C. Vafa, “The Point of E_8 in F-theory GUTs,” [arXiv:0906.0581 \[hep-th\]](#).
- [33] J. Marsano, N. Saulina, and S. Schafer-Nameki, “Monodromies, Fluxes, and Compact Three-Generation F-theory GUTs,” *JHEP* **08** (2009) 046, [arXiv:0906.4672 \[hep-th\]](#).
- [34] J. P. Conlon and E. Palti, “On Gauge Threshold Corrections for Local IIB/F-theory GUTs,” *Phys. Rev.* **D80** (2009) 106004, [arXiv:0907.1362 \[hep-th\]](#).
- [35] A. Font and L. E. Ibáñez, “Matter wave functions and Yukawa couplings in F-theory Grand Unification,” *JHEP* **09** (2009) 036, [arXiv:0907.4895 \[hep-th\]](#).
- [36] R. Blumenhagen, T. W. Grimm, B. Jurke, and T. Weigand, “Global F-theory GUTs,” [arXiv:0908.1784 \[hep-th\]](#).
- [37] S. Cecotti, M. C. N. Cheng, J. J. Heckman, and C. Vafa, “Yukawa Couplings in F-theory and Non-Commutative Geometry,” [arXiv:0910.0477 \[hep-th\]](#).
- [38] T. Li, D. V. Nanopoulos, and J. W. Walker, “Fast Proton Decay,” [arXiv:0910.0860 \[hep-ph\]](#).
- [39] J. P. Conlon and E. Palti, “Aspects of Flavour and Supersymmetry in F-theory GUTs,” [arXiv:0910.2413 \[hep-th\]](#).
- [40] K.-S. Choi, “Extended Gauge Symmetries in F-theory,” [arXiv:0910.2571 \[hep-th\]](#).
- [41] H. Hayashi, T. Kawano, Y. Tsuchiya, and T. Watari, “Flavor Structure in F-theory Compactifications,” [arXiv:0910.2762 \[hep-th\]](#).
- [42] C. Córdova, “Decoupling Gravity in F-Theory,” [arXiv:0910.2955 \[hep-th\]](#).
- [43] F. Marchesano and L. Martucci, “Non-perturbative effects on seven-brane Yukawa couplings,” [arXiv:0910.5496 \[hep-th\]](#).
- [44] Y.-C. Chung, “Abelian Gauge Fluxes and Local Models in F-Theory,” [arXiv:0911.0427 \[hep-th\]](#).

- [45] C. Vafa, “Geometry of Grand Unification,” [arXiv:0911.3008](#) [[math-ph](#)].
- [46] J. Marsano, N. Saulina, and S. Schafer-Nameki, “Compact F-theory GUTs with $U(1)_{PQ}$,” [arXiv:0912.0272](#) [[hep-th](#)].
- [47] E. Dudas and E. Palti, “Froggatt-Nielsen models from E_8 in F-theory GUTs,” [arXiv:0912.0853](#) [[hep-th](#)].
- [48] J. J. Heckman, “Particle Physics Implications of F-theory,” [arXiv:1001.0577](#) [[hep-th](#)].
- [49] R. Dermisek, H. Verlinde, and L.-T. Wang, “Hypercharged Anomaly Mediation,” *Phys. Rev. Lett.* **100** (2008) 131804, [arXiv:0711.3211](#) [[hep-ph](#)].
- [50] H. Verlinde, L.-T. Wang, M. Wijnholt, and I. Yavin, “A Higher Form (of) Mediation,” *JHEP* **02** (2008) 082, [arXiv:0711.3214](#) [[hep-th](#)].
- [51] T. W. Grimm and A. Klemm, “U(1) Mediation of Flux Supersymmetry Breaking,” [arXiv:0805.3361](#) [[hep-th](#)].
- [52] M. Buican and S. Franco, “SUSY breaking mediation by D-brane instantons,” [arXiv:0806.1964](#) [[hep-th](#)].
- [53] J. P. Conlon, F. Quevedo, and K. Suruliz, “Large-Volume Flux Compactifications: Moduli Spectrum and D3/D7 Soft Supersymmetry Breaking,” *JHEP* **08** (2005) 007, [hep-th/0505076](#).
- [54] J. P. Conlon, D. Cremades, and F. Quevedo, “Kähler Potentials of Chiral Matter Fields for Calabi-Yau String Compactifications,” *JHEP* **01** (2007) 022, [hep-th/0609180](#).
- [55] J. P. Conlon, “Mirror Mediation,” *JHEP* **03** (2008) 025, [arXiv:0710.0873](#) [[hep-th](#)].
- [56] J. P. Conlon and F. Quevedo, “Astrophysical and Cosmological Implications of Large Volume String Compactifications,” *JCAP* **0708** (2007) 019, [arXiv:0705.3460](#) [[hep-ph](#)].
- [57] J. P. Conlon, S. S. Abdussalam, F. Quevedo, and K. Suruliz, “Soft SUSY Breaking Terms for Chiral Matter in IIB String Compactifications,” *JHEP* **01** (2007) 032, [hep-th/0610129](#).
- [58] S. P. Martin and J. D. Wells, “Cornering gauge-mediated supersymmetry breaking with quasi-stable sleptons at the Tevatron,” *Phys. Rev.* **D59** (1999) 035008, [hep-ph/9805289](#).

- [59] I. Hinchliffe and F. E. Paige, “Measurements in gauge mediated SUSY breaking models at LHC,” *Phys. Rev.* **D60** (1999) 095002, [hep-ph/9812233](#).
- [60] S. Ambrosanio, B. Mele, S. Petrarca, G. Polesello, and A. Rimoldi, “Measuring the SUSY breaking scale at the LHC in the slepton NLSP scenario of GMSB models,” *JHEP* **01** (2001) 014, [hep-ph/0010081](#).
- [61] S. Ambrosanio *et. al.*, “SUSY long-lived massive particles: Detection and physics at the LHC,” [hep-ph/0012192](#).
- [62] J. R. Ellis, A. R. Raklev, and O. K. Øye, “Gravitino dark matter scenarios with massive metastable charged sparticles at the LHC,” *JHEP* **10** (2006) 061, [hep-ph/0607261](#).
- [63] T. Ito, R. Kitano, and T. Moroi, “Measurement of the Superparticle Mass Spectrum in the Long-Lived Stau Scenario at the LHC,” [arXiv:0910.5853 \[hep-ph\]](#).
- [64] M. Dine, W. Fischler, and M. Srednicki, “Supersymmetric Technicolor,” *Nucl. Phys.* **B189** (1981) 575–593.
- [65] S. Dimopoulos and S. Raby, “Supercolor,” *Nucl. Phys.* **B192** (1981) 353.
- [66] M. Dine and W. Fischler, “A Phenomenological Model of Particle Physics Based on Supersymmetry,” *Phys. Lett.* **B110** (1982) 227.
- [67] C. R. Nappi and B. A. Ovrut, “Supersymmetric Extension of the $SU(3) \times SU(2) \times U(1)$ Model,” *Phys. Lett.* **B113** (1982) 175.
- [68] M. Dine and W. Fischler, “A Supersymmetric GUT,” *Nucl. Phys.* **B204** (1982) 346.
- [69] L. Alvarez-Gaumé, M. Claudson, and M. B. Wise, “Low-Energy Supersymmetry,” *Nucl. Phys.* **B207** (1982) 96.
- [70] S. Dimopoulos and S. Raby, “Geometric Hierarchy,” *Nucl. Phys.* **B219** (1983) 479.
- [71] M. Dine and A. E. Nelson, “Dynamical supersymmetry breaking at low-energies,” *Phys. Rev.* **D48** (1993) 1277–1287, [hep-ph/9303230](#).
- [72] M. Dine, A. E. Nelson, and Y. Shirman, “Low-energy dynamical supersymmetry breaking simplified,” *Phys. Rev.* **D51** (1995) 1362–1370, [hep-ph/9408384](#).
- [73] M. Dine, A. E. Nelson, Y. Nir, and Y. Shirman, “New tools for low-energy dynamical supersymmetry breaking,” *Phys. Rev.* **D53** (1996) 2658–2669, [hep-ph/9507378](#).

- [74] G. F. Giudice and R. Rattazzi, “Theories with Gauge-Mediated Supersymmetry Breaking,” *Phys. Rept.* **322** (1999) 419–499, [hep-ph/9801271](#).
- [75] R. Rattazzi and U. Sarid, “Large $\tan\beta$ in gauge-mediated SUSY-breaking models,” *Nucl. Phys.* **B501** (1997) 297–331, [hep-ph/9612464](#).
- [76] J. A. Bagger, K. T. Matchev, D. M. Pierce, and R.-J. Zhang, “Weak-scale phenomenology in models with gauge-mediated supersymmetry breaking,” *Phys. Rev.* **D55** (1997) 3188–3200, [hep-ph/9609444](#).
- [77] S. Martin, “Predictions of the sign of μ from supersymmetry breaking models,” *Phys. Rev.* **D65** (2002) 035003, [hep-ph/0106280](#).
- [78] B. C. Allanach, “SOFTSUSY2.0: a program for calculating supersymmetric spectra,” *Comput. Phys. Commun.* **143** (2002) 305–331, [hep-ph/0104145](#).
- [79] OPAL Collaboration, G. Abbiendi *et. al.*, “Search for Stable and Long-Lived Massive Charged Particles in $e^+ e^-$ Collisions at $\sqrt{s} = 130$ GeV to 209 GeV,” *Phys. Lett.* **B572** (2003) 8–20, [hep-ex/0305031](#).
- [80] M. Ibe and R. Kitano, “Sweet Spot Supersymmetry,” *JHEP* **08** (2007) 016, [arXiv:0705.3686 \[hep-ph\]](#).
- [81] M. Muhlleitner, A. Djouadi, and Y. Mambrini, “SDECAY: A Fortran code for the decays of the supersymmetric particles in the MSSM,” *Comput. Phys. Commun.* **168** (2005) 46–70, [hep-ph/0311167](#).
- [82] B. S. Acharya *et. al.*, “Identifying Multi-Top Events from Gluino Decay at the LHC,” [arXiv:0901.3367 \[hep-ph\]](#).
- [83] T. Sjöstrand, S. Mrenna, and P. Skands, “PYTHIA 6.4 Physics and Manual,” *JHEP* **05** (2006) 026, [hep-ph/0603175](#).
- [84] P. Meade and M. Reece, “BRIDGE: Branching Ratio Inquiry / Decay Generated Events,” [hep-ph/0703031](#).
- [85] P. Skands *et. al.*, “SUSY Les Houches Accord: Interfacing SUSY Spectrum Calculators, Decay Packages, and Event Generators,” *JHEP* **07** (2004) 036, [hep-ph/0311123](#).
- [86] A. De Roeck, J. Ellis, F. Gianotti, F. Moortgat, K. Olive, and L. Pape, “Supersymmetric benchmarks with non-universal scalar masses or gravitino dark matter,” *Eur. Phys. J.* **C49** (2007) 1041–1066, [hep-ph/0508198](#).

- [87] J. Chen and T. Adams, “Searching for high speed long-lived charged massive particles at the LHC,” *Eur. Phys. J.* **C67** (2010) 335–342, [arXiv:0909.3157 \[hep-ph\]](#).
- [88] **The ATLAS** Collaboration, G. Aad *et. al.*, “Expected Performance of the ATLAS Experiment - Detector, Trigger and Physics,” [arXiv:0901.0512 \[hep-ex\]](#).
- [89] G. L. Kane, A. A. Petrov, J. Shao, and L.-T. Wang, “Initial determination of the spins of the gluino and squarks at LHC,” [arXiv:0805.1397 \[hep-ph\]](#).
- [90] **D0** Collaboration, V. M. Abazov *et. al.*, “Search for Long-Lived Charged Massive Particles with the D0 Detector,” *Phys. Rev. Lett.* **102** (2009) 161802, [arXiv:0809.4472 \[hep-ex\]](#).
- [91] **CDF** Collaboration, T. Aaltonen *et. al.*, “Search for Long-Lived Massive Charged Particles in 1.96 TeV $\bar{p}p$ Collisions,” *Phys. Rev. Lett.* **103** (2009) 021802, [arXiv:0902.1266 \[hep-ex\]](#).
- [92] W. Buchmuller, K. Hamaguchi, M. Ratz, and T. Yanagida, “Supergravity at Colliders,” *Phys. Lett.* **B588** (2004) 90–98, [hep-ph/0402179](#).
- [93] K. Hamaguchi, Y. Kuno, T. Nakaya, and M. M. Nojiri, “A study of late decaying charged particles at future colliders,” *Phys. Rev.* **D70** (2004) 115007, [hep-ph/0409248](#).
- [94] J. L. Feng and B. T. Smith, “Slepton trapping at the Large Hadron and International Linear Colliders,” *Phys. Rev.* **D71** (2005) 015004, [hep-ph/0409278](#).
- [95] K. Hamaguchi, M. M. Nojiri, and A. de Roeck, “Prospects to study a long-lived charged next lightest supersymmetric particle at the LHC,” *JHEP* **03** (2007) 046, [hep-ph/0612060](#).
- [96] **MACRO** Collaboration, M. Ambrosio *et. al.*, “Measurements of atmospheric muon neutrino oscillations, global analysis of the data collected with MACRO detector,” *Eur. Phys. J.* **C36** (2004) 323–339.
- [97] A. Arvanitaki, S. Dimopoulos, A. Pierce, S. Rajendran, and J. Wacker, “Stopping gluinos,” *Phys. Rev.* **D76** (2007) 055007, [hep-ph/0506242](#).
- [98] S. Asai, K. Hamaguchi, and S. Shirai, “Stop and Decay of Long-lived Charged Massive Particles at the LHC detectors,” *Phys. Rev. Lett.* **103** (2009) 141803, [arXiv:0902.3754 \[hep-ph\]](#).

- [99] N. Arkani-Hamed, G. L. Kane, J. Thaler, and L.-T. Wang, “Supersymmetry and the LHC Inverse Problem,” *JHEP* **08** (2006) 070, [hep-ph/0512190](#).
- [100] J. Hubisz, J. Lykken, M. Pierini, and M. Spiropulu, “Missing energy look-alikes with 100 pb^{-1} at the LHC,” *Phys. Rev.* **D78** (2008) 075008, [arXiv:0805.2398](#) [[hep-ph](#)].
- [101] G. L. Kane, P. Kumar, and J. Shao, “LHC String Phenomenology,” *J. Phys.* **G34** (2007) 1993–2036, [hep-ph/0610038](#).
- [102] G. L. Kane, P. Kumar, and J. Shao, “Unravelling Strings at the LHC,” *Phys. Rev.* **D77** (2008) 116005, [arXiv:0709.4259](#) [[hep-ph](#)].
- [103] P. Meade, N. Seiberg, and D. Shih, “General Gauge Mediation,” *Prog. Theor. Phys. Suppl.* **177** (2009) 143–158, [arXiv:0801.3278](#) [[hep-ph](#)].
- [104] M. Buican, P. Meade, N. Seiberg, and D. Shih, “Exploring General Gauge Mediation,” *JHEP* **03** (2009) 016, [arXiv:0812.3668](#) [[hep-ph](#)].